

# Filière Systèmes industriels

## Orientation Power and Control

# Diplôme 2007

## *Mikaël Rodriguez*

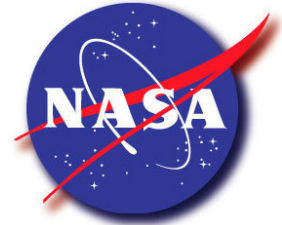
*Wireless sensor for the  
in-vivo monitoring  
of astronaut health*

Professeur

Martial Geiser

Experts

Rafat R. Ansari, Luca Pollonini



# Design and development of a wireless sensor for the in-vivo monitoring of astronaut health

Author  
**Mikaël Rodriguez**

Supervisors  
**Dr. Rafat R. Ansari**  
**Dr. Luca Pollonini**  
**Prof. Martial Geiser**



## ACKNOWLEDGEMENTS

I wish to thank all the people without whom my stay here in Texas would never have been so attractive, in particular:

- Prof. Martial Geiser, who gave me the opportunity to complete my diploma work in United States
- Dr. Rafat Ansari, for offering me the chance to work on this very interesting project
- Dr. Luca Pollonini, for his excellent help, support and collaboration on this work, and without whom this project would never have gone so far
- Dr. Jeffrey Jones and his colleagues, for their interest and collaboration on this project
- Prof. Gilbert Maitre, for his support and recommendations during the entire work
- Marga Pollonini, for taking the time to correct this document
- Dr. James Turley, Dr. Robert Vogler and their families, for their very kind hospitality and for having helped me to move in Houston after my arrival
- Rahila Ansari, Benafsha Irani, Marga & Luca Pollonini, for keeping me entertained during my stay and for making me discovering the city of Houston
- My friends from Switzerland who joined me in Florida for the winter vacations

and finally all the people I did not mention in particular, but who played a role in the success of my work.

## ABSTRACT

### PURPOSE

The aim of this project is to develop a prototype of a miniaturized system able to perform blood flow and pulse-oxymetry measurements on a fingertip. The motivation is to monitor the evolution of those parameters in the astronauts' fingers, since they suffer from injuries in this part of the body when they carry out extra-vehicular activities in space. By integrating such a measurement system in their suit, it could be possible to understand and quantify this phenomenon, and maybe avoid further injuries to their fingers. Therefore, the system has to meet several requirements such as compact size, low-power, ease of operation, and wireless communication.

### APPROACH

The measurements are based on the non-invasive *Laser Doppler Flowmetry* and *pulse-oxymetry* techniques. The use of a laser beam which is shined on the skin, scattered within the tissues, reflected out of the body, collected and finally analyzed, has been demonstrated to be an appropriate method for this purpose: the use of the laser light is totally painless, very sensitive, and appropriate to this kind of in-vivo measurements.

### DEVELOPMENT

A prototype system made of two laser sources, a miniaturized probe, a photodiode, several fiber optics and a customized electronic circuit board responsible for managing the whole system and to compute the data has been developed. A standard laptop computer displays the results and controls the system through a wireless transmission using the *Bluetooth* technology.

The main features of this system are the low power consumption, the small space requirement, the portability and the ability to communicate wirelessly with a remote laptop.

### CONCLUSION

The initial engineering tests show that the system is functional. However, detailed testing in humans needs to be performed.



# CONTENTS

Section	Page
<b>1 Introduction .....</b>	<b>1</b>
1.1 Purpose.....	1
1.2 System requirements .....	2
1.3 Approach .....	3
<b>2 Laser Doppler flowmetry and pulse-oxymetry.....</b>	<b>5</b>
2.1 Principles of laser Doppler flowmetry.....	5
2.2 Implementation of the LDF in this application.....	8
2.3 Principles of pulse-oxymetry.....	9
2.4 Implementation of the pulse-oxymetry in this application.....	9
<b>3 Design and development of a new system .....</b>	<b>10</b>
3.1 Background.....	10
3.2 Concept .....	17
3.3 Development and detailed design .....	25
<b>4 Characterization of the system.....</b>	<b>61</b>
4.1 Characterization of the electronic part.....	61
4.2 Characterization of the software part.....	64
4.3 Characterization of the optical set-up.....	67
4.4 First measurements.....	68
<b>5 Conclusion and future development .....</b>	<b>72</b>
5.1 Summary .....	72
5.2 Known weaknesses and problems .....	73
5.3 Ideas and further development .....	74
<b>Appendices.....</b>	<b>78</b>

# 1 INTRODUCTION

## 1.1 PURPOSE

When astronauts carry out *extra-vehicular activities (EVA)* in the space, they are exposed to a severe environment consisting of, among other things: abrupt temperature changes due to the orbit the astronauts follow around the Earth (the temperature can be as high as 85 °C when the astronauts are facing the sun, or as low as -130 °C when they are over the shadowed side of Earth), lack of oxygen due to the absence of atmosphere, and high levels of radiation since, as opposed to every living being on the Earth, they are not protected by the ozone layer. Therefore, the astronauts must wear specially designed suits for their protection against these phenomena, which must also allow them the required flexibility and level of mobility to perform the assigned tasks. For this purpose, the *EVA mobility unit suits (EMUs)* are commonly used. The EMUs are made of a variety of different synthetic polymers (nylon, neoprene, mylar, gortex, kevlar, nomex), and they provide the basic elements for life support such as oxygen, temperature control, pressurized enclosure, carbon dioxide removal, and protection from sunlight, solar radiation and tiny micrometeoroids.



Picture 1  
EVA mobility unit suit

Despite the high-technology EMUs, fatigue and discomfort can occur in the fingers of astronauts during the space walks outside the orbiting spacecrafts. After several hours of EVA, the fingers of the majority of the astronauts present bruises and a deep pain is felt in this part of the body. This temporary situation is usually resolved once the astronaut is back in a normal environment (such as the inside of the space station), without any intervention. This fact remains to date unexplained, although several hypotheses have been expressed: one conjecture is that, despite the insulation and protections within the astronauts' suits, the severity of the environment (particularly the coldness) causes restricted blood circulation in their extremities, which consequently can cause fatigue.

There is therefore a critical interest in monitoring the blood circulation in the capillaries of the astronauts' distal fingertips during missions. First of all, being able to quantify different parameters such as the blood volume, the blood flow or the oxygenated hemoglobin rate in this part of the body could help to understand if these discomforts are really related to the blood circulation, as mentioned in the previous hypothesis; if it is correct, these parameters would clearly represent how serious this phenomenon is. The collected data could then be used to develop better countermeasures to help the astronauts avoid further discomfort or even injuries to their fingers. Having a real time measurement of the blood circulation during EVA's could offer important advantages like, for instance, relating the evolution of the monitored parameters to the astronauts' conditions (facing the sun or in the dark, moving or staying still, bending the fingers or not, etc.), or, more than just understanding the phenomenon, taking some decisions during the mission in order to limit the impairing to the astronauts' fingers.

This project is based on the development of a prototype for such measurement system. Obviously, before the flight model is approved, the concept will be modified, optimized and tested step by step on Earth; this document shows how the first embedded system has been created and which technologies are used, as well as the results obtained after the first tests. Considering its peculiar use, it has to meet several requirements that are enumerated in the next section.

## 1.2 SYSTEM REQUIREMENTS

The aim is to develop a portable, miniaturized system able to measure the blood circulation (blood volume, velocity and flow) as well as the oxygenated hemoglobin rate in the distal fingertips. Its design, especially the place of each component and interconnections between them, has to be well considered so that it can be embedded in the astronaut suit.

This system has to satisfy the following points:

- The method used for the measurement has to be non-invasive, based only on the contact with the skin. The inner glove of the astronaut system can eventually be modified, but the outer glove has to be kept unchanged since it consists of the main protection of the hand; therefore, the sensors have to be very tiny so that they can fit in the glove.
- The other components of the system can be placed within the *display and control module* (located on the belly) or within the *backpack* (hard upper torso part of the suit); even though the exact dimensions of the system and its placement within this box are not the main concern so far, its volume has to be kept as small as possible. Details about the different EMU's parts are shown in appendix 1.
- The power consumption has to be kept as low as possible, since the available energy is clearly limited, and the system cannot be fond of it. There are no particular voltage requirements for the main power input of the system: this part will be adapted on later.
- The results of the measurement have to be displayed on a control unit in real time, and these data have to be stored for further analysis.
- The astronaut, while executing his tasks during the mission, will not be able to monitor the results of the measurement by himself. Therefore, the system has to be remote controlled, so that somebody else can supervise the measurement and watch the results. Since a physical connection between the astronaut and the environment nearby is not available, the system has to communicate wirelessly with the remote control unit. The existing wireless communication system that is currently used to transmit data between the astronaut and space shuttle cannot be used: a totally independent transmission system has to be developed for this purpose.



Picture 2  
Glove of an EMU

Most of the requirements above don't mention any absolute value (e.g. dimensions, power consumption). This offers more freedom for the development of the system and avoids spending too long on these points which can be solved afterwards: first, the system has to prove that such measurement done by an embedded system is reliable; then its integration can be thoroughly studied and optimized.

Since this model is a first prototype and is therefore not going to fly, the conception restrictions and required robustness and immunity related to the space environment are not applicable.

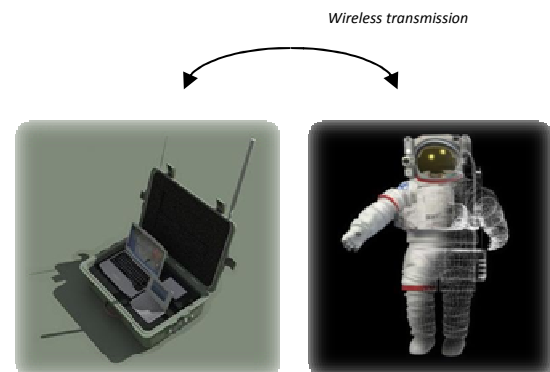


Figure 1  
Expected configuration of the system

### 1.3 APPROACH

In order to perform non-invasive measurements, the use of a laser beam which is shined on the skin, scattered within the tissues, reflected out of the body, collected and finally analyzed, has been demonstrated to be an appropriate method for this purpose: the use of the laser light is totally painless, very sensitive, and appropriate to this kind of in-vivo measurements. Several laser-based measurement techniques have been studied for many years at *NASA Glenn Research Center (Cleveland, Ohio)*, which provides a strong basis and deep knowledge as a starting point for this project.

One possibility to quantify the blood circulation in the astronauts' fingers is to measure the hemodynamic of the capillaries in their fingertips; therefore, *laser Doppler flowmetry (LDF)* has a significant potential. In order to determine the oxygenated hemoglobin rate, the *pulse-oxymetry* technique will perfectly complement the LDF since it requires some features that are also needed for the LDF measurement.

The Doppler shift effect, caused by the reflection of the light on red blood cells, can be used to detect the volume, velocity and flow of the blood. This method has been successfully developed, e.g. by Martial H. Geiser and al., in the foveal region of the human choroidal vascular system [1]. A pilot study [2] provides sufficient evidence that the LDF measurements are suitable for monitoring microcirculation in the distal fingertips; the experimental setup consisted of a laser emitter, detector, support mount for the test subject's finger, and a computer controlling the data acquisition system. The aim of a previous project was the miniaturization of the probe [3], which involved the design of a fiber optic based system that offers the possibility to mount larger components further away from the sensor.

The *pulse-oxymetry* technique is appropriate to determine the oxygenated hemoglobin rate: it is based on the differential optical density of red and infrared light as projected through a vascular bed and calculates a ratio of the optical densities (since red and infrared light absorption characteristics of oxygenated and deoxygenated hemoglobin are different). Utilizing the optical density ratio, an arterial oxygen saturation ( $SpO_2$ ) value is empirically reported based on the ratio obtained.

As required, a probe able to fit in the glove could be developed: its aim is to assure good contact with the skin so that the laser light can penetrate the finger in the desired position, and the reflected light is collected. All the other components of the system could be placed further away, within the *display and control module* or within the *backpack*. That's why several fiber optics will connect the sensor with the rest of the system, particularly the laser source(s), which provides the original, pure laser light, and a photodiode, responsible of converting the collected light into an electrical signal, which can be processed afterwards. The work done in the previous project [3] consists of a very useful background for this part of the development, as well as for the LDF measurement.

Another electronic part should also take place within the *display and control module* or *backpack*: it actually consists of the major development of the project, and the "brain" of the system. It would complement the photodiode, it would process the electrical signal coming out of it, and it would transmit the resulting data wirelessly to the remote controller. This electronic part should also be able to control the lasers and obviously, manage its own operations. The choice of the components used for this part of the system must be carefully considered, so that the power consumption can be minimized; in order to reduce the space, as many as possible *surface mounted devices (SMDs)* components would be chosen and finally assembled on a customized *printed circuit board (PCB)*. However, the fact that the laser sources, the photodiode and the processing board are remotely located and connected to the fingertip-probe by fiber optics, offers a lot

more possibilities for its mechanical design (having placed it in the arm, for instance, would result in too many restrictions).

The *Bluetooth* standard is a low-power wireless technique which is able to achieve a perfect transmission within a distance of 10 meters at least. It is relatively easy to integrate and moreover, most of the laptop computers possess it now. It makes it a good option for transmitting the data in this application, and could allow the system (and therefore the astronaut) to be connected to whatever laptop or computer located at a reasonable distance from him. This wireless transmission standard should have enough capabilities to fit the data transmission rate requirements, as well as the expected real-time display.

Finally, if the *Bluetooth* integration can be considered, the control application, responsible of displaying the results of the measurements and controlling the embedded system, could be developed in a commonly used programming language based on a *Microsoft Windows* environment; this could avoid any other unnecessary financial expenses since it's not a problem to find an already existing and available laptop or desktop computer, which doesn't need to satisfy any special requirements (even if the *Bluetooth* is not integrated in it yet, a quite cheap external module can simply be plugged in).

As a first step, the miniaturizing of the lasers as well as the photodiode will be left aside: tiny, portable lasers do already exist and could be used without any modification as a starting point for the system; some existing photodiode modules are available in the laboratories and are satisfactory enough to begin with. Therefore, the main concern is the measurement processing as well as the wireless transmission, both of which have to be totally developed, as shown in figure 2. Some work has to be done on the probe design and the corresponding fiber optics too. Therefore, the work will start by several tests which will provide a useful background to design this system, customized for this very particular application.

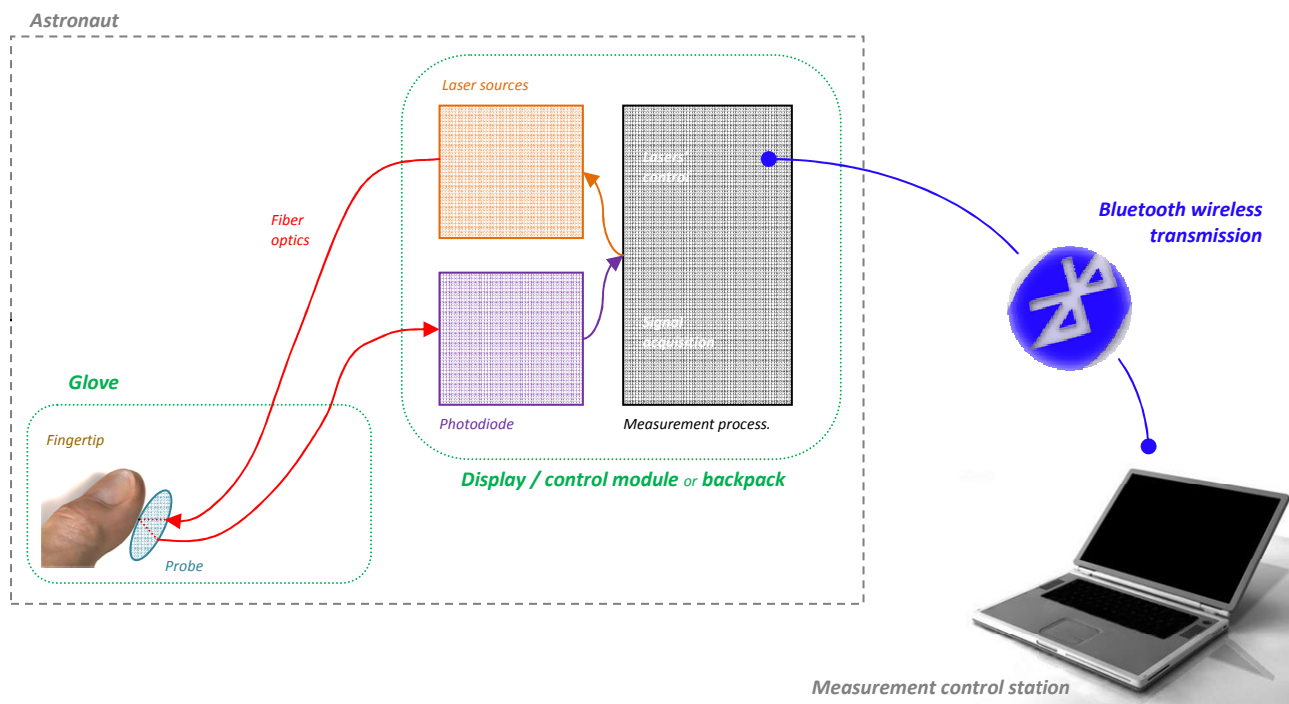


**Figure 2**  
Principle scheme of the system to develop

## 2 LASER DOPPLER FLOWMETRY AND PULSE-OXYMETRY

### 2.1 PRINCIPLES OF LASER DOPPLER FLOWMETRY

#### 2.1.1 Introduction

Light is capable of measuring the velocity of the red blood cells even at the slow speeds with which they move through capillaries; laser Doppler blood flowmetry thus uses the upper visible range and the near-infrared light (600-1'200 nm) to measure tissue perfusion by exploiting the Doppler shifts that moving red blood cells impart to light [4]. The spectral purity of the laser makes it practical to detect the slight frequency shifts produced by the interactions between photons and moving red blood cells.

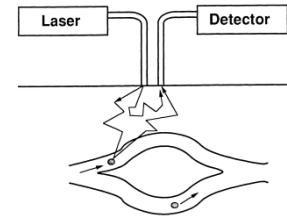


Figure 3  
Laser Doppler measurement of tissue perfusion

The laser light is typically delivered to the tissue and returned to a detector by fiber optic light guides. Light in the tissue is diffusely scattered by stationary tissue. This light reaches the detector without being Doppler-shifted. Photons that encounter moving red blood cells experience a Doppler shift, as shown in figure 3.

#### 2.1.2 Fundamentals of the Doppler effect

Figure 4 illustrates the Doppler effect as it applies to sound waves. Figure 4a depicts a stationary source of sound emitting a particular frequency and a listener located at some distance from the source. If both listener and source are stationary, the listener receives  $C \cdot T / \lambda$  waves in  $T$  seconds, where  $C$  is the speed of sound and  $\lambda$  is the wavelength. Figure 4b illustrates the situation in which the listener will receive an additional  $v_L \cdot T / \lambda$  waves in time  $T$  due to his movement at the velocity  $v_L$ . Because the frequency that the listener experiences ( $f_0$ ) is simply the number of waves per unit of time,

$$f_0 = \frac{\left(\frac{C \cdot T}{\lambda} + \frac{v_L \cdot T}{\lambda}\right)}{T} = \frac{(C + v_L)}{\lambda}$$

The frequency at the source that the listener hears when stationary is just  $f_s = C / \lambda$ . The difference between the two perceived frequencies defines the Doppler frequency shift ( $f_d$ ), which can be expressed as

$$f_d = f_0 - f_s = f_s \left(1 + \frac{v_L}{C}\right) - f_s = \frac{v_L \cdot f_s}{C}$$

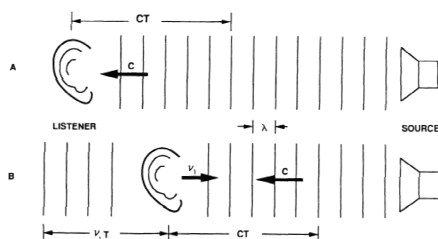


Figure 4  
Acoustic example of the elementary Doppler principle



For sound waves, the motion of the source has a different Doppler shift frequency to the same motion on the listener's part. In other words, it is not just the relative motion between source and listener that is important, but which of the two is in motion. In addition, as the velocity of the source approaches the velocity of sound, the Doppler shift frequency becomes infinite. On the other hand, the situation is fundamentally different for Doppler effects with light. The difference can be explained in terms of Einstein's theory of relativity, which states that the speed of light is a constant in all reference frames. Light needs no material medium for its propagation, and its speed relative to the source or observer is always the same. Therefore, it is only the relative motion between the observer and the source that determines the Doppler shift frequency. Thus,

$$f_0 = \left[ f_s \frac{(1 - v_{os}/C)}{\sqrt{1 - (v_{os}/C)^2}} \right] - f_s$$

Where  $C$  is the velocity of light and  $v_{os}$  is the relative velocity of the source with respect to the observer.

This equation can be applied to light entering tissue, but two other factors must be considered. If light hits a stationary object and is reflected directly to a receiving detector, the returning light will have the same frequency as the emitted light. However, if the returning light has reflected from an object in motion, such as a red blood cell, the returning light will undergo a Doppler shift that is twice that predicted by the equation. The reason is that the structure reflecting the light acts as both the observer and the source. Because the red blood cell is in motion, the transmitted frequency it receives is Doppler-shifted according to the equation, and the reflected light that leaves the red blood cell is shifted again because the red blood cell also acts as a source in motion relative to the stationary receiver. The second factor to consider is that only the component of the velocity vector directed toward or away from the receiver (observer) contributes to the Doppler shift frequency. Thus, for direct backscattering, one must actually scale the frequency shift by the cosine of the angle between the red blood cells' velocity vector and the line connecting the object to the receiver. Although the Doppler shifts imparted to light by moving red blood cells are quite small compared to the frequency of light, the method is practical because of the spectral stability of laser light.

### 2.1.3 Theory of Doppler measurement

The classical Doppler effect is normally experienced as the increase of the pitch (or frequency) of a train whistle as it moves towards the observer, and a decrease as it moves away. Doppler ultrasound techniques are easily explained by this analogy: an ultrasound wave principally moves on a straight path through tissue (as does sound in air), and a small fraction is scattered back (i.e., reflected) toward the source by moving red blood cells. If the cell has a velocity  $-v_x$  in the direction of the source of the ultrasound and its detector, the ultrasound frequency will be shifted to lower frequencies by an amount  $\Delta f = 2 \cdot v_x / \lambda$ , where  $\lambda$  is the wavelength of the ultrasound in the tissue. Thus a Doppler ultrasound probe is sensitive to motion in a specific direction, and it can record the distribution of velocities in that direction. Because the wavelengths of the applied ultrasound field are 0.1-0.3 mm, the relatively high velocities of blood cells moving in large vessels (3-150 cm/s) result in frequency shifts between 100 and 10'000 Hz. However, the velocities in capillaries are significantly lower (about 1 mm/s), so the shifts they produce are immeasurably small (about 5 Hz).

For particles suspended in a clear fluid, the laser Doppler backscatter techniques give frequency shifts from which distributions of particle velocities can be determined. Because the wavelengths of light are approximately 500-fold smaller than ultrasound wavelengths, the corresponding Doppler shifts are 500 times greater. More generally, the Doppler shifts of scattered laser light are determined by the speed of the particle, a scale factor, and the cosine of the angle between the velocity direction and the direction of the Bragg scattering angle.

This light which is Doppler shifted, is optically mixed with the light which has been scattered by the static structural components as show in figure 5, and detected by a photo detector. Only 1‰ to 1% of the detected light has been Doppler shifted; the remainder of light that has not been Doppler shifted acts as a reference signal.

The photodetected voltage is analyzed according to the scheme developed by Bonner and Nossal [6] to obtain the LDF parameters:

$$\text{Blood volume} = \frac{1}{A_{DC}^2} \cdot \int P(f)df \equiv \left[ \frac{W}{V^2} \right]$$

$$\text{Blood speed} = \frac{\int f \cdot P(f)df}{\int P(f)df} \equiv [Hz]$$

$$\text{Blood flow} = \text{Blood volume} \cdot \text{Blood speed} = \frac{1}{A_{DC}^2} \cdot \int f \cdot P(f)df \equiv \left[ Hz \cdot \frac{W}{V^2} \right]$$

Where  $P(f)df$  is the power spectrum and  $A_{DC}$  the voltage of the analyzed signal.

The *blood volume* in the detected section is expressed in  $W/V^2$ ; the *blood speed* has a unit of  $Hz$  and is proportional to the mean speed of the blood within the volume sampled by the laser light. Finally, the *blood flow*, which is the product of the two other values, is expressed in  $Hz \cdot W/V^2$ . The detected light contains Doppler shift frequencies which can be positive or negative, depending on the direction of movement of the red blood cells with regard to the event and scattered light directions.

In order to apply the LDF theory to the real measurements, it is first necessary to filter out the low-frequency artifacts due to the tissue motion (e.g., a subject's breathing, muscle twitch, motion of the probe relative to the tissue). Several instruments therefore utilize the following algorithm to calculate the effective Doppler-shift frequency (see figure 6):

$$\text{Blood flow} = \frac{1}{A_{DC}^2} \cdot \int_{30Hz}^{30,000Hz} f \cdot P(f)df \equiv \left[ Hz \cdot \frac{W}{V^2} \right]$$

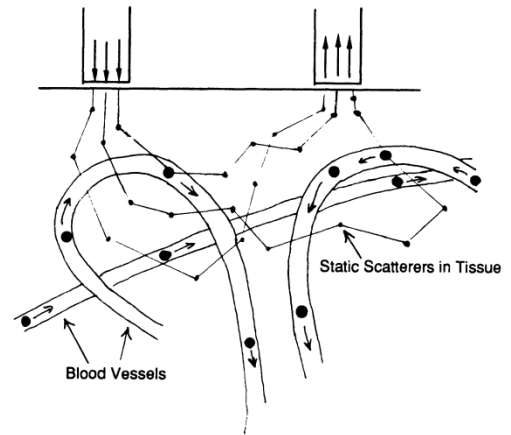
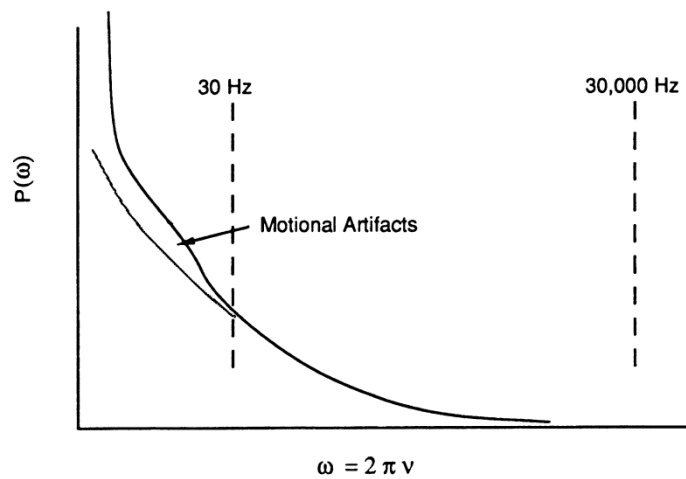


Figure 5  
Schematic diagram of light diffusing through vascularized tissue





**Figure 6**  
Schematic representation of the power spectrum of the detected photocurrent, showing 30 Hz and 30 kHz cutoffs

## 2.2 IMPLEMENTATION OF THE LDF IN THIS APPLICATION

In this work, the interest is to apply the method described above to measure the three blood parameters (volume, speed, flow) on a fingertip.

The wavelength of the laser source determines the depth the light goes into the skin, and therefore the probability that a photon is absorbed by the tissue depends on this very wavelength. The useable wavelengths for the measurement on a fingertip are located between 600 and 1'200 nm; this is named the therapeutic window for the tissue.

After being transformed in an electrical signal, the scattered light presents a different behavior depending on which part of the body is analyzed. The expected signal to process has therefore a particular shape after the scattering into the fingertip tissue as shown in figure 7.

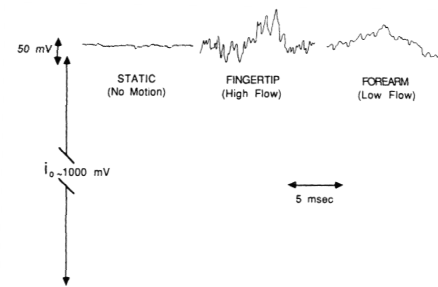


**Figure 7**  
Schematic of typical signal detected with a laser Doppler flowmeter (photodiode voltage versus time)

A previous project [3] showed a system with a configuration that was able to achieve good results for such a measurement: among other things, it recommends to use a high-stability laser with a wavelength of 780 nm, and a core-to-core fiber separation of 3 mm. Other technical details are explained in chapter 3.1.1 since this existing project will serve as a background for further development.

## 2.3 PRINCIPLES OF PULSE-OXYMETRY

The principle of pulse-oxyometry is based on the red and infrared light absorption characteristics of oxygenated and deoxygenated hemoglobin. Oxygenated hemoglobin (HbO<sub>2</sub>) absorbs more infrared light and allows more red light to pass through, while deoxygenated (or reduced) hemoglobin (Hb) absorbs more red light and allows more infrared light to pass through, as shown in figure 8. Red light is in the 600-750 nm wavelength light band, near-infrared in the 850-1'000 nm.

The wavelength at which the two substances absorb the same amount of light is called *isosbestic point*. The isosbestic point of oxygenated hemoglobin and deoxygenated hemoglobin occur at 805 nm. This point may be used as a reference point where light absorption is independent of the degree of saturation. Thus, comparison of absorbancies at different wavelengths allows estimation of the relative concentrations of HbO<sub>2</sub> and Hb. Modern pulse-oxyimeters may use two or more wavelengths, not necessarily including an isosbestic point.

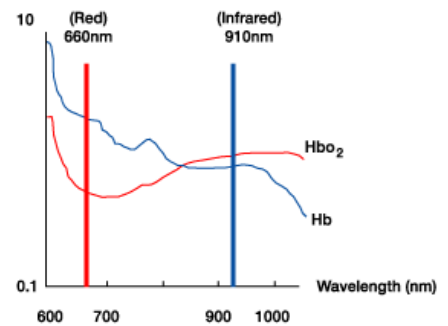


Figure 8

Relative absorption of red and infrared light by oxy- and deoxygenated hemoglobin (absorption coefficient versus wavelength)

After the transmitted red (R) and infrared (IR) signals pass through the measuring site and are received at the photodetector, the *R/IR* ratio is calculated. This ratio is compared to a "look-up" table (made up of empirical formulas) that converts the ratio to a SpO<sub>2</sub> value. Typically *R/IR* ratios are shown in the table 1 below.

$$Ratio = \frac{A_r}{A_{ir}} \rightarrow \% SpO_2$$

R/IR ratio	SpO <sub>2</sub>
0.5	100%
1.0	82%
2.0	0%

Table 1

*R/IR* ratio to SpO<sub>2</sub> conversion

## 2.4 IMPLEMENTATION OF THE PULSE-OXYMETRY IN THIS APPLICATION

The idea is to combine both the LDF and pulse-oxyometry measurements in this system. The principle mentioned in the previous section has proved its abilities to measure reliable values for the oxygenated hemoglobin rate: several instruments based on this process are commercially available.

Since the pulse-oxyometry technology requires two different wavelengths, a good option could be using the already existing LDF wavelength along with a second one belonging to the visible red range. This will also require a particular optical configuration, since the laser light coming from two different sources has to be emitted by one single common emitter on the finger.

The wavelength used for the LDF measurement (780 nm) is located in the near-infrared range, which is quite close to the isosbestic point of figure 8. Therefore, given the limited choice to the existing lasers available in the laboratory, complementing the LDF wavelength with a red laser of 635 nm wavelength should return good results, considering that the absorption of those two lights is definitely different according to the graph of figure 8.

### 3 DESIGN AND DEVELOPMENT OF A NEW SYSTEM

#### 3.1 BACKGROUND

##### 3.1.1 Existing blood flowmeter

In 2006, a desktop computer-based system able to perform LDF measurement was developed in Dr. Ansari's laboratory at NASA Glenn research center [3]. It is made up of, among other things:

- A 780 nm laser, featuring user-selectable output power (max 5 mW), and a high stability (wavelength variation < 0.1 nm; output power stability < 0.025 dB); this point is critical since the frequency shift is used to derive the LDF parameters.
- A *clip-probe*, where the contact between the fibers' termination and the skin is assured and both emitter and receiver fibers are separated by a core-to-core distance of 3 mm.
- An avalanche photodiode module with a photosensitive area of  $\varnothing$  3 mm and a sensitivity of  $-150 \cdot 10^6$  V/W
- Two multimode fiber optics with FC/PC terminations and a core diameter of 50  $\mu$ m.
- A PCI-bus acquisition card, dedicated to the conversion of the analog signal coming out of the photodiode to a numerical signal that the computer can process. The analog signal is sampled at a frequency of 242 kHz and converted with a resolution of 16 bits over a 2V range.
- A desktop computer for the processing of the data and the visualization of the results



Picture 2  
Clip-probe

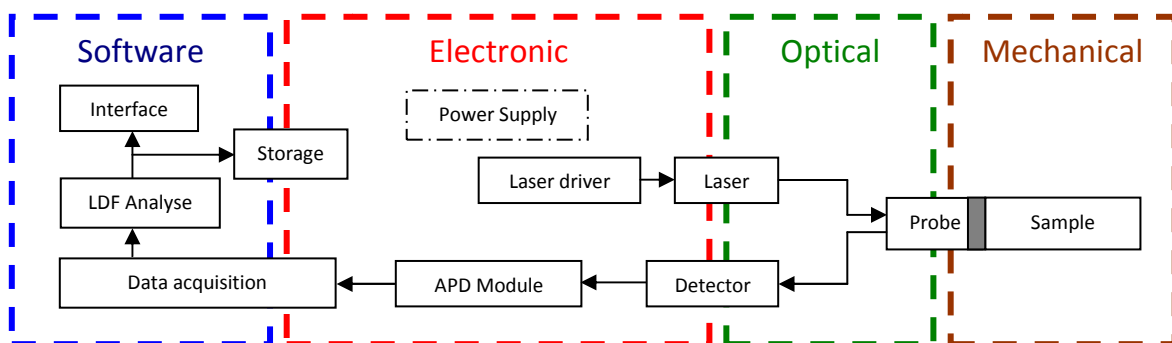
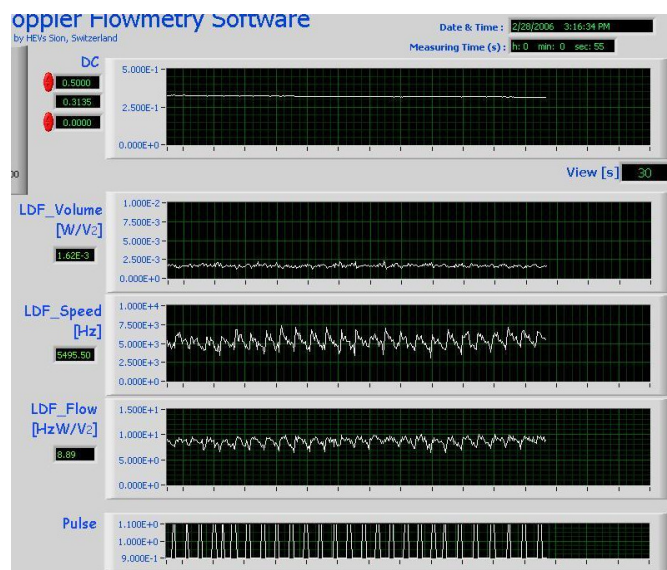


Figure 9  
Block diagram of the computer-based system

The distance between the core of the two fibers affects the number of times that a photon can be shifted: using a small separation, the light will not penetrate very deep inside of the tissue and most of it will be reflected without striking any moving cell, and without a significant loss of power, therefore the photodiode can be saturated; an excessive distance between the emitter and receiver can result in photons to be shifted multiple times, which means that the analysis will be unable to calculate meaningful results, since the LDF theory assumes that the photon is shifted once only. Good results were achieved by using a separation of 3 mm core-to-core.

In order to compute the power spectrum of the analyzed signal, a *fast Fourier transform (FFT)* routine was executed on each block of  $2^{14}$  (16'384) samples provided by the external acquisition card. Therefore, the result of each calculated parameter is updated at a rate of 14.77 Hz, which provide a good real-time displaying. The processing and displaying software has been developed with *LabView 7.0*.



**Figure 10**  
Display of the existing system, while taking a measurement on the fingertip. Voltage of photodiode, blood volume, speed and flow, as well as heart beat (external sensor) are graphically display over the time.

### 3.1.2 Available components

Some electronic components to be used in a previous system had already been purchased before the beginning of this project. The previous system did not offer the desired results, and in order to save time and money it was decided to re-use them in the new project, since in theory they met the necessary requirements. They are principally amplifiers, filters, regulators, but particularly:

- A digital signal processor from Microchip, *dsPIC33F series*, with development board and corresponding softwares
- A Bluetooth module from Sena, *Parani ESD-200*, with interface board and corresponding software

### 3.1.3 The Bluetooth technology

#### Basics

*Bluetooth* wireless technology is a short-range communication system intended to replace the cables connecting portable and/or fixed electronic devices. The key features of *Bluetooth* wireless technology are robustness, low power, and low cost. The *Bluetooth* core system consists of an RF transceiver, the baseband, and the protocol stack. The system offers services that enable the connection of devices and the exchange of a variety of data classes between these devices.

The *Bluetooth* RF (physical layer) operates in the unlicensed ISM band at 2.4GHz. The system employs a frequency hop transceiver to combat interference and fading, and provides many FHSS carriers. RF operation uses a shaped, binary frequency modulation to minimize transceiver complexity. The symbol rate is 1 Megasymbol per second (MSPS) supporting the bit rate of 1 Megabit per second (Mb/s) or, with Enhanced Data Rate, a gross air bit rate of 2 or 3Mb/s. These modes are known as *Basic Rate* and *Enhanced Data Rate* respectively.

#### Frequency bands and channel arrangement

The *Bluetooth* system operates in the 2.4 GHz ISM band. This frequency band is 2'400 – 2'483.5 MHz. The 79 RF channels are ordered from channel number 0 to 78 and are spaced of 1 MHz beginning at 2'402 GHz. The radio frequency tolerance of the transmitter is fixed at  $\pm 75$  kHz from the center frequency  $f_c$ .

In order to comply with out-of-band regulations in each country, a guard band is used at the lower and upper band edge: the lower guard band is 2 MHz and the upper is 3.5 MHz.

#### Power classes

The following table shows the power requirements for each of the 3 existing power classes for *Bluetooth*:

Power class	Max. output power $P_{max}$	Nominal output power	Min. output power* $P_{min}$	Power control	Operating range
1	100 mW (20 dBm)	(not assigned)	1 mW (0 dBm)	$P_{min}$ (< 4 dBm) to $P_{max}$ Optional: $P_{min}^{**}$ to $P_{max}$	100 meter
2	2.5 mW (4 dBm)	1 mW (0 dBm)	0.25 mW (-6 dBm)	Optional: $P_{min}^{**}$ to $P_{max}$	10 meter
3	1 mW (0 dBm)	(not assigned)	(not assigned)	Optional: $P_{min}^{**}$ to $P_{max}$	1 meter

Table 2

\* minimum output power at maximum power setting

\*\* the lower power limit  $P_{min} < -30$ dBm is suggested but is not mandatory

Power class 1 devices implement power control. The power control is used for limiting the transmitted power over +4 dBm. Power control capability under +4 dBm is optional and could be used for optimizing the power consumption and overall interference level.

On the receiver side, the actual sensitivity level is defined as the input level for which a raw bit error rate of 0.1% is met; the receiver sensitivity shall be below or equal to -70 dBm with any *Bluetooth* transmitter. Therefore, it can operate over a distance of 10 meters or 100 meters depending on the *Bluetooth* device class.

### Bluetooth baseband

The *Bluetooth* baseband is the part of the *Bluetooth* system that specifies or implements the medium access and physical layer procedures between *Bluetooth* devices. Two or more devices sharing the same physical channel form a piconet. One *Bluetooth* device acts as the master of the piconet, whereas the other device(s) act as slave(s). Up to seven slaves can be active in the piconet. Additionally, many more slaves can remain connected in a parked state, as shown in figure 11.

Data is transmitted over the air in packets. The symbol rate for all modulation schemes is 1 Msps. The gross air data rate is 1 Mbps for basic rate. Each *Bluetooth* device is allocated a unique 48-bit *Bluetooth* device address (BD\_ADDR) obtained from the IEEE registration authority. The general basic rate packet consists of 3 entities: the access code, the header, and the payload, as shown in figure 12.

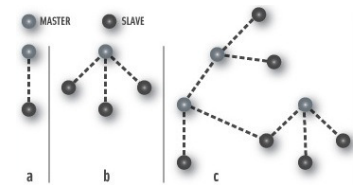


**Figure 11**  
Piconets with...  
a single slave operation (a),  
a multi-slave operation (b),  
a scatternet operation (c).



**Figure 12**  
Standard basic rate packet format

### Bluetooth wireless technology profiles

In order to use *Bluetooth* wireless technology, a device must be able to interpret certain *Bluetooth* profiles. The profiles define the possible applications. *Bluetooth* profiles are general behaviors through which *Bluetooth* enabled devices communicate with other devices. *Bluetooth* technology defines a wide range of profiles that describe many different types of use cases. By following a guidance provided in *Bluetooth* specifications, developers can create applications to work with other devices also conforming to the *Bluetooth* specification. At a minimum, each profile specification contains information on the following topics:

- Dependencies on other profiles
- Suggested user interface formats
- Specific parts of the *Bluetooth* protocol stack used by the profile. To perform its task, each profile uses particular options and parameters at each layer of the stack. This may include an outline of the required service record, if appropriate.

Among many others, one of the existing profiles is the *Serial Port Profile (SPP)*. It defines how to set up virtual serial ports and connect two Bluetooth enabled devices. A scenario would be using two devices, such as PCs or laptops, as virtual serial ports and then connecting the two devices via *Bluetooth* technology.

The SPP defines two roles, Device A and Device B. The first one is the device that takes initiative to form a connection to another device (initiator), and the second one is the one that waits for another device to make initiative to connect (acceptor).

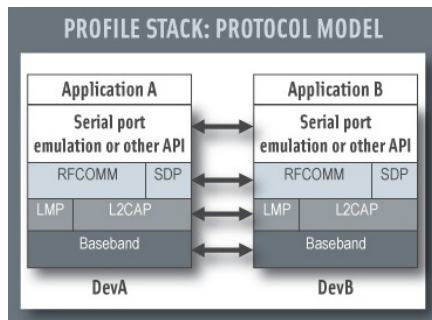


**Figure 13**  
Connection between two devices A and B with the SPP profile

In the figure 13, the baseband, LMP and L2CAP are the OSI layer 1 and 2 *Bluetooth* protocols. RFCOMM is the *Bluetooth* adaptation of GSM TS 07.10, providing a transport protocol for serial port emulation. SDP is the *Bluetooth Service Discovery Protocol*. The port emulation layer is the entity emulating the serial port, or providing an API to applications. The applications on both sides are typically legacy applications, able and wanting to communicate over a serial cable (which in this case is emulated). But legacy applications cannot know about *Bluetooth* procedures for setting up emulated serial cables, which is why they need help from some sort of *Bluetooth* aware helper application on both sides.

### 3.1.4 Preliminary measurements on the photodetected signal

An important part of this project will be focused on the development of the processing board, including the acquisition, conditioning and filtering of the photodetected signal. After the light is scattered in the tissue, it is returned to a photodiode through a fiber optic, and it is converted into an electrical signal that will be acquired and processed by the circuit board. In order to improve the signal conditioning part, and to make the good choices for the electronic components that will be used for this part, it is necessary to analyze how the signal coming out of the photodiode (future input of the circuit board) behaves.

A measurement according to the configuration of figure 14 has been taken on two subjects, with a laser source from *OZ-2000 series* of *OZ Optics* (wavelength 780 nm) and a photodiode *C5460-01* from *Hamamatsu*. The existing *clip-probe* has been used.

For each subject, the output power has been stabilized at ~18 mW first, and then at 25 mW. The details of the experiment as well as the results obtained are shown in appendix 3.

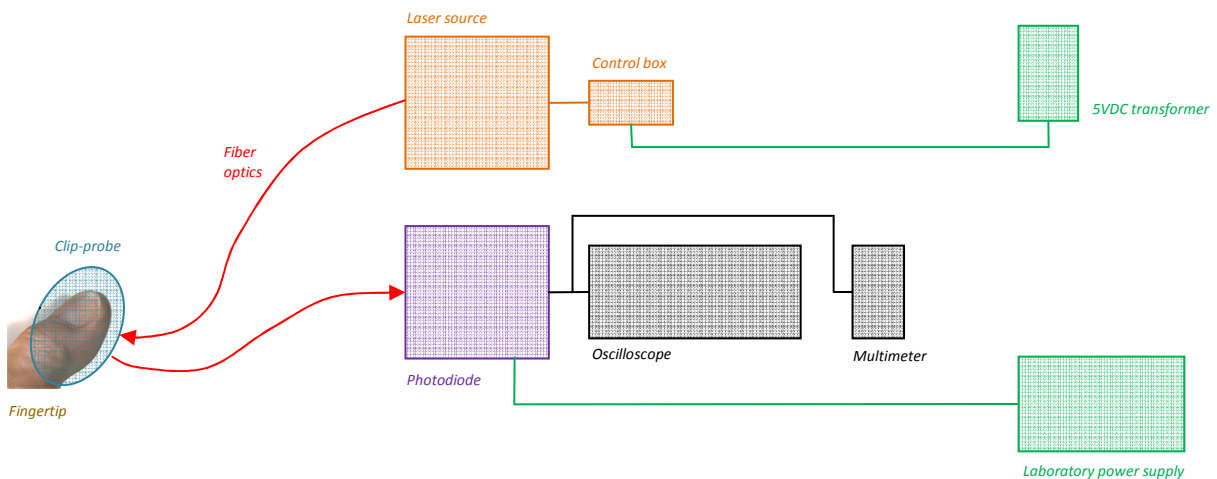


**Figure 14**  
Devices and setup used for the experiment. Refer to appendix 2 for details about the instruments and devices.



The conclusion is that the signal to be analyzed has, during the measurement and considering the worse case (highest voltage), a **static component that can go down to -2.8V**, and a **dynamic component oscillating in the range of -300..+300 mV** after adding a safety margin of 10% on each value and rounding the results. Figure 15 shows one of the oscilloscope screenshots obtained with this experiment (the others are shown in appendix 3).

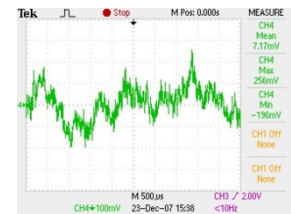


**Figure 15**  
Oscilloscope screenshot obtained with this exp.

After comparing these results and the oscilloscope screenshots with the figure 7 (part  *fingertip*) of section 2.2, a visual appreciation permits to say that the shape of the signal has the same behavior, and the static and dynamic range are perfectly comparable to the sample 5 of appendix 3. The four first samples, which have been taken at higher powers, return higher static and dynamic voltages.

The modification of a normal blood flow obtained, for example, with an occlusion or a significant temperature variation, will alter only the dynamic part of the signal (of which range decreases), and the static part will remain the same value.

### 3.1.5 Power spectrum

The LDF algorithm requires that a power spectrum is computed on the analyzed signal in order to extract the expected parameters, as shown in figure 16. It is obtained thanks to a *fast Fourier transform (FFT)* (refer to appendix 4 for a more detailed explanation of how this spectrum is obtained starting from the signal):

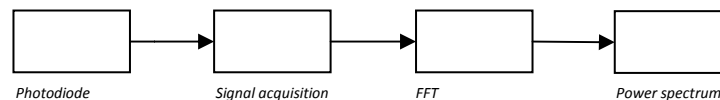


**Figure 16**  
Different steps of the signal before being computed for the FFT and power spectrum

The quality and resolution of this power spectrum depends on the quantity of samples that are processed in the same time for the FFT. As mentioned in section 3.1.1, the existing system uses blocks of 16'384 samples to perform this calculation in the computer. Since this application wants the system to be miniaturized (i.e. this calculation is going to be done by a processor for instance), and considering that the calculation power is usually lower in the miniaturized components compared to the computers, it is necessary to test if the measurement is altered or still reliable when the number of samples used for the FFT is lower.

Figure 17 shows a typical LDF spectrum. Generally, the magnitude of the power spectrum decreases as the frequency increases. The determination of the LDF parameters is based on the portion of the power spectrum included between 30Hz and 35 kHz; the range from 35 kHz to 40 kHz is used to calculate the noise. The part related to higher frequencies is not used in the LDF process and are therefore not displayed here.

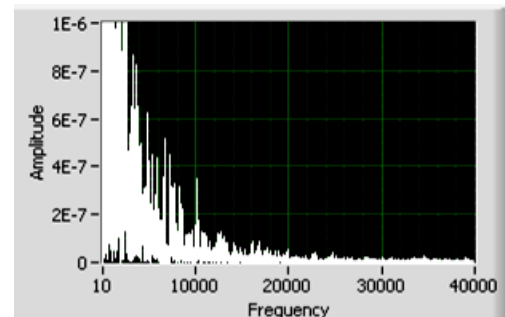


**Figure 17**  
Typical power spectrum representing the frequency shifts after light scattering in a fingertip. It has been computed by the existing system [3].



More details about the whole processing of the signal for this purpose will be given in section 3.2.4.

In changing the value of the corresponding variable of the software of the existing system [3], it is possible to visually evaluate how the measurement works when the number of samples used for the FFT decreases. The test started with the original number of samples  $2^{14}$  (16'384) and the exponent has been decreased by 1 until  $2^{10}$  (1'024). The configuration and devices used correspond to the original one, meaning that it's basically the same as on figure 14, with the only difference that the output of the photodiode is connected to the acquisition card of the computer instead of the oscilloscope and the multimeter. As shown in figure 18, the quality of the measurement is a little affected (some noise is added), but is satisfactory enough.

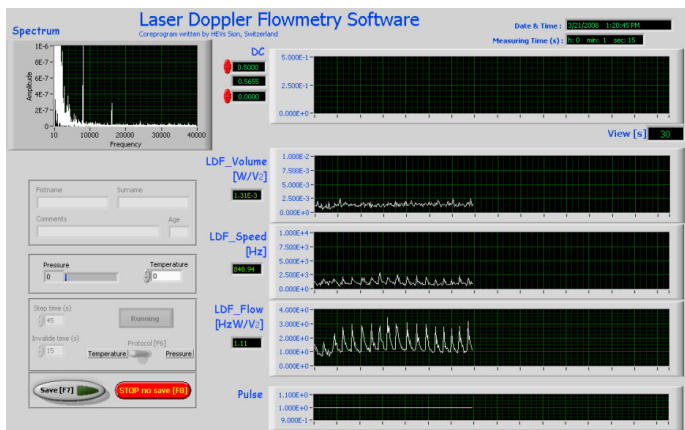


**Figure 18**

Existing system taking a blood circulation measurement with  $f_s = 242$  kHz and the FFT processed on blocks of 1'024 samples. The measurement, especially the blood flow, shows the pulsations of the body added by a little noise compared to the high resolution original FFT (done on 16'384 samples).

## 3.2 CONCEPT

Based on the theoretical principles as well as the preview background, a new concept can now be developed. Before going in deep into it, some scheme and preliminary calculations will be done in this section in order to verify if the previous approach is feasible and if it really meets the requirements. Then, some more ideas will be explored and evaluated so that a definitive principle can be decided, allowing the further detailed design to take place.

### 3.2.1 Optical configuration

#### Laser sources

According to chapters 2.2 and 2.4, two different laser sources will be used in this application. The first one, with a wavelength of 780 nm, will be shared by the two measurements (LDF and pulse-oxymetry). The second one, with a wavelength of 635 nm, is only necessary for the pulse-oxymetry. Both lasers are laboratory models (*OZ-2000 series*) from *OZ Optics* and cannot be worn or integrated in the suit. However, they offer interesting features for a first step of the development, and the use of other miniaturized, portable laser sources will be considered afterwards.

The output power can be controlled up to respectively 25 mW and 20 mW, which is enough for a measurement based on the light scattering in the finger. Their high stability (wavelength variation < 0.1 nm; output power stability < 0.025 dB) make them ideal for this application. Each output is directly fiber-coupled (single mode fiber, 5  $\mu\text{m}$  core), that is terminated by a FC/PC connector.

The operating nominal voltage is 5VDC and the control of the laser is done thanks to several digital and analog signals, as explained in section 3.2.2.

#### Miniaturized probe

The main weakness of the existing *clip-probe* is that it is definitely too big to be integrated in a glove. Another point that makes its integration difficult is that the fibers are placed perpendicularly to the finger.

The idea is to develop a configuration where the fibers could be conducted parallel to the arm, the hand, and finally the finger, before entering the probe. The latter, composed of several mirrors, could steer the light from the fiber to the skin (and vice versa) by reflecting the light at 90° as shown in figure 19. The source light and the scattered light will obviously be kept separated one from each other.

#### Photodiode

The fiber optic containing the light that has been scattered in the finger conducts this luminous signal to the photodiode, which is responsible to convert it into an electrical signal. The latter is actually an *Avalanche Photodiode (APD) Module* with an active area of  $\varnothing$  3 mm and a sensitivity of  $-150 \cdot 10^6$  V/W. It has to be powered by a very stable bipolar voltage of  $\pm 12\text{V}$  and 0V (ground). It can connect the fiber thanks to an originally FC/PC connector, but this one can be mechanically changed to an SMA connector, as it will be needed in this case.

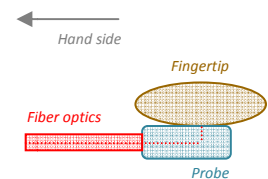


**Figure 19**  
Concept for the miniaturized probe

## Interconnections

All the above mentioned devices have to be connected each other using the optical fibers. A particularity is that only one fiber has to emit both types of light in the finger (i.e. at the input of the probe), otherwise the pulse-oxyometry measurement will not be reliable. Therefore, the light coming out from both sources have to be conducted into one single fiber; for this purpose, a combiner with SMA termination will be used. Figure 20 shows the setup of this part of the system:

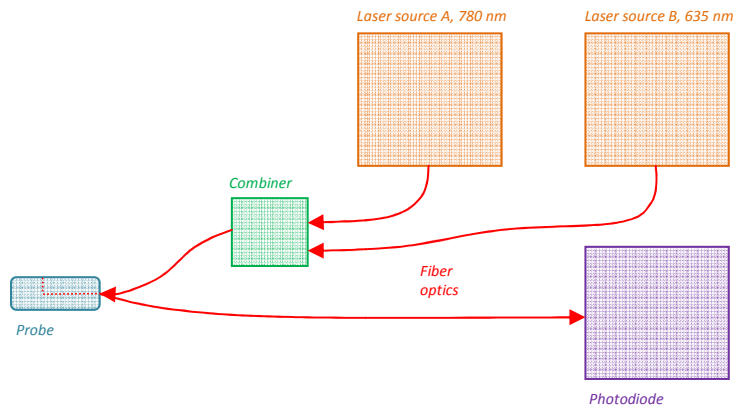


**Figure 20**

Optical connection between the laser sources, the probe and the photodiode

Apart from the fiber that is physically coupled with each laser, all the other will be multimode fibers. Good results have been achieved with 50  $\mu\text{m}$  core, but several diameters from this value up to 600  $\mu\text{m}$  will be tested here in order to find the best compromise.

### 3.2.2 Lasers control

The two lasers used in this application (*OZ-2000 series* from *OZ Optics*) possess each a 9-pin DB connector, which is used to monitor and control the laser. It can be directly connected to a *control box*, such as the one used for the experiment in section 3.1.4, or to the provided connection cable which offers, on the other side, 10 wires corresponding each to one of the connector's signals. Table 3 summarizes these connections:

Pin-nr*	Wire color	I/O	Type	Designation
1	Blue	Input	Power supply	+5V input
2	White	Input	Power supply	+5V input
2	Red	Input	Power supply	+5V input
3	Yellow	Input	Digital (0V / 5V)	Laser enable
4	Green	Output	Digital (0V / 5V)	Temperature OK
5	Orange	Input	Analog (0..5V)	Power control
6	Black	Input	Power supply	Ground
7	Brown	Input	Power supply	Ground
8	Purple	Output	Analog	LD I op (monitor)
9	Grey	Output	Analog	PD I mon (monitor)

**Table 3**

Functionalities of the input and output wires of the laser of *OZ-2000 series* from *OZ Optics*

\*Refer to the user's manual of the laser to recognize the pinout of the DB connector, or use the cables' colors

The red and black wires are not naked, but terminated by a 2.1 mm in-line power jack; this offers the possibility to supply the laser through this connector, using ideally a power supply such as the 5V transformer used in the experiment of section 3.1.4.

After being powered, the laser requires several seconds to warm up. When it is ready to operate, the digital output *Temperature OK* is tied up at 5V; it is at 0V in the opposite case.

Once the laser is ready to operate (after warming up completed), it can be enabled or disabled by applying a voltage of respectively 5V or 0V on the digital input *Laser enable*.

The light power can be modulated thanks to the analog input *Power control*. The light power increases or decreases linearly in its own range, according to the voltage applied on the analog input. However, the relation between the electrical signal and the output power is inverted. For example, the output power of the 635 nm laser (max power 20 mW) has to be controlled according to the relationship in table 4.

Applied voltage on pin 5	Light power at the output
0 V	20 mW
1 V	16 mW
2 V	12 mW
4 V	4 mW
5 V	0 mW

**Table 4**

Example to control the light power of a 20 mW laser of OZ-2000 series from OZ Optics

In this application, the laser will be powered by the external 5V transformer through its jack connector. The other alternative power wires (such as blue and brown) will be used to provide the power to the rest of the system (processing board and photodiode after voltage conversion). Each laser will be controlled by the future processing board: the latter will be able to monitor the temperature of the laser, to enable or disable it, and to module its power respectively through the signals *Temperature OK*, *Laser enable* and *Power control*.

Pins 8 and 9 are advanced features that are not used in this application.

### 3.2.3 Signal conditioning

According to chapter 2.1.3, the LDF parameters must be extracted from the photodetected signal coming out of the photodiode by calculating first:

- The FFT on a fixed number of samples, in order to compute the power spectrum  $P(f)$  of the signal
- An average of the signal's voltage  $A_{DC}$  based on the same number of samples as the FFT.

The experiment of chapter 3.1.4 is now useful to define an effective signal conditioning. Since the frequency-shift only (reflected in the dynamic part of the signal) is significant for the evolution of the blood parameters and the static part stays rather constant since it's dependent on the subject, the idea here is to perform a high-resolution acquisition on the dynamic part only. Therefore, the static component has to be filtered out before this acquisition. However, since the mean value of the signal (i.e. including the static part) has also to be acquired, two different acquisitions (a *DC-coupled acquisition* and an *AC-coupled acquisition*) will be needed as shown in figure 21.

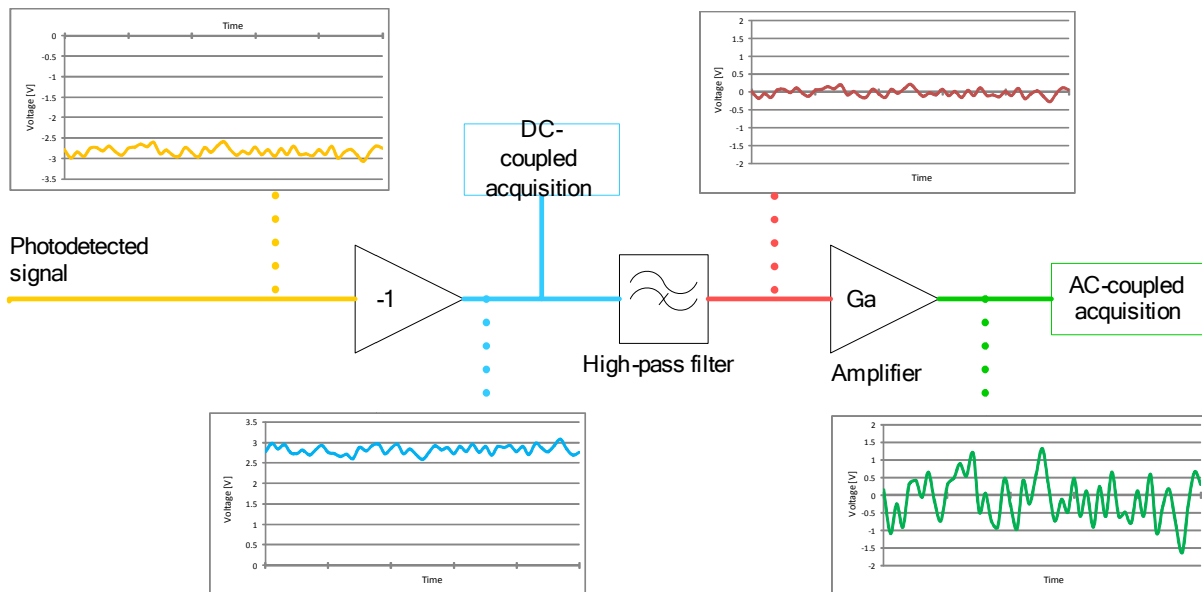


**Figure 21**

Conditioning and acquisition of the photodetected signal. It is first inverted, and the global acquisition takes place (blue). Then the static component can be filtered out thanks to a high-pass filter (red), and finally the remaining dynamic part is amplified and acquired (green).

The first inversion (yellow to blue) will be necessary depending on the components used for the signal conditioning and acquisition. The multiplication by  $G_a$  is necessary to match the dynamic signal's range to the input range of the A/D converter that will be used for the *AC-coupled acquisition*; using almost the entire input range of this converter will result in a higher accuracy of the sampled values for further processing.

The electronic components able to perform the signal conditioning will be described in section 3.3.4. Depending on the electrical configuration, some additional components will be added (anti-aliasing filters, voltage limiters, etc.).

### 3.2.4 Signal processing

#### Digital signal processor

The processing of the signal after the two acquisitions will be done within a *Digital Signal Processor (DSP)*. A *dsPIC33FJ256GP710* from Microchip is available: it's a high-performance, 16-bit digital controller with among other things, some features like:

- Modified Harvard architecture
- C compiler optimized instruction set
- Up to 85 programmable digital I/O pins
- Up to nine 16-bit timers

- Up to 2 *Inter Integrated Circuits (I<sup>2</sup>C)* modules
- Up to 2 UART modules
- UP to 2 AD converters
- 3.3 V operating voltage and low power consumption
- 30 KByte *Random Access Memory (RAM)*
- Can process up to 40 millions of instructions per second

If the latter is powerful enough to meet the requirements of this application, it will be used. The most concern is the abilities of this device to compute the data after the acquisition, especially the FFT processing that requires speed and memory.

At this stage of the design, it is difficult to predict any precise value since nothing has been developed so far. However, some estimation can be calculated and will permit deciding if this DSP can be used or not.

Microchip provides a routine<sup>1</sup> to perform FFTs in devices from *dsPIC30F* series; since the *dsPIC33F* belongs to a similar family of devices, it should be possible to adapt this routine for it. Among other things, this routine offers the possibility to store the FFT results in the same location as the input of the FFT. For instance, if the FFT is computed on 512 samples (i.e. 512 memory locations), another similar 512 memory locations are not needed to write the results: it can overwrite the input data. This offers an advantage in order to save memory in the DSP. With this routine, each computed value (either at the input or at the output) has to be represented in a numerical 16-bit variable. Therefore, the absolute maximal number of values that this DSP is able to compute with this FFT routine is, according to the memory size:

$$\text{Max FFT block length} = \frac{\text{DSP RAM size}}{\text{FFT variables size}} = \frac{30 \text{ KByte}}{16 \text{ bit}} = \frac{30 \cdot 1024 \cdot 8 \text{ bit}}{16 \text{ bit}} = 15'360$$

Obviously, the computation of the FFT is not the only part of the processing that requires memory, so that a well considered margin has to be taken into account in order to define what the max. *FFT block length* can be.

This result shows, first of all, that this DSP is not able to reach the same calculation power as the existing system [3] which performs the FFT on 16'384 samples. However, the results achieved after the tests of section 3.1.5 show that performing an FFT on block lengths down to 1'024 can provide good results, and this is clearly in the capabilities of this DSP. Therefore, the memory requirements are satisfactory enough for its use in this application.

The second concern is about the time that the DSP takes to compute the FFT. The principle is easy to understand: the FFT and following calculation (such as LDF processing) are done on a fixed number of samples (*block length*); **the whole process has to be computed in less time than the sampling of this quantity of samples requires**. For instance, the existing system [3] works with a *block length* of 16'384 samples and a sampling frequency of 242 kHz. Therefore, it takes

$$\frac{16'384}{242 \text{ kHz}} = 67.7 \text{ ms}$$

to sample the whole block of data. Then the FFT and LDF processing are computed on this block, and during this time the sampling of the signal keeps running. That's why both FFT and LDF processes have to be

<sup>1</sup> Available from Microchip website ([www.microchip.com](http://www.microchip.com)), section *dsPIC30F code examples*, folder *CE018*

completed in less than 67.7 milliseconds, so that when the new block is available, the last calculation has been completed and the new block can be computed at its turn.

Even though the processing speed of this DSP is known, it is difficult, to predict how long the computation of a whole block will require. The only way to find this out is to develop the algorithm and to perform some measurements on the device. That will be done in the further development.

### LDF algorithm

Based on the theory of *Laser Doppler Flowmetry* and the existing system [3], the LDF algorithm reported in appendix 5, representing the calculation and process that has to be done by the DSP in order to return the expected results, has been designed. In this application (LDF measurement on a fingertip), the limits of the integrals reported in section 2.1.3 have been redefined, and a reduction of the noise has been taken into account. This algorithm follows the signal conditioning and it takes the *DC-coupled acquisition* and the *AC-coupled acquisition* as inputs. The outputs will be, as expected, the LDF parameters such as *blood volume*, *blood speed*, and *blood flow*.

### Pulse-oxymetry algorithm

As described in section 2.3, the pulse-oxymetry measurement is based on the calculation of a ratio between two average values; it doesn't require any special features like an FFT for instance. Therefore, this DSP will be able to process this algorithm, as long as the lasers can be controlled. The global acquisition only will be needed to sample the signal, since this measurement is not based on the analysis of the dynamic part of the signal.

## 3.2.5 Wireless transmission

The wireless transmission between the embedded system and the remote control laptop will be using the *Bluetooth* technology. On one side, the laptop just requires having the Bluetooth integrated (or an external module as an alternative); this part is discussed in section 3.2.6. On the remote device side, the available *Parani ESD-200* module can be used: it's a module device for wireless serial communication using *Bluetooth* technology. This module communicates with other *Bluetooth* devices that support the *Serial Port Profile* (such as a laptop).

Table 5 summarizes the features of the *Parani ESD-200* module:

<b>Interface</b>	Serial interface
<b>Serial speed</b>	1'200 bps to 230'400 bps
<b>Bluetooth version</b>	1.2
<b>Bluetooth profile</b>	serial port profile (SPP)
<b>Power class</b>	2
<b>Power level</b>	Max. 4 dBm
<b>Nominal working distance</b>	30 m
<b>Supply current</b>	Min. 150 mA

**Table 5**  
Main features of the *Parani ESD-200*



All these features make the *Parani ESD-200* ideal for this application: its serial interface is totally compatible with the *UART* port of the *dsPIC33F*, and on the side of the laptop, the *SPP* protocol is appropriate to interface any application with the serial port related to this *Bluetooth* connection. Moreover, it introduces a delay no bigger than 30 ms in the transmission, which makes it appropriate for this kind of real-time monitoring. However, it is necessary to make sure that this kind of wireless transmission offers a baudrate that is high enough to transmit all the data without any interruption.

As a first approximation will be considered the transmission of the results of the LDF measurements from the embedded system to the laptop. In order to improve this part of the process, it has been decided that only the *blood volume* and the *blood speed* would be transmitted; the *blood flow*, which is just a multiplication of the two other values, can be computed by the control application itself. Moreover, each group of results corresponds to a temporal value which indicates when the result has been acquired and processed; this value has to be transmitted as well. The  $A_{DC}$  value will be transmitted from the embedded device to the laptop too, since it is a very useful indication in order to verify that the measurement is behaving properly (it is now known that this value should neither exceed a certain voltage, nor oscillate more than hundreds of millivolts, therefore a different behavior can be a sign to alert that something is wrong). Finally, even if the values to transmit are not clearly organized in a frame yet, a place has to be reserved for a special symbol indicating the beginning of the frame and its content. Therefore, the symbols or values to transmit each time that an LDF result is available are:

- Start of frame
- Time stamp
- ADC value
- Blood volume
- Blood speed

It has been decided that the representation of these values will be done accordingly to the *IEEE 754* standard, *single-point* precision. The IEEE standard for binary floating-point arithmetic (IEEE 754) is the most widely-used standard for floating-point computation, and is followed by many CPU (central processing unit) and FPU (floating point unit) implementations; please refer to appendix 6 for further description. As an exception, the time stamp will be coded on 32 bits too, as a standard integer value.

Finally, the frequency at which a "LDF results packet" containing the above symbols or values is transmitted depends on the speed of the LDF algorithm, which depends itself particularly on the length of the data block to compute. According to the previous section, the bigger is the block, or the smaller is the sampling frequency, the higher is the interval of time between two groups of LDF results available, i.e. the smaller is the frequency at which they will be transmitted.

Considering an unfavorable case where the block length is of 1'024 samples, and the sampling frequency is 100 kHz, the time interval between two transmission set becomes 10.24 ms, i.e. 97.65 Hz. Therefore, the required baudrate for the wireless transmission can be calculated based on the five values, each made of 32 bits:

$$97.65 \text{ Hz} \cdot 5 \cdot 32 \text{ bit} = 15'624 \text{ bit/s}$$

According to the maximal baudrate that the *Parani ESD-200* offers, the above required baudrate is fully achievable. However, it has to be taken into account that other frames will be transmitted along with the LDF frame that has been used for this approximation. They are, for instance, the results of the pulse-oxymeter (if both measurements are running in the same time), in addition to some frames that will be



responsible to maintain the connection status, or some commands or status will be sent respectively from or to the laptop. These additional frames will not need the baudrate to increase significantly since they will be either not very frequent or smaller than the LDF frame, that's why the development will start with a baudrate that has been arbitrarily fixed at 57'600 bit/s. The baudrate that the total amount of data require will be calculated during the detailed design and the value of 57'600 bit/s will be increased afterwards if needed.

### 3.2.6 Control and monitoring of measurements

The last part to consider is the displaying of the results and the control of the embedded system from a remote location. It had been chosen to use a laptop for this purpose, and the previous section confirmed that the *Bluetooth* module offers a perfect compatibility with any laptop, desktop or handheld device since it works with the SPP interface.

When the *Parani ESD-200* and a laptop equipped with a *Bluetooth* interface are connected, the computer's *Bluetooth* management system (peculiar to the manufacturer) allocates a serial COM port to this connection. Any application can use this COM port, such as *hyper terminal*, to communicate with the *Parani ESD-200*. However, the port's configuration has to be the same on both laptop and *Parani ESD-200*.

For a developer, the access to this COM port can be totally integrated in the application: no other software is required to run the connection with the *Parani ESD-200* (i.e. the connected DSP). For this work, it has been chosen to develop the control application in the *VisualBasic.NET* language. In order to improve the displaying of the results, an additional development tool (*Measurement Studio, National Instruments*) will be used, offering the possibility to potentiate the graphical capability of the *VisualBasic.NET* application.

### 3.3 DEVELOPMENT AND DETAILED DESIGN

The approach described in the section 1.3, the theory of the measurements in the chapter 2, and the background of the section 3.1 are the basis to develop a new system starting from the concept explained in the previous section. The latter confirms, by its calculations and approximations, that such a concept is feasible. Therefore, the system has been developed based on this principle; many details have been considered, several tests on subsystems have been performed in order to evaluate the strengths and weaknesses of every option. The solutions providing the best compromises have finally been chosen and the resulting system has been created. Among other things, the design of the miniaturized probe and the processing board required a particular attention. Therefore, this circuit board has been developed by manufacturing two versions of it (prototype boards 1 and 2): the first prototype was meant to be an intermediate step to the final version and it was equipped with LEDs and test points to assess the correct functionalities in an easier way. The second prototype that is described in this section is the miniaturized version of the first prototype but without the unnecessary test components.

#### 3.3.1 Set-up of the system

This section provides an overview of the entire system. The details of each part are explained in the following sections. Figure 22 shows the set-up of the system; table 6 enumerates the corresponding components.

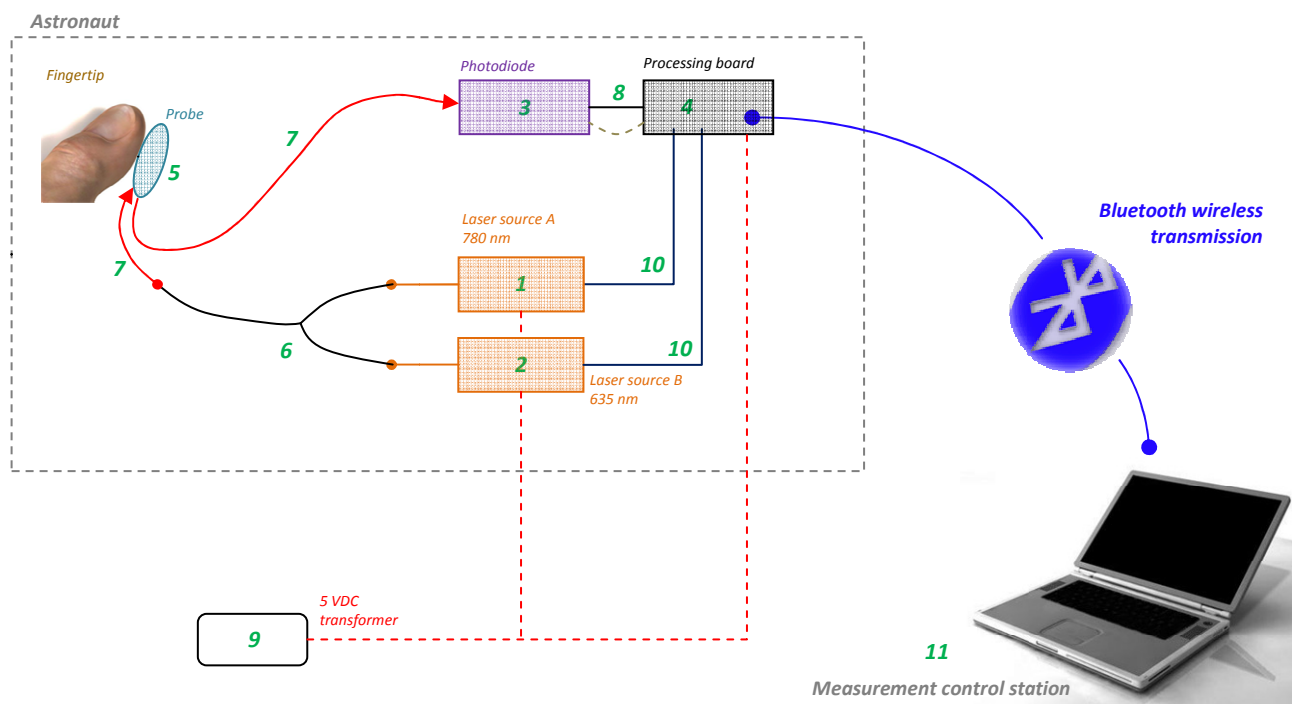


**Figure 22**  
Final set-up of the system.

Landmark	Device	Section-nr.
1	Laser source A, 780 nm	3.3.3
2	Laser source B, 635 nm	3.3.3
3	Photodiode	3.3.3
4	Processing board	3.3.4
5	Miniaturized probe	3.3.2
6	Fibers combiner	3.3.3
7	Fiber optics	3.3.2
8	BNC cable	3.3.3/4
9	5 VDC transformer	3.3.4
10	Connection cable	3.3.4
11	Laptop	3.3.7

Table 6

Caption of the figure 22.

So far, the system is not battery-powered, but one single transformer (9) is used to provide a 5VDC voltage to the two lasers and to the processing board. The photodiode (3), which requires a bipolar voltage of  $\pm 12V$  and the ground, is supplied by the processing board which generates these voltages. The laptop (11) is powered by its own transformer or its battery.

The processing board (4) controls the two lasers (1, 2) (according to 3.2.2); it is able to monitor the temperature of the lasers, to turn them on/off, and to control their output power.

The fibers originally coupled with the laser sources are combined together using a fiber combiner (6), which is itself connected to the input fiber (7) of the probe.

The probe is in contact with the skin on the fingertip, shoots the light coming from the lasers into it and collects the scattered light, that is directed to the output fiber (7) (similar to the input fiber). The latter is directly connected to the photodiode (3).

The photodiode converts the received light into an electrical signal and transmits it to the processing board (4) through a BNC cable (8).

Finally, this circuit board (4) processes the data and transmits them to the laptop (11) which is responsible to display the results. It is also able to control the measurement by sending commands to the processing board.

### 3.3.2 Miniaturized probe

The design of the probe has been based on the considerations of section 3.2.1, i.e. it has to fit in the glove while, as much as possible, not to alter the mobility of the hand. The main requirements of the probe are:

- the probe has to be as tiny as possible
- It has to be fiber-coupled
- the fibers will be placed parallel to the hand until it reaches the probe, but the light has to penetrate and exit the skin perpendicularly

Following from that, the fibers have to be well considered so that they offer enough pliability to fit in the glove.

As a first prototype of this probe, the solution that has been carried out is an assembly of two prisms and one mechanical part as shown in figure 24. The visible part of the fibers (red) is made of the core of the fiber, the cladding, and the external protection; the outer diameter at this location is 830  $\mu\text{m}$ .

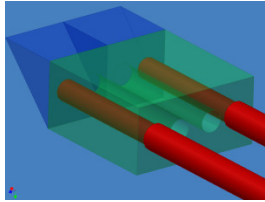


**Figure 24**  
Cross-sectional view of the mechanical parts of the probe

The mechanical precision part (grey) is made of aluminium and is responsible to maintain the fibers aligned so that the light can penetrate the prisms (blue) perpendicularly, as shown in figure 23. Inside of this piece, just the core and the cladding of the fiber remain (totalizing  $\varnothing$  635  $\mu\text{m}$ ): the mechanical part protects it from external damages. 4 holes of  $\varnothing$  650  $\mu\text{m}$  each allow the fiber to fit in it only without the external jacket. Even though two holes would have been enough for this application (only two fibers – emitter and receiver – are needed), having 4 of them allows to test different configurations as a matter of distance between the core of the two fibers.

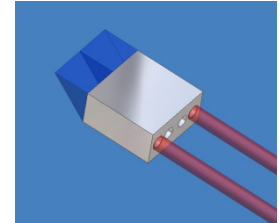


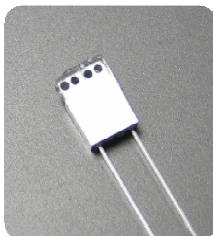
**Figure 23**  
3D-conception of the optical probe

In order to achieve a good contact between the output of the fiber and the prism, the jacket has been properly stripped and the extremity of the fibers have been successively polished with sheets of 5, 3, 1 and 0.3  $\mu\text{m}$  abrasive grain, and eventually verified with a microscope.

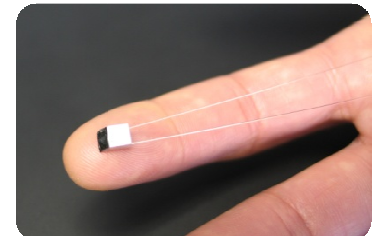
Once the light gets out of the fiber, it is reflected at right angle by the prism. The finger is placed on the upper flat-part of the sensor, the fibers going along the arm. The light is scattered in the finger and collected symmetrically through the second fiber.

The three components are glued all together from the outer surfaces, where the probe is not in contact with the skin. On the other side, each fiber is terminated with a standard SMA connector.

Each prism is 2 mm side big, and the mechanical holder is 4 x 2 x 4 mm, therefore the probe's clutter is no bigger than 4 mm width, 6 mm long and 2 mm high. Pictures 3 and 4 respectively show the probe assembled, and on a finger.



**Picture 3**  
Probe after assembly



**Picture 4**  
Probe positioned on the fingertip

Thanks to the 650  $\mu\text{m}$  diameter holes, this prototype probe can be tested with different fibers of which external diameter (core + cladding) is up to 635-640  $\mu\text{m}$ . Fibers with different apertures will be tested as well. Appendix 7 contains the technical references of the components used for this assembly, and appendix 8 is the mechanical drawing for the manufacturing of the metallic holder.

### 3.3.3 Optical set-up

The optical part of the system is made of the following components:

- one 780 nm laser from *OZ-2000 series*, variable output power (max. 25 mW) (Laser A)
- one 635 nm laser from *OZ-2000 series*, variable output power (max. 20 mW) (Laser B)
- two connection cables (one for each laser)
- two FC/PC – SMA adapters
- one fiber combiner
- one probe fitted with two fiber optics (emitter and receiver) according to section 3.3.2
- one photodiode

Figure 25 shows in detail how these components are connected together:

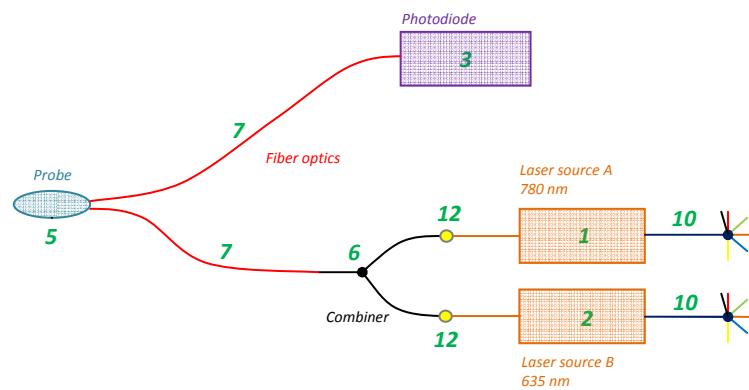
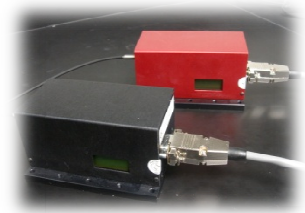


Figure 25  
Optical set-up of the system

The lasers (1, 2) provide a high stability (wavelength variation < 0.1 nm; output power stability < 0.025 dB) which is ideal for this application. They are powered by an external 5VDC voltage provided through the connection cables (10) (red and black wires). For each laser, three other wires (yellow, green, orange) which respectively correspond to the *laser enable*, *temperature ok* and *power control* signals, are connected to the processing board that is responsible to control them (see picture 5).



Picture 5  
Lasers A and B

Both lasers are fiber pigtailed (single mode fiber, 5  $\mu\text{m}$  core), and are terminated by a FC/PC connector. Therefore, two FC/PC-SMA adapters (12) are required to connect them with the combiner (6). The latter is made of multimode fibers with a 400  $\mu\text{m}$  diameter core. On the other side, the combiner is connected to the input fiber (7) of the probe (SMA to SMA). The output fiber of the probe is connected to the photodiode (3) with SMA connection as well. The photodiode is powered from the processing board.

Table 7 below gives more technical information about the lasers and the photodiode, and the appendix 7 contains the technical references of these optical components.

Landmark	Device	Brand and model	Features	
1	Laser A	OZ Optics, OZ-2000-780-5/125-S-40-3S-3A-1-25	Wavelength	780 nm
			Max. output power	25 mW
			Coupled fiber	SM, 5 μm core
			Operating voltage	5 VDC
			Max. operating current	2.5 A
2	Laser B	OZ Optics, OZ-2000-635-4/125-S-40-3S-3A-1-20	Wavelength	635 nm
			Max. output power	20 mW
			Coupled fiber	SM, 5 μm core
			Supply voltage	5 VDC
			Max. operating current	2.5 A
3	Photodiode	Hamamatsu, C5460-01	Active area	∅ 3.0 mm
			Photo sensitivity	-1.5 · 10 <sup>8</sup> V/W
			Frequency bandwidth	DC to 100 kHz
			Operating voltages	±12V, 0V
			Current dissipation (max)	+45 mA; -16 mA

**Table 7**  
 Technical features of the lasers and the photodiode

### 3.3.4 Processing board

This circuit board (4) is not only one of the main parts of the system, but also a significant improvement in terms of miniaturization: it is able to control every other main component such as the lasers, the probe and the photodiode, to coordinate their operations, and to perform the measurement in a way comparable to the computer-based system [3]. Its main features are the conditioning of the signal through several electronic components, the data processing in a DSP, and the transmission of the results to the remote laptop via *Bluetooth*.

The following describes how the *prototype board 2* is made (last version at this date).

#### Board inputs and outputs

According to the general set-up of the system presented in section 3.3.1 and the details about the lasers' control, the circuit board can first be considered as a "black-box" with the following inputs and outputs (described in tables 8a and 8b):

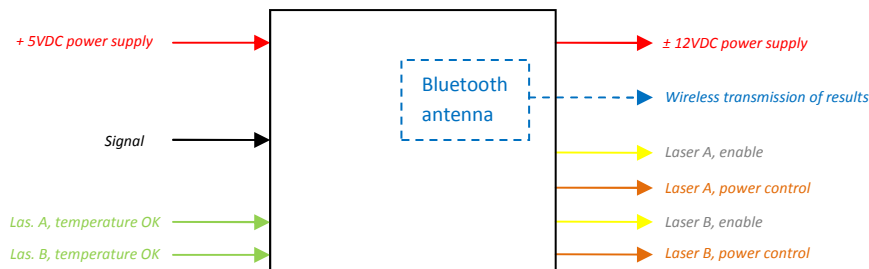


**Figure 26**  
 Inputs and outputs of the processing board

Inputs		
Name	Type	From
5 VDC power supply	Power	Transformer
Signal	Analog	Photodiode
Laser A, temp. OK	Digital 5V	Laser A
Laser B, temp. OK	Digital 5V	Laser B

Outputs		
Name	Type	To
±12 VDC power supp.	Power	Photodiode
Wireless transm.	Radio	Laptop
Laser A, enable	Digital 5V	Laser A
Laser A, power ctrl.	Analog 0.. 5V	Laser A
Laser B, enable	Digital 5V	Laser B
Laser B, power ctrl.	Analog 0.. 5V	Laser B

Tables 8a and 8b

Description of inputs and outputs of the circuit board

Signal conditioning

The conditioning of the signal prepares it for the sampling. It has to be done in a way that optimizes the acquisition of the interesting data, while respecting the feasibility rules that the electronic components impose. In this case, the scheme presented in section 3.2.3 is applied to the input signal: it particularly optimizes the acquisition of the signal's dynamic variations.

According to the LDF algorithm of section 3.2.4, only the frequencies up to 40 kHz are interesting for this measurement. Therefore, according to the *Shannon's theorem* which mentions that the sampling frequency of a signal has to be at least the double of the maximal frequency that the signal contains, the sampling frequency of this system has to be chosen 80kHz or higher. For this work, the arbitrary sampling frequency of 100 kHz has been chosen; it satisfies this condition imposed by *Shannon's theorem*.

For the same reason, since the behavior of the photodetected signal is unpredictable and can contain frequencies higher than the theoretical limit of 50 kHz (for a sampling at 100 kHz), an anti-aliasing filter has to be placed in the processing chain, before any A/D conversion.

The block-diagram of the signal processing finally becomes:

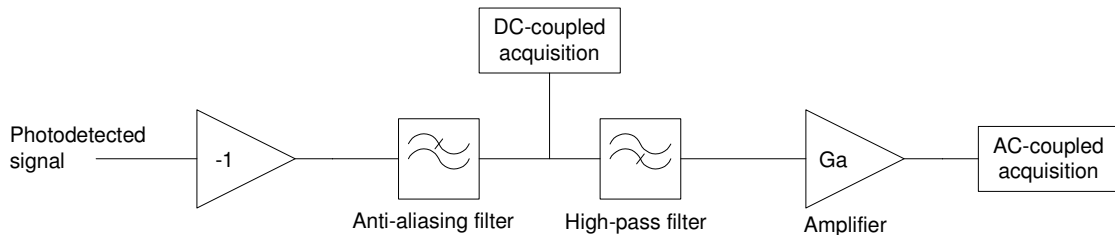
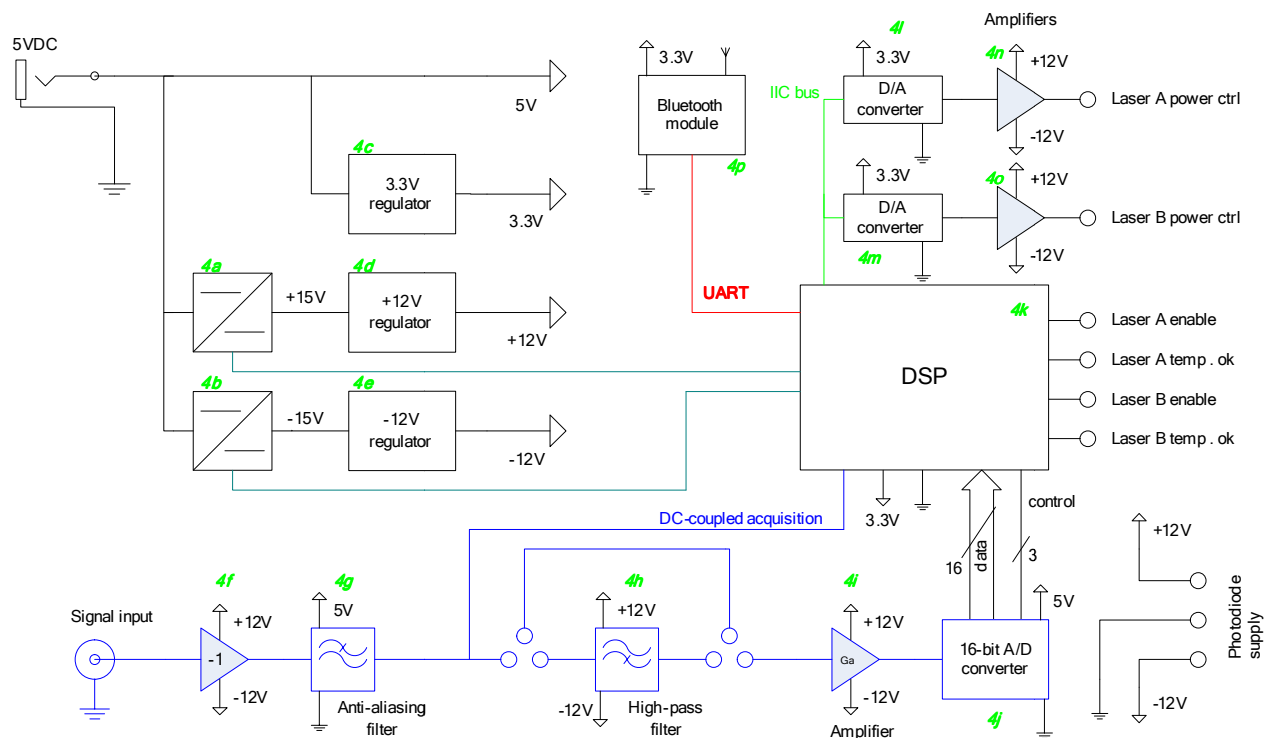


Figure 27

Block-diagram of the signal processing

Hardware architecture of the board

Apart from the signal conditioning part described above, the circuit board also includes the DSP that is responsible to perform the calculation on the acquired signal, a wireless transmission part, a lasers control part, and a power management part. Figure 28 shows how they are interfaced together:



**Figure 28**  
Hardware architecture of the circuit board

The board is powered by a single 5VDC source. This voltage (provided by the external transformer) is used without any modification for supplying the 5V-components, and is regulated down to 3.3V for some others. The 5VDC is also converted to +15V and -15V first (DC/DC converters), and then regulated down to respectively +12V and -12V for a use by bipolar components such as the amplifiers or the photodiode. These converters can be enabled/disabled by the DSP through a digital signal.

The photodetected signal is connected to the board through a BNC cable, and its processing corresponds to what has been discussed earlier in this section. The *DC-coupled acquisition* is done by the DSP itself, which is fitted with several internal A/D converters (12 bits resolution over 3.3V in this case), and the *AC-coupled acquisition* is done by an external A/D converter with a 16 bits resolution over a range of -10..+10V. It is controlled by the DSP by means of three digital signals, and the data are transmitted on a 16-bit parallel bus. For some reasons related to the prototyping, the high-pass filter can be bypassed.

The DSP can monitor and control the lasers through the three known signals *Laser enable*, *Temperature OK* and *Power control*. The two firsts are managed with two digital outputs and two digital inputs. In order to generate the analog signal related to the power control, for each laser, one external D/A converter followed by an amplifier are used. The presence of the amplifier is justified since the D/A converters offer an output voltage in the range 0..3.3V only. They are connected to the DSP through an *Inter Integrated Circuits (I<sup>2</sup>C)* bus.

Finally, the Bluetooth module communicates with the DSP through the UART port. It consists of four digital signals, two used to transmit or receive the data (*Tx*, *Rx*), and two for the *hardware flow control* of this transmission (*RTS*, *CTS*).



One last feature that is not related to the operation of the system is not shown in this scheme: the DSP can be programmed from a computer through an interface called *MPLAB ICD2* that connects the DSP through a 5-pin connector. Since this is a prototype (i.e. the algorithm and process have to be developed and can change very often), it is necessary to have the possibility to modify the algorithm contained in the DSP.

### Electrical design

This section explains in details which models of electronic components are used, what their features are, and how they are connected and used. The corresponding electrical scheme is attached in appendix 9.

#### DC/DC converters (4a, 4b)

*📄 scheme landmark: U2, U3*

Two DC/DC converters are used to generate voltages of +15V and -15V. The purpose is, afterwards, to regulate them respectively to +12V and -12V for use by the concerned components.

In this system, two *MAX629* from *Maxim* are used. They are low power DC/DC converters with internal N-channel *mosfet* switch and programmable current limiting. They can generate a voltage up (down) to +28V (-28V) with a current of 500 mA, and the switching frequency can go up to 300 kHz.

Figure 29 shows a typical connection for a positive output voltage:

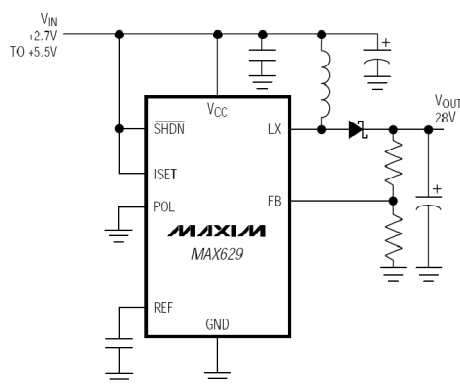


**Figure 29**

Typical connection of MAX629 for a positive output voltage

- $V_{cc}$  is the power supply input that provides energy to the component (not related to the conversion). In this system, it is powered at 3.3V
- *SHDN* (active low) is a digital signal that is used to turn on/off the converter. It is connected to the DSP.
- *ISET* is the input that sets the current limit. In order to have a 500 mA current limit like in this application, it has to be connected to  $V_{cc}$ .
- *POL*, the polarity input, has to be grounded for a positive output voltage, or connected to  $V_{cc}$  for a negative output voltage.
- *REF* is a reference output that is bypassed with a 0.1  $\mu\text{F}$  capacitor.
- *GND* is related to the power supply and is simply grounded
- *FB* is a feedback input for setting the output voltage. It is connected to an external voltage divider made of two resistors that, depending on their values, set the output voltage.
- *LX* is the internal N-channel DMOS switch drain.

Contrary to this typical connection, the power supply input  $V_{cc}$  and the "conversion input voltage" applied to the top of the coil are not the same: the conversion here starts from 5V. Since separate supplies are used for these two inputs, the noise injection onto  $V_{cc}$  is reduced by isolating it from the switching transients.

<b>Manufacturer</b>	Maxim
<b>Model</b>	MAX629ESA+
<b>Package</b>	8-pin SO
<b>Input voltage before conversion (in this system)</b>	5V
<b>Output voltage after conversion (in this system)</b>	+15V (4a); -15V (4b)
<b>Supply voltage (for integrated circuit functioning) (in this system)</b>	3.3V
<b>Max. current absorption ( for integrated circuit functioning)</b>	120 $\mu$ A
<b>Required quantity</b>	2

Table 9  
Specifications of MAX629

The resistors dividers made of  $R_2$  and  $R_3$  for the positive output voltage and  $R_4$  and  $R_5$  for the negative output voltage must be calculated as follows:

$$R_2 = R_3 \cdot \left( \frac{V_{out}}{V_{ref}} - 1 \right) \qquad R_4 = R_5 \cdot \frac{|V_{out}|}{V_{ref}}$$

Where  $V_{ref} = 1.25$  V.

With  $R_2 = 220$  k $\Omega$  and  $R_3 = 20$  k $\Omega$ ,  $V_{out} = 15$  V (positive output voltage), and with  $R_4 = 240$  k $\Omega$ ,  $R_5 = 20$  k $\Omega$ ,  $V_{out} = -15$  V (negative output voltage).

These output voltages are both satisfactory to be regulated respectively to +12V and -12V afterwards.

### 3.3V regulator (4c)

 scheme landmark: U1

A low-dropout linear regulator is responsible to generate the 3.3V voltage starting from the original VDC. For this purpose, a LM1117-3.3 of National Semiconductors has been chosen. It offers current limiting and thermal shutdown. Its circuit includes a Zener trimmed bandgap reference to assure output voltage accuracy to be within  $\pm 1\%$ . This component doesn't require any external adjustment to set the targeted voltage: it is designed so that its output is fixed at 3.3V. Only two external tantalum capacitors are needed to achieve a very stable voltage, as shown in figure 30.

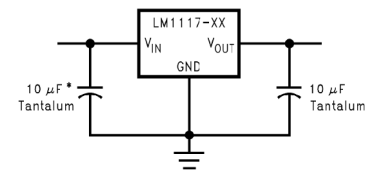


Figure 30  
Typical application of a LM1117 as a fixed output regulator

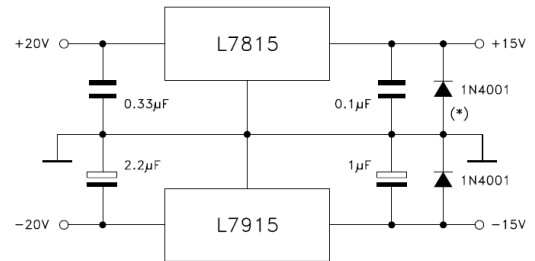
<b>Manufacturer</b>	National Semiconductors
<b>Model</b>	LM1117I-3.3
<b>Package</b>	SOT-223
<b>Input voltage (in this system)</b>	5V
<b>Output voltage (in this system)</b>	3.3V
<b>Max. output current</b>	800 mA
<b>Quiescent current</b>	10 mA
<b>Required quantity</b>	1

Table 10  
Specifications of LM1117-3.3

±12V regulators (4d, 4e)

*📄 scheme landmark: U4, U5*

The +12V and -12V voltages are generated from the +15V and -15V outputs from the DC/DC converters (respectively 4a, 4b). For this purpose, two different regulators are used. They are both from the manufacturer ST. Like the previous one, they are three-terminal regulators with fixed output voltage. Each type employs internal current limiting, thermal shut-down and safe area protection, making them essentially indestructible. Figure 31 shows a typical assembly of both components together, generating a bipolar output voltage.



**Figure 31** Split power supply similar to the assembly used in this application. The two diodes are against potential latch-up problems.

	L7812C	L7912C
Manufacturer	ST	ST
Model	L7812CD2T-TR	L7912CD2T-TR
Package	D <sup>2</sup> pack	D <sup>2</sup> pack
Input voltage (in this system)	+15V	-15V
Output voltage (in this system)	+12V	-12V
Max. output current	> 1A	> 1A
Quiescent current	8 mA	3 mA
Required quantity	1	1

**Table 11**  
Specifications of L7812C and L7912C

Instrumentation amplifier (4f)

*📄 scheme landmark: U7*

The photodetected signal is first inverted by this part of the signal processing. It always has a negative voltage (that can go down to -12V since this is the extreme negative voltage that the photodiode can provide). In order to minimize the noise introduced in the signal processing, an instrumentation amplifier has been chosen for inverting the photodetected signal. The precision, low-power instrumentation amplifiers INA129 of Texas Instruments offers a very low offset voltage (50 µV), drift (0.5 µV/°C), and high common-mode rejection (120 dB at G ≥ 100). Figure 32 shows the internal circuitry of this component.

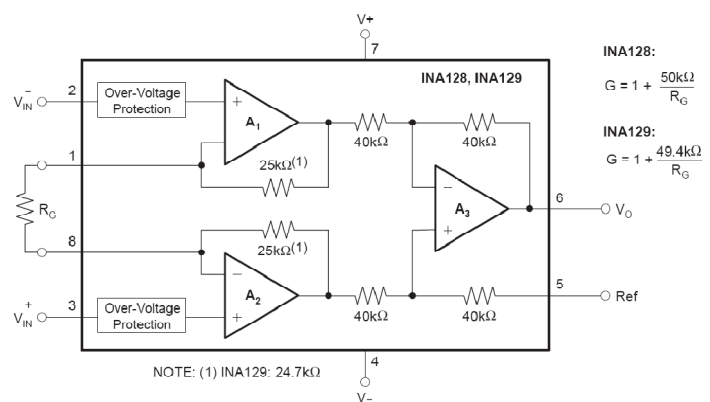


**Figure 32** Internal circuitry of INA129 and calculation of the gain based on the value of R<sub>G</sub>

Since the photodetected signal just has to be inverted (gain  $G = 1$ ), no resistor will be connected between pins 1 and 8, so that  $R_g = \infty$  and therefore  $G = 1$ . However, in order to invert the polarity of the signal, the latter has to be connected on the negative input pin 2 ( $V_{in^-}$ ), and its reference to the positive input pin 3 ( $V_{in^+}$ ). The instrumentation amplifier will be supplied by  $\pm 12V$  applied on pins 7 and 4. Finally, the pin 6 ( $V_o$ ) delivers the signal for further processing, and pin 5 ( $Ref$ ) is the 0V reference.

<b>Manufacturer</b>	Texas Instruments
<b>Model</b>	INA129U
<b>Package</b>	8-pin SO
<b>Power supply (in this system)</b>	$\pm 12V$
<b>Current absorption</b>	$\pm 700 \mu A$
<b>Required quantity</b>	1

Table 12  
Specifications of INA129

### Anti-aliasing filter (4g)

 scheme landmark: U8

This component is an anti-aliasing filter which aim is to assure that no frequencies higher than 50 kHz are forwarded to the further circuit (acquisitions at 100 kHz). For this purpose, an 8<sup>th</sup>-order switched capacitor, Butterworth lowpass filter *MAX295* of *Maxim* has been chosen. With this component, the design task is limited to the choice of an external capacitor related to the cutoff frequency, which can be set up to 50 kHz. A reason for having chosen a Butterworth filter is that it provides the maximally flat passband response, which is ideal for this application since it requires minimum deviation from the DC gain. Figure 33 shows the ideal connection of the *MAX295* for this application.

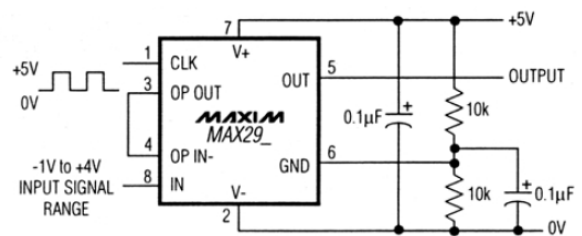


Figure 33  
Mounting of the MAX29x for 5V single-supply operation

Considering that the frequencies higher than 50 kHz have to be cut out according to *Shannon's theorem*, and that the useful portion of the signal is contained up to 40 kHz, a good compromise is to fix the cutoff frequency  $f_c$  at 45 kHz. The set up of the cutoff frequency is done by driving the *CLK* pin by an external capacitor; depending on the size of the capacitor, the internal clock frequency  $f_{clk}$  changes, and the cutoff frequency of the filter is linearly related to this internal clock. The relations are the following:

$$f_c = \frac{f_{clk}}{50} \quad f_{clk}[kHz] \cong \frac{10^5}{3 \cdot C_{osc}[pF]}$$

With  $f_c = 45$  kHz,  $C_{osc} = 14.81$  pF. Since this capacitor's size is not available, the closest existing value has to be used: with the normalized value  $C_{osc} = C_{22} = 15$  pF,  $f_c \approx 44.4$  kHz.

<b>Manufacturer</b>	Maxim
<b>Model</b>	MAX295CSA+
<b>Package</b>	8-pin SO
<b>Power supply (in this system)</b>	5V
<b>Current absorption</b>	7 mA
<b>Required quantity</b>	1

**Table 13**

Specifications of MAX295

Another thing that has to be taken into consideration is that the previous component (instrumentation amplifier *U7*) can technically provide a signal within the range  $-12V..+12V$ , but this filter only accepts inputs from  $0V$  to  $5V$ . Therefore, a voltage limitation has to be placed before the filter. In order not to place a second voltage limitation after the filter (since, as it will be mentioned in the next section, a voltage limitation is required for the DSP as well), it has been chosen to limit the voltage range only once before this filter. A second limitation is required for the analog input of the DSP which has to be in the range  $-0.3V..+3.6V$ .

In order to limit the upper voltage, a Zener diode (*D6*) with a Zener voltage of  $3.6V$  is placed before the filter. Since the positive short-circuit current of the previous component (instrumentation amplifier *U7*) is  $6\text{ mA}$ , the Zener diode has to be able to absorb and dissipate the power in this worse case (where  $V_z = 3.6V$ ). Its power dissipation is  $500\text{ mW}$ , which is perfectly appropriate to absorb the maximal power of  $3.6V \cdot 6\text{ mA} = 21.6\text{ mW}$  in case of a voltage exceed on this track.

In order to limit the lower voltage, a limitation at  $0V$  is not achievable, but it can be approached by using a Schottky diode such as *D7*: its very low forward voltage permits to limit the negative voltage at  $-0.25\text{ V}$ . If there's an excess of negative voltage on this track, the diode will conduct, and the previous instrumentation amplifier will deliver up to  $-15\text{ mA}$ . Here again, the maximal power dissipation of the diode, which is  $75\text{ mW}$ , is definitely higher than the power delivered by the instrumentation amplifier, which is  $-0.25V \cdot -15\text{ mA} = 3.75\text{ mW}$ .

### Highpass filter (4h)

 *scheme landmark: U9 (a and b)*

The highpass filter responsible to cutoff the static component of the signal is a 4<sup>th</sup>-order filter made of passive components and two operational amplifiers. The cutoff frequency has been fixed at  $10\text{ Hz}$ , which provides a good compromise between the filtering of the static component and the lowest frequency interesting for the LDF process, which is  $30\text{ Hz}$  according to section 3.2.4. The type chosen is again a Butterworth filter, with a gain of 1. The components' values have been calculated with the *Filter Pro* software of *Texas Instruments*.

In order to realize it, the amplifiers that have been chosen are the high precision, low noise operational amplifiers *OPA228* series of *Texas Instruments*. Particularly its high speed with a slew rate of  $10V/\mu\text{s}$  makes it ideal for this application. Since two amplifiers are required for this filter, an *OPA2228*, which combines two amplifiers in the same package, has been used.

<b>Manufacturer</b>	Texas Instruments
<b>Model</b>	OPA2228U
<b>Package</b>	8-pin SO
<b>Power supply (in this system)</b>	±12V
<b>Current absorption</b>	2 · ±3.7 mA
<b>Required quantity</b>	1

**Table 13**  
Specifications of OPA2228

### Pre-conversion amplifier (4i)

*📄 scheme landmark: U10a*

After being high-pass filtered by the previous component, only the dynamic part of the signal will remain at the input of this amplifier. According to section 3.1.4, the oscillation will be in the range of -300..+300 mV. As mentioned in the next section, the following A/D converter operates with an input range of -10..+10V. In order to fit the dynamic of the signal within this range, it has to be multiplied by a theoretical factor of  $10V/300mV \approx 33.3$ . In order to have a safety margin, it has been chosen to keep a lower value: by using  $R_{17} = 150 \text{ k}\Omega$  and  $R_{18} = 5.11 \text{ k}\Omega$ , the gain of the amplifier in this non-inverting configuration becomes:

$$G = \frac{R_{17} + R_{18}}{R_{17}} \approx 30.35$$

Here as well, a high slew rate is required to follow the important variations that the LDF signal can contains, that's why another *OPA2228* (using only one amplifier in the package) will be used.

### External A/D converter (4j)

*📄 scheme landmark: U11*

This external A/D converter is responsible to sample the dynamic part of the signal after amplification by the previous component. An *AD976A* from *Analog Devices* has been chosen.

The resolution of the acquisition is 16 bits over a range of -10..+10V, which theoretically corresponds of  $\sim 305.176 \mu V$ . The result of the sampling is written on a 16 bit bus directly connected to 16 digital I/O of the DSP. In order to improve the acquisition procedure within the DSP, the connection of the components has been optimized by using only one DSP's digital port (*PORT D*), and by connecting them in the correct bit order (bit 0 of the result connected to input D0 of DSP, bit 1 to D1, etc.), so that it is not necessary to reconstruct the value in the program.

The DSP controls the A/D converter through two signals called *R/C*, and *CS* (active low), and monitor its state through a third signal *BUSY* (active low). To initiate a conversion and place the sample/hold circuit into the hold state, both the *R/C* and *CS* signals must be brought low for no less than 50 ns. Once the conversion process begins, the *BUSY* signal will go low until the conversion is complete. At the end of a conversion, *BUSY* will return high, and the resulting valid data will be available on the data bus.

In the mode of conversion used for this application, the conversion timing is controlled by a negative-going  $R/C$  signal, at least 50 ns wide. In this mode the  $CS$  pin is always tied low, and the only limit placed on how long the  $R/C$  signal can remain low is the desired sampling rate (100 kHz in this case). Less than 83 ns after the initiation of a conversion, the  $BUSY$  signal will be brought low and remain low until the conversion is complete and the output shift registers have been updated with the new binary two's complement data.

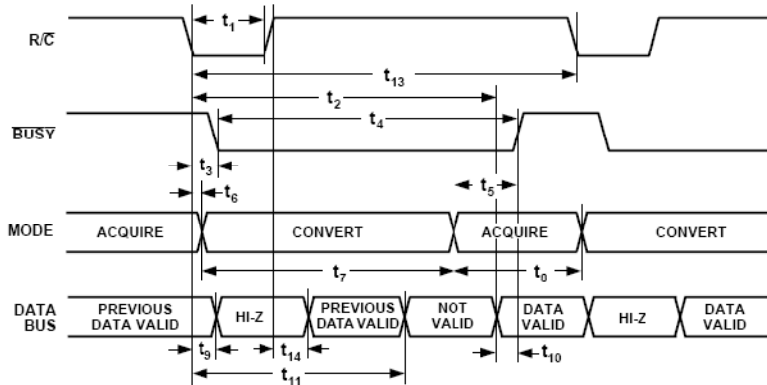


Figure 34 Conversion timing with outputs enabled after conversion ( $CS$  tied low).

<b>Manufacturer</b>	Analog Devices
<b>Model</b>	AD976ABRZ
<b>Package</b>	28-pin SO
<b>Power supply</b>	5V
<b>Power consumption</b>	Max 100 mW
<b>Required quantity</b>	1

Table 14 Specifications of AD976A

[Lasers' power control D/A converters \(4l, 4m\)](#)

*U12, U13*

In order to generate the analog signals that set the lasers' powers (known as *power control*), one D/A converter per laser is used. *DAC7571* of *Texas Instruments* have been chosen: they are low-power, single-channel, 12-bit buffered voltage output D/A converters. They communicate with the DSP over a single I<sup>2</sup>C compatible two-wire serial interface that operates, in this case, at 100 kHz.

Since the output range of these devices is 0..3.3V, they are each followed by an operational amplifier that multiplies the output of the D/A so that the nominal 0..5V range of the laser is reached.

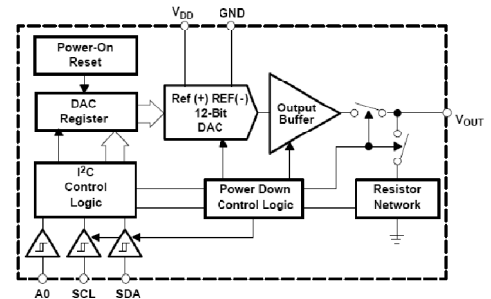


Figure 35 Internal block diagram of the DAC7571

Figure 35 shows the internal diagram of a *DAC7571*. The power supply ( $V_{dd}$ ) is 3.3V since this is the operating voltage of the I<sup>2</sup>C bus when it is connected with the DSP. The two lines of the bus are the clock signal *SCL* and the data line *SDA*. When the bus is not transmitting (state called *idle mode*), those two lines have to be in a high logic state, i.e. 3.3V. Therefore, the lines are each tied-up by a pull-up resistor (*R21*, *R22*).

The I<sup>2</sup>C address of the converter is coded on 8 bits with a fixed-part and a configurable part as follows:  $100110A_00$ , where  $A_0$  corresponds of the logic electrical state of the corresponding pin. In this system, the set up is done according to the following table:

HW architecture	Scheme	I <sup>2</sup> C address	Corresponding laser
<i>4l</i>	<i>U12</i>	1001 1010	Laser A
<i>4m</i>	<i>U13</i>	1001 1000	Laser B

Table 15

Addresses used on the I<sup>2</sup>C bus of the system

<b>Manufacturer</b>	Texas Instruments
<b>Model</b>	DAC7571
<b>Package</b>	SOT-23
<b>Power supply</b>	3.3V
<b>Max. current consumption in normal operation</b>	160 $\mu$ A
<b>Required quantity</b>	2

Table 16

Specifications of DAC7571

### Post D/A conversion amplifiers (for lasers' power control) (4n, 4o)

*📖 scheme landmark: U14 (a and b)*

These are the post-amplifiers of the D/A converters. Their output is directly connected to the analog input of the lasers, setting the lasers' powers by an analog signal of 0..5V. *U14a* is dedicated to laser A and *U14b* to laser B.

Since the output voltage is rather constant (doesn't present any spurious voltage changing as the LDF signal for instance), an important requirement of these amplifiers is the stability but not the slew rate. For this purpose, the performances of an *OPA227* amplifier are appropriate. This operational amplifier is basically the same as the *OPA228* with a lower slew rate of 2.3V/ $\mu$ s.

<b>Manufacturer</b>	Texas Instruments
<b>Model</b>	OPA227U
<b>Package</b>	8-pin SO
<b>Power supply (in this system)</b>	$\pm$ 12V
<b>Current absorption</b>	2 · $\pm$ 3.7 mA
<b>Required quantity</b>	2

Table 17

Specifications of OPA227



They are both mounted in a non-inverter configuration with a gain that should ideally be  $G = 5V/3.3V \approx 1.515V$ . The values of  $R_{23} = 5.11 \text{ k}\Omega$  and  $R_{24} = 10 \text{ k}\Omega$ , related to  $U14A$ , return

$$G = \frac{R_{23} + R_{24}}{R_{24}} \approx 1.511$$

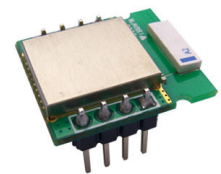
that is a gain satisfactory enough for this part of the system.

### Bluetooth module (4p)

 scheme landmark: U6

The *Bluetooth* module is directly connected to the DSP and is in charge to transmit the data wirelessly to the remote control laptop. The available component *Parani ESD-200* from *Sena* is used in this system.

The *Parani ESD-200* communicates with the DSP through a serial communication. The transmitter and receiver pins *Txd* and *Rxd* are connected to the corresponding input and output of the DSP's *UART* port: these are the lines on which the data transit.



Picture 6  
Parani ESD-200

The pins *Rts* and *Cts* consist of the "hardware flow-control" of this serial transmission. This optional feature is used in this system in order to improve the chances to achieve a communication without errors between those two components. The DSP's *UART* port is also fitted with these corresponding input and output, which are connected to the *Parani ESD-200*.

The *RST* input can be used to reset the module to its manufactory settings, which is not needed here. Therefore, it has to be tied up at the operating voltage of the module, i.e. 3.3V. Finally, *DCD* is an active-low output that indicates when the *Bluetooth* connection has been established with another device; this signal is watched by a simple digital input of the DSP.

<b>Manufacturer</b>	Sena
<b>Model</b>	Parani ESD-200
<b>Dimensions (L x W x H) [mm]</b>	18 x 20 x 11.7
<b>Weight</b>	2 g
<b>Power supply (in this system)</b>	3.3V
<b>Current absorption</b>	Max 29 mA
<b>Required quantity</b>	1

Table 18  
Specifications of Parani ESD-200

This device offers several modes of operation related to the way that it connects (or is connected by other devices). In this application, in order to offer more flexibility, it is interesting that the *Parani ESD-200* can connect (or be connected by) any other *Bluetooth* device. A connection with only one device at a time can be achieved, but with this mode of operation (mode 3), there's no only one laptop allowed to connect the device, for instance. Therefore, it is not necessary to change its settings if the remote *Bluetooth* laptop is different from the last one used.

To change the settings of the *Parani ESD-200*, the dedicated interface board and the *Parani ESD-200 configuration* software have to be used. It offers the possibility to change the mode of operation, the name of the device, and the serial port settings.

In this application, the settings of the DSP's UART port, the *Parani ESD-200* and the COM-port of the remote laptop have to be the same. The default settings are shown in the following table:

<b>Baudrate</b>	57'600 bps
<b>Data bit</b>	8
<b>Parity</b>	None
<b>Stop bit</b>	1
<b>Hardware flow control</b>	enabled

Table 19  
Default settings of the serial port for this application

### DSP (4k)

 *scheme landmark: DSP*

The DSP used in this application is the *dsPIC33FJ256GP710* from *Microchip*. It offers many features such as many digital I/O ports and analog inputs, I<sup>2</sup>C bus interface, and UART interface that are all used in this system. Table 20 below summarizes the main specifications of this device:

<b>Manufacturer</b>	Microchip
<b>Model</b>	dsPIC33FJ256GP710
<b>Package</b>	100-lead plastic thin-quad flatpack (PF) 14x14x1 mm body, 1.0/0.10 mm lead form (TQFP)
<b>Power supply</b>	3.3V
<b>Current absorption</b>	< 90 mA in operation
<b>Required quantity</b>	1

Table 20  
Specifications of dsPIC33FJ256GP710

Appendix 10 shows the pinout of the DSP.

The input clock of the DSP is provided by an external crystal that oscillates at its nominal frequency of 8 MHz. It is afterwards multiplied by the internal PLL so that the final oscillating frequency  $f_{osc}$  is 80 MHz. Therefore, according to equation 8-3 of the DSP's datasheet:

$$F_{cy} = \frac{F_{osc}}{2} = 40 \text{ MIPS}$$

The device can process the algorithm at 40 millions of instructions per second.

Finally, the DSP is also in charge for the *DC-coupled acquisition* through one of its internal AD converters (pin 3, AN29). The resolution of the acquisition is 12 bits over a range of 0..3.3V, which theoretically corresponds of  $\sim 805.664 \mu\text{V}$ . The sampling frequency is 100 kHz according to the signal conditioning section. The result of the sampling is written to the internal register *ADC1BUF0*.

### Power calculation

Now that all the power consumers in the circuit are well know, it is possible to verify if the DC/DC converters and the voltage regulators are able to provide the required energy. The following tables regroup the consumers by voltage category:

+12V			
Landmark	Component	Absorbed current [mA]	Corresponding power [mW]
-	Photodiode	45	540
U7	Instrumentation amplifier	$700 \cdot 10^{-3}$	8.4
U9	Operational amplifier (high-pass filter)	$2 \cdot 3.7$	88.8
U10a	Operational amplifier	3.7	44.4
U14	Operational amplifier	$2 \cdot 3.7$	88.8
<b>Total</b>			<b>771</b>

✓ 12V-regulator U4 can provide up to 12W

-12V			
Landmark	Component	Absorbed current [mA]	Corresponding power [mW]
-	Photodiode	-16	192
U7	Instrumentation amplifier	$-700 \cdot 10^{-3}$	8.4
U9	Operational amplifier (high-pass filter)	$2 \cdot -3.7$	88.8
U10a	Operational amplifier	-3.7	44.4
U14	Operational amplifier	$2 \cdot -3.7$	88.8
<b>Total</b>			<b>423</b>

✓ -12V-regulator U5 can provide up to 12W

+15V			
Landmark	Component	Absorbed current [mA]	Corresponding power [mW]
-	(all the 12V components)		771
U4	+12 V regulator	8	120
<b>Total</b>			<b>891</b>

✓ 15V DC/DC U2 can provide up to 7.5W ( $500 \text{ mA} \cdot 15\text{V}$ )

-15V			
Landmark	Component	Absorbed current [mA]	Corresponding power [mW]
-	(all the -12V components)		423
U5	-12 V regulator	3	45
<b>Total</b>			<b>468</b>

✓ -15V DC/DC U3 can provide up to 7.5W ( $-500 \text{ mA} \cdot -15\text{V}$ )

3.3V			
Landmark	Component	Absorbed current [mA]	Corresponding power [mW]
U2	+15V DC/DC (chip supply)	$120 \cdot 10^{-3}$	$40 \cdot 10^{-3}$
U3	-15V DC/DC (chip supply)	$120 \cdot 10^{-3}$	$40 \cdot 10^{-3}$
DSP	DSP	90	297
U6	Bluetooth module	29	95.7
U12	D/A converter	$160 \cdot 10^{-3}$	$528 \cdot 10^{-3}$
U13	D/A converter	$160 \cdot 10^{-3}$	$528 \cdot 10^{-3}$
<b>Total</b>			<b>394</b>

✓ 3.3V regulator U1 can provide up to 2.64 W ( $800 \text{ mA} \cdot 3.3\text{V}$ )

5V			
Landmark	Component	Absorbed current [mA]	Corresponding power [mW]
-	(all the 3.3V components)		394
-	(all the +15V components)		891
-	(all the -15V components)		468
U1	3.3V regulator	10	50
U8	Anti-aliasing filter	7	35
U11	External A/D converter		100
<b>Total board and photodiode consumption</b>			<b>1'938</b>

Entire system (on 5V)			
Landmark	Component	Absorbed current [mA]	Corresponding power [mW]
<b>1</b>	Laser A	240	1'200
<b>2</b>	Laser B	240	1'200
<b>3,4</b>	Board and photodiode		1'938
<b>Total system consumption</b>			<b>4'338</b>

✓ External transformer 9 provides up to 20 W ( $4\text{A} \cdot 5\text{V}$ ); safety margin is higher than 75%

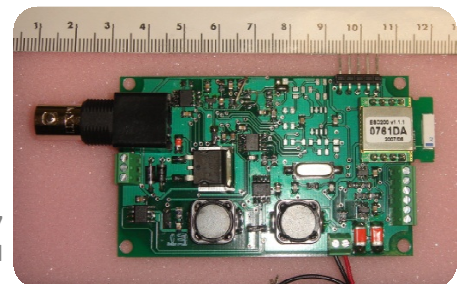
Note: at start-up, both lasers have to warm up. During this time that last for about 30 sec, the absorbed current per laser can go up to 1'100 mA., totalizing a power of about 13W for the whole system. This requirement is still achievable by the used transformer.

### Layout design

The circuit has been assembled and soldered on a printed circuit board with two layers. The outer dimensions are 80 x 50 mm, just like the photodiode, so that they can be stacked and save space. Picture 7 shows the board itself after final assembly.

Picture 7

Top view of the processing board



### 3.3.5 DSP software

The DSP algorithm has been developed in the *Microchip MPLAB IDE 8.00* environment. This development tool is an easy interface to program and debug the process that the DSP will execute during the operation of the system. The code is written in the C- language, and the compiler used is the *MPLAB C30*.

The entire *MPLAB* project contains several files that are sorted out by type. Among other things, the *.h* files contain definitions such as constant values or variables, and the *.c* files contain the methods (or classes) that basically constitute the several parts of the algorithm. The following table represents the tree of the *MPLAB* project and describes the content of each file.

Astronaut measurements MPLAB project		
Source files	<b>ad.c</b>	Contains the initializations of both internal and external AD converters, and the code related to the signal sampling at 100kHz.
	<b>calculation.c</b>	Contains the code related to the FFT routine, as well as the two measurements procedures ( <i>LDF processing</i> and <i>Pulse-oxymeter processing</i> )
	<b>clock.c</b>	Contains the initialization of the clock, including the PLL settings
	<b>dcdc.c</b>	Contains the methods to turn on/off the two DC/DC converters
	<b>fast_copy.s</b>	Assembler code used in the FFT routine
	<b>I2c_bus.c</b>	Contains the initialization method of the I <sup>2</sup> C module, the I <sup>2</sup> C driver, and a method to write on the bus.
	<b>lasers.c</b>	Contains the methods to turn on/off the lasers, and to set their power
	<b>main.c</b>	Starting point of the code: contains the variable declarations, the variables initializations, and the main program
	<b>measurements.c</b>	Contains all the procedures to start or stop the requested measurement, and to switch from one state to each other (state machine). Also contains the procedure executed when a command is received from the remote device.
	<b>ports.c</b>	Contains the initialization of the ports, and methods to read or write these inputs / outputs
	<b>subtract_means.s</b>	Assembler code used in the FFT routine
	<b>timers.c</b>	Contains the initialization of the timers and the related interrupt routines
<b>twiddle_factors.c</b>	Contains the hexadecimal factors that represent the window used by the FFT routine	
<b>wireless_transmission.c</b>	Contains the initialization of the UART port, the related interrupts, several methods to send different types of data via Bluetooth, and the procedures to initiate or check the wireless connection with the remote device.	
Header files	<b>constant_values.h</b>	Contains all the constant values used in the code
	<b>p33FJ256GP710.h</b>	Definition file of the device
	<b>system.h</b>	Call the internal or external libraries / header files that are required in this program
	<b>variables_types.h</b>	Defines customized variable types in order to make the programming more efficient

Table 21  
Organization of the MPLAB *Astronaut measurements* project

During the project, two different circuit boards have been developed: the first prototype was meant to be an intermediate step to the final version and it was equipped with LEDs and test points to assess the correct functionalities in an easier way. The second prototype that has been described in the previous section is the miniaturized version of the first prototype but without the unnecessary test components. The circuit is basically the same on both boards, that's why this program can be used on both prototypes. As mentioned in the next section, it is just necessary to change a parameter before uploading the firmware in the desired device.

### Constant variables

The file *variable\_types.h* is clearly separated in two parts that are related to "board 1" and "board 2". Since two types of prototypes circuit boards have been developed and that they don't have the same pinout, the definition of the input/output pins as well as their initialization differs from one board to the other. Therefore, the code has to be adapted in order to load the correct settings to the desired device. Here, instead of modifying the configuration of each pin and to adapt it with the electrical configuration of the desired board (e.g. setting which pins are digital outputs, analog inputs, etc.), the program offers the possibility to set the variable *BOARD* with the correct setting (1 or 2 for respectively prototype 1 or 2), which will take care about compiling the correct settings.

For each board, the defined constant values are almost the same. They are principally:

- **Signal conditioning variables:** the value of gain of the electronic devices in the signal conditioning part such as amplifiers and filters
- **Signal sampling and numerical conversion:** the sampling frequency value, the block length for acquisition and processing, and the parameters of both internal and external ADs converters
- **Signal processing:** limitation of some LDF results
- **Wireless transmission frames:** some time limitations related to the wireless connection, and the different "start of frame" possible values
- **Lasers parameters:** the maximal power of the laser used, and the switching interval for the pulse-oxymetry application
- **I<sup>2</sup>C bus:** the address default size, the number of attempts, and some driver constants
- **External AD converter signal ports:** the DSP's pins where its control signals are connected
- **External DA converter I<sup>2</sup>C addresses:** the assigned physical addresses of the two DA converters
- **Lasers control:** the DSP's pins where the laser's digital signals are connected
- **Bluetooth connection signal:** the DSP's pins where the Bluetooth module status pin is connected
- **DC/DC converters control:** the DSP's pins connected to the *SHDN* pin of each DC/DC converter

### General structure of the program

The whole program is based on a simple structure that initiates all the hardware and software initializations, and then cyclically repeats some procedures such as checking the wireless connection, reading the inputs or writing the outputs, executing the commands if received or sending the status if needed, or calling a measurement routine if selected. The program can exit this cycle if a reset is requested: in this case, it will simply restart the initializations (except the clock initialization). Figure 36 shows the flow chart of the main program.

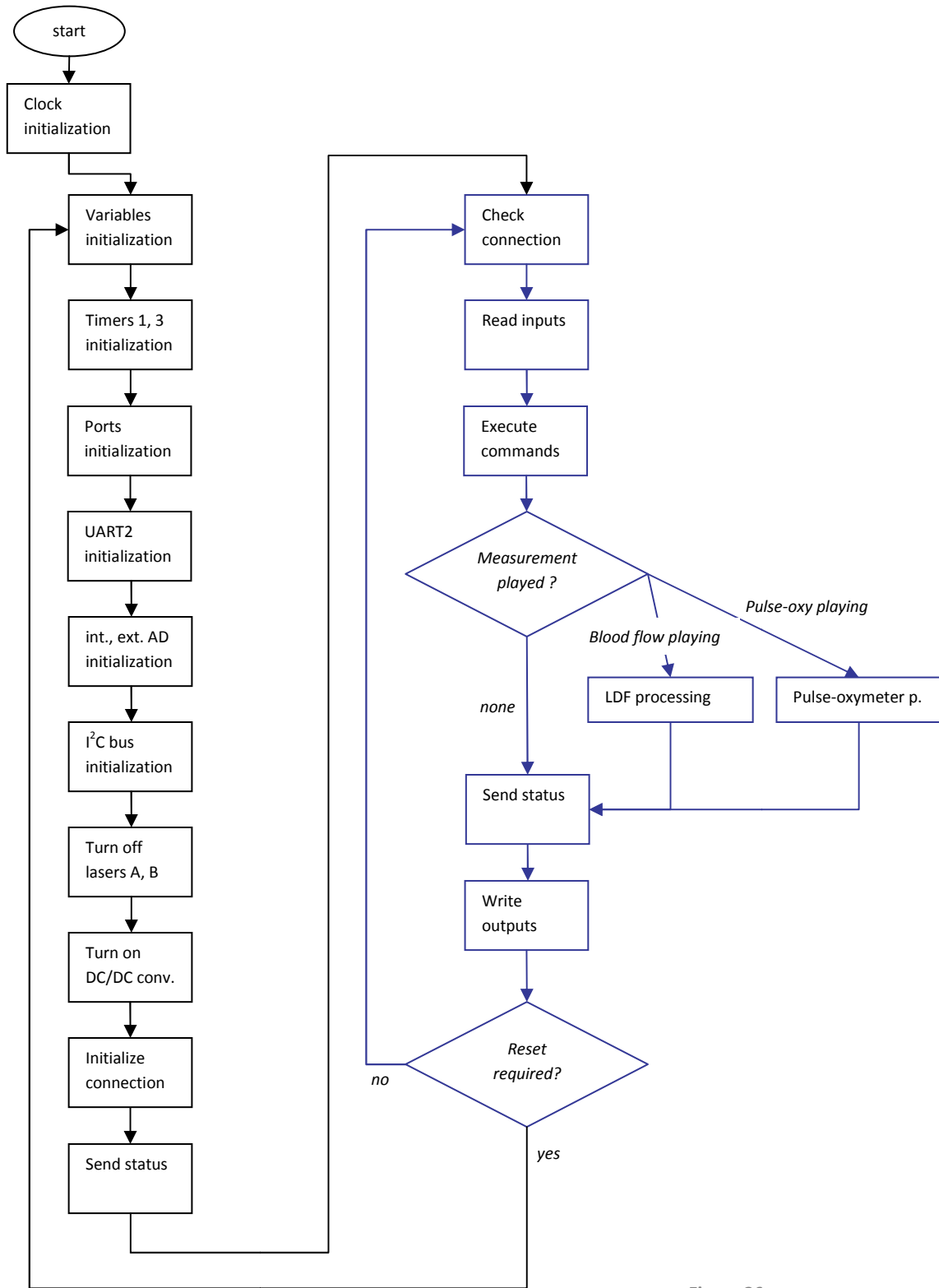


Figure 36  
 Flow chart of the main program

After power-up of the system, the clock is first initialized. It particularly configures the internal PLL to reach an internal cycle frequency  $f_{cy}$  of 40 MIPS. This initialization is called only once, even in the case of a software reset.

Then all the variables are initialized. There's a dedicated method *InitVariables* that contains all the initial values for each variable: in the part of the program where the variables are declared only, no value is assigned, so that it is possible to guarantee that the state of the system after a software reset is the same as after the start-up.

After that, the *timer 1* and *timer 3* are initialized. *Timer 1* is responsible to generate the time-base as explained in the next section; *timer 3* is used for the A/D acquisitions as explained in the corresponding section as well.

The *UART2* is then initialized with the same settings as the *Bluetooth* module as mentioned in section 3.3.4.

Then the two A/D converters are initialized: the internal A/D converter has to set the input pin where the acquisition will take place, and configure it with a 12 bit resolution. After initialization, this A/D converter remains disabled. The initialization of the external A/D converter only consist of tiding the *CS* signal low, and the *RC* signal high, according to the communication protocol between the converter and the DSP as shown in the previous section.

After that the I<sup>2</sup>C bus is initialized. A particularity is that both pins *SCA* and *SDA* have to be configured as open-drain because of the particularity of this communication system.

Then the two lasers are disabled since at the beginning no measurement is supposed to start without the intervention of the control application: both lasers can be turned off.

The two DC/DC converters that actually allow the  $\pm 12V$  components to be supplied are here turned on.

After all the above initializations, the system is ready to operate and the connection with the remote control laptop can be initiated according to section 3.3.6.

Once it has been completed, the embedded device sends its status to the remote control laptop so that they are synchronized before the cycling operation begins.

The main cycle is then infinitely repeated unless the software reset condition occurs: it can appear in two cases only:

- The remote control laptop asks for the DSP to perform a reset
- The maximal time allowed without the wireless connection is checked has elapsed (see 3.3.6)

The software reset restarts the program from the initialization of variables.

The main cycle starts by checking the connection with the remote control laptop. This method is called each time the program enters the cycle. Its detailed operations are explained in section 3.3.6. This part of the program is the responsible for a software reset if certain connection conditions occurs.

The reading of the inputs simply scans the digital inputs of the system and updates the corresponding variables (example: *LaserX.TemperatureOK*). Oppositely, the further writing of the outputs is simply the update of the output pins according to the state of the related variables (example: *LaserX.Enable*).

The *Execute commands* part checks if an order from the remote control device has arrived to the DSP, and executes it accordingly.



Then a switching structure executes the corresponding measurement routine if either the *blood flow measurement* or *pulse-oxymetry measurement* has been started by the remote control device.

Finally, the embedded system sends its status to the remote control device only if they have changed since the last cycle. It updates the outputs as mentioned above, and returns to the beginning of the cycle unless a software reset is necessary.

During the operation of the system, several interruptions can occur. These are, ordered from the highest to the lowest priority:

- A/D acquisition interrupt
- Timer 1 interrupt
- UART receiver interrupt
- UART transmitter interrupt
- I<sup>2</sup>C bus interrupt

The parts of the program that require further explanations are discussed in the next parts of this section.

#### Variables organization

In this program, most of the variables are global. Particularly, some customized structures have been created for the variables related to the measurements, the acquired signal, and the lasers control. These definitions are available in the file *variables\_types.h*.

Each measurement, such as *BloodFlow* or *Pulsoxymeter*, contains four statuses that can be either true or false. They are, for the blood flow measurement for instance:

- BloodFlow.Selected
- BloodFlow.Stop
- BloodFlow.Play
- BloodFlow.Pause

Only one measurement type can be selected at a time. Then, for each measurement, only one of the three status *stop*, *play* or *pause* is true. Therefore, the fact that a measurement is selected doesn't mean that it is running: in order to perform the measurement, it has to be both selected and played.

A second simple structure is used for each laser. The parameters for the laser A are, for instance:

- LaserA.main
- LaserA.TemperatureOK
- LaserA.Enable
- LaserA.Power

When the parameter *main* is true, the corresponding laser will be used for the LDF measurement. The parameter *TemperatureOK* indicates if the laser is ready to operate; it is updated when the inputs are read thanks to the electrical signal coming from the laser. The parameter *Enable* is true when the laser is turned on, and the corresponding DSP's output is updated when the outputs are written by the main cycle. Finally, the parameter *Power* contains the value of the corresponding laser's power in milliwatts. The corresponding analog output has to be changed through a function described in the Lasers control part below.

The most complicate structure of this program is the one that stores all the indications related to the signal acquisition. The following array shows how it is made:

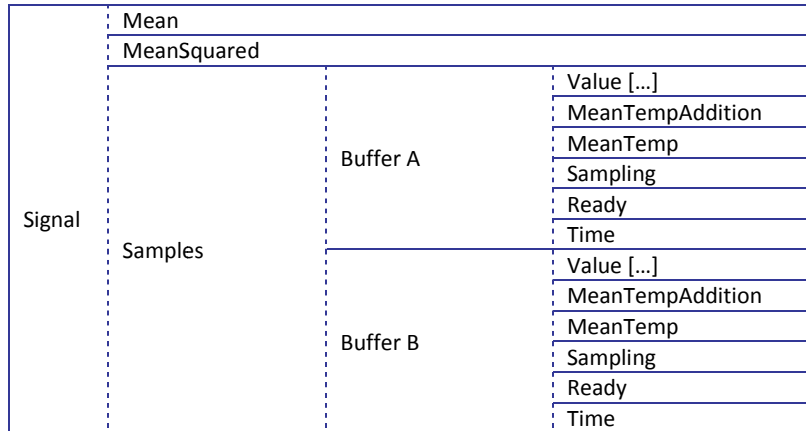


**Figure 37**  
Structure of the signal variable. The parameter *Mean* for instance is called with the syntax *Signal.Mean*

Its use will be discussed in the A/D conversion part of this section.

### Internal time reference

*project file: timers.c*

In order to perform the synchronization with the remote control application and to keep the time stamps of the measurements, the DSP must have a real time-base. For this purpose, the *timer 1* of the device is used and benefits from the second interrupt priority of the system (the first one being the signal acquisition). It is configured so that an interrupt occurs every millisecond: at this moment, the two variables *RunTime* and *MeasurementTime* are increased by 1. The first one represent the elapsed time (in ms) since the device has been started or reset, the second one is the elapsed time from the moment the measurement has started, therefore this variable is set at 0 each time the measurement starts.

### Lasers control

*project file: lasers.c*

The lasers are controlled by the three following methods:

- TurnOnLaser(*laser*)
- TurnOffLaser(*laser*)
- SetLaserPower(*laser*, *power*)

The values in parentheses are the parameters required to call the function. The character corresponding to the laser name has to be putted in place of *laser* in the parentheses and the number corresponding to the power value in milliwatts has to replace *power* in the third function. For instance, to turn on the laser A, the syntax in c-code is:

```
TurnOnLaser('A');
```

The operation of the third method is described here since it has some particularities. The inputs of this method are the concerned laser, and the power to assign to it; the output is a value that is written on the I<sup>2</sup>C bus with the corresponding address and the output voltage that the D/A converter has to provide.

According to table 3 of section 3.2.1, the relationship between the output power and the applied voltage is inverted. Moreover, the D/A converter accepts as a command 12 bits integer values that are linearly related to the output voltage as follows, considering that the output voltage range of the D/A converter is 0..3.3V:

$$\text{Output voltage} = \frac{\text{Integer value}}{2^{12} - 1} \cdot 3.3V$$

Where the integer value ordered must be in the range 0..4095. Then it is possible to determine the *integer value* that has to be sent to the D/A converter with the following formula:

$$\text{Integer value} = -(\text{Power} - \text{MaxPower}) \cdot \frac{4095}{\text{MaxPower}}$$

Where *MaxPower* is the maximal power of the corresponding laser in mW, and *Power* is the desired power in mW.

The flow chart of appendix 11 shows how this procedure is implemented.

### A/D conversion

 *project file: ad.c*

The signal acquisition is done by two different A/D converters: the internal one of the DSP for the *DC-coupled acquisition* and the external one for the *AC-coupled acquisition*. Both have the same sampling frequency of 100 kHz and in order to simplify the procedure, they always work together.

The internal A/D converter is physically coupled to the *timer 3* of the DSP. By setting the overflow value of this timer in order that it reaches it and resets its counter at a frequency of 100 kHz, the *ADC1Interrupt* will occur at the same frequency. Then, the code corresponding of the acquisition process can be placed in this interrupt for both converters: it guarantees that they will always acquire the data at the same moment and thus at the same frequency.

In order to store the acquired data before they are processed, the variable *Signal* and its subvariables are used. As shown in figure 37 above, it is divided in two identical buffers: this is necessary since after the acquisition of one block of samples, this block will be processed by the LDF algorithm for example. However, during this time, the sampling of the signal is still running and another free location is required in order to store the data that are currently acquired. Once the second buffer is full, it can be processed and at this time, the first buffer should have been released by the previous calculation. Appendix 12 shows the flow chart of the acquisition procedure of one sample, with one buffer only in order to simplify the understanding of the principle.

## Measurements management

 project file: *measurements.c*

The system offers the four following different types of measurements:

- **BloodFlow:** measures the blood volume, speed and flow only with the LDF processing
- **PulseOxymeter:** measures the oxygenated hemoglobin rate only with pulse-oxymetry processing
- **Alternate:** performs the two first measurements by regularly switching from one to the other
- **Simultaneous:** performs the two first measurements without interruption

As mentioned in the variable section, each measurement has 4 possible status: *selected*, *stop*, *play*, *pause*. These parameters are basically boolean values that can be used to check the status in certain functions, but the management of the measurement selection and state is not based on these variables: a state machine with 12 different states is used for this purpose.

Each of the four measurements can take one of the three different states *stop*, *play*, or *pause*. A state number between 1 and 12 is assigned to each state and is stored in the global variable *MeasurementState*. Figure 38 shows the state machine for one measurement type only, appendix 13 shows the entire state machine.

From whatever state, another *stop* state can be reached; appendix 13 shows this principle only to jump to the stop state of the *alternate* measurement. The other arrays haven't been design for reading reasons.

The method *MeasurementSelection()* contains the algorithm that manages the whole state machine.

When the machine is in a *stop* state and that it has been asked to switch to the corresponding *play* state, it will call either the *StartBloodFlowMeasurement* method if the state number 2 is requested, or the *StartOtherMeasurement* method for another *play* state. These methods will verify that the required laser(s) is (are) ready to be used, and turn it (them) on if yes. It will also turn on the A/D converters and reset the variable *MeasurementTime* that paces the measurement. If an error occurs, such as a required laser that is not ready to be used (warm-up not completed for instance), the variable *CommandAccepted* will be set at 0, indicating that the machine cannot switch to the required state.

When the machine is in a *pause* state, the lasers that are used for the measurement are not turned off (they will be when the *stop* state is reached only).

Finally, when a measurement is running and that another *stop* state is requested, the system simply turns off the lasers and the A/D conversion by calling either the *StopBloodFlowMeasurement* or *StopOtherMeasurement* method. This request is always accepted.

The boolean states such as *BloodFlow.Play*, *Alternaly.Pause*, etc. are automatically updated according to the state of the machine.

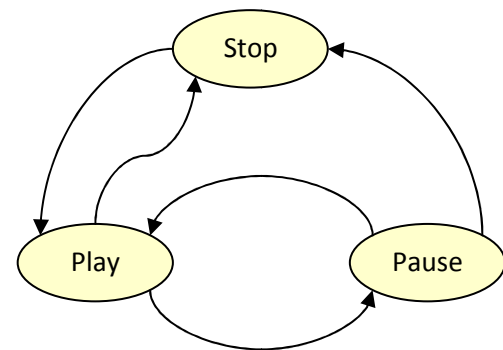


Figure 38  
State machine principle for one measurement type only

## LDF processing

 project file: *calculation.c*

The LDF processing is the most difficult calculation done in this system. The DSP has basically to compute the whole algorithm shown in appendix 5. The following explanation first discusses when the calculation starts, then the detailed calculation of the FFT, and finally the rest of the algorithm.

After having talked about the main cycle of the program, the state machine that manages the measurements, and the A/D acquisition, it is simple to understand when the method *LDFProcessing* is called by the program. According to the figure 36, the main cycle goes through a "switch" condition at each cycle, which occurs at a frequency that is difficult to estimate precisely, but it is in the range of several kHz when the DSP is not processing any other calculation. In order to call the *LDFProcessing*, a measurement using the LDF algorithm has to be started by the state machine. For instance, as soon as the state machine is set on state 2 (state *play* of *BloodFlow*), the "switch" condition will call the *LDFProcessing* method at each cycle. Even though this method is called at the same frequency as the main cycle is executed, it doesn't mean that the LDF algorithm is executed so often: the beginning of this method is a condition that expects the sampling buffer to be ready for processing before entering the further calculation. This can be represented by the simplified flow chart of figure 39.

The buffer is set as "ready for processing" in the variable *Signal.Samples.BufferX.Ready* that is set by the A/D conversion. Since, according to the functioning of the state machine, the A/D conversion is turned on when the state of the measurement is *play*, there's a moment when the block of samples will be totally filled and then the *LDFProcessing* method will be allowed to enter the LDF algorithm part and computes it on the block of samples.

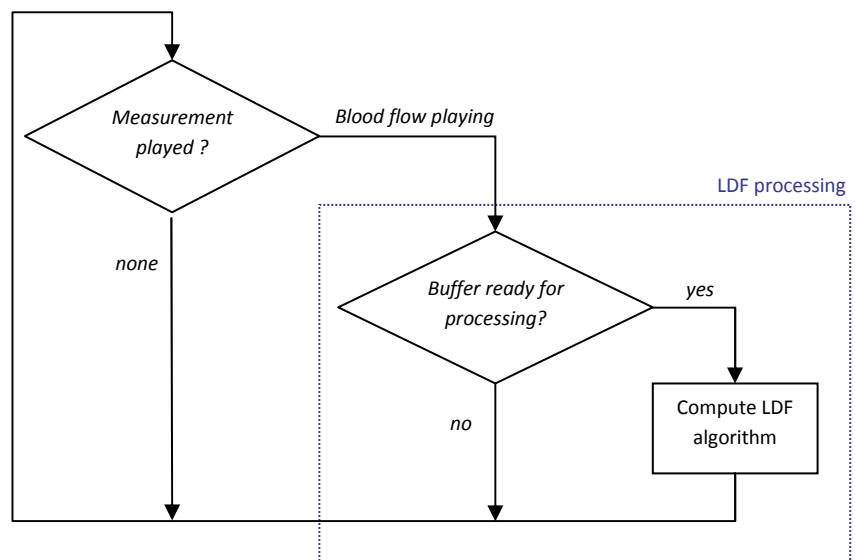


Figure 39

Simplified flow chart to show under which conditions the LDF algorithm is executed

In this system, the FFT is computed on blocks of 1'024 samples. The routine used is originally provided by *Microchip* and has been integrated in this part of the program without any major modifications. This routine has the particularity to work with the normalized 1.15 format: it is a fixed-point representation that can represent numbers in a range from -1 ( $8000_{16}$ ) to 0.999969482 ( $7FFF_{16}$ ); this range is enough to compute Fourier transforms (since *sin* and *cos* functions are defined between -1 and 1). The variable type associated at the input of the FFT is a *fractional* type: it corresponds of the known type *integer* but is interpreted in the 1.15 format. For instance, if the *integer* value 15'000 ( $3A98_{16}$ ) is a sample of the block to be analyzed by the FFT, the latter will interpret it as the value  $15'000/2^{15} \approx 0.45776$ .

Another particularity of this routine is that it accepts inputs in the normalized range of -0.5..0.5 only. This is the reason why the samples acquired by the external A/D converter are divided by 2 before being stored in the block, and then acquired: by doing that, the maximum positive value that this 16-bit bipolar A/D converter can provide becomes  $2^{14} = 16'384$ , which corresponds, in the 1.15 format, to  $2^{14}/2^{15} = 0.5$ . The maximum positive voltage at the input of the converter corresponds to the maximal normalized value of the FFT routine. The same reasoning can be applied for the negative values.

Therefore, there's a normalization factor called *KPreFFT* in the code that expresses the relationship between the real voltage applied at the input of the A/D converter and the normalized value. In the case of the external A/D converter that has an input range of -10..+10V (20V width) and that is normalized to -0.5..+0.5 (width 1), the normalization factor is calculated by  $1/20 = 0.05$ . This factor will be used afterwards to denormalize the result of the FFT.

The window that is used to compute the FFT is defined in the file *twiddle\_factors.c* and obviously depends on the length of the analyzed block. In this application, the window used is a Hanning window and its factors  $\omega(n)$  can be calculated thanks to the following formula:

$$\omega(n) = \frac{2^{16}}{2} \cdot \left(1 - \cos\left(\frac{2 \cdot \pi \cdot n}{1023}\right)\right) \quad \text{where } 0 \leq n < 1'024$$

After the FFT has been computed, the following calculation can be applied on the interesting part of the results, according to appendix 4:

$$Amp^2 = Re^2 + Im^2$$

However, applying this calculation only would return a normalized result. In order to denormalize it, *Amp*<sup>2</sup> is multiplied by the factor *KPostFFT*, which is calculated as follows if the external A/D converter is used:

$$KPostFFT = \left( \frac{1}{2^{15}} \cdot 2^{16-15} \cdot \frac{1}{G_{ia} \cdot G_{lpf} \cdot G_{hpf} \cdot G_a \cdot KPreFFT} \right)^2$$

The whole factor is squared since the correction is done on *Amp*<sup>2</sup> which is a squared value as well. The first division by  $2^{15}$  compensates the normalized interpretation of the compiler: the result of the FFT is normalized in the 1.15 format, but the compiler interprets it as an integer value. For instance, if the FFT would return the normalized value 1 for a given index (or frequency), the compiler will interpret it as 32'767, which is wrong. The multiplication by  $2^{16-15}$  is related to the resolution of the A/D conversion: the external A/D converter actually returns a result on 15 bits since the sampled value is directly divided by two after acquisition. If the internal A/D converter is used to perform the FFT for instance, this factor would become  $2^{16-12}$  since the resolution of the internal one is 12 bits. The last division includes the normalization factor *KPreFFT* as well as the gains of the instrumentation amplifier  $G_{ia}$ , the anti-aliasing (low-pass) filter  $G_{lpf}$ , the high-pass filter  $G_{hpf}$ , and the pre-conversion amplifier  $G_a$ . In fact, the voltage applied at the input of the external A/D converter has been amplified and therefore this has to be taken into account in order to have, in the final spectrum, the power corresponding to the photodetected signal, and not to the signal after conditioning. These four constant gains can be modified in the file *constant\_values.h*.

The last part of the algorithm, which basically consists of the whole scheme of appendix 5 without the FFT, requires some explanations about the integrals calculation: in C-programming, the integrals have to be transformed into sums in order to compute them. There are two types of integrals used in the LDF theory, and they can be transformed according to the following formulas:

$$\int P(f)df = \sum PSD(f) \cdot \Delta f$$

$$\int f \cdot P(f)df = \sum f \cdot PSD(f) \cdot \Delta f = \sum index \cdot \Delta f \cdot PSD(f) \cdot \Delta f = \sum index \cdot PSD(f) \cdot (\Delta f)^2$$

Where  $PSD(f)$  is the resulting vector of the FFT (calculation of  $Amp^2$  at each index). These index start at 0 and go up to 1'023 since the FFT has been computed on blocks of 1'024 samples. Each index represent a frequency that can be calculated in multiplying the index by  $\Delta f$ , where

$$\Delta f = \frac{f_s}{Block\ length} = \frac{100\ kHz}{1'024} = 97.65625\ Hz$$

In this application, the resulting spectrum has to be processed in two phases according to the algorithm of appendix 5: a first time with the results from 30 Hz to 35 kHz, and a second time with the results from 35 kHz to 40 kHz. These frequencies are mathematically the lower and upper limits of the integrals. In order to apply them in the code (loops), they have to refer to the index of the results, which are simply the division of these limits by  $\Delta f$ . Therefore the rounded index are respectively 1, 358 and 410.

Oppositely to the mathematical model of appendix 5, the *blood flow* is not calculated here: this multiplication is later done by the control application. Finally, the results are sent to the remote control laptop with a time stamp and the mean value of the voltage (see next section for details about the wireless transmission).

### Pulse-oxymeter processing

Compared to the LDF processing, the pulse-oxymeter calculation is mathematically very simple, but has a different structure since it is based on a sequential procedure.

The call of the *PulseOxymeterProcessing* method works exactly the same way as the call of the *LDFProcessing* described above: it is called at each main cycle of the program as long as this measurement is played (set by the state machine, state 5 in this case).

The variables *Signal.Samples.BufferX.Ready* have been initially created to indicate if the buffer is ready for the LDF processing or not. The pulse-oxymeter processing uses these variables to steer the sampled values in the appropriate buffer: when the value of the variable is true, the A/D acquisition will not use this buffer for the acquisition: it is locked.

The flow chart of figure 40 shows the sequence executed to obtain one result of the pulse-oxymetry process.



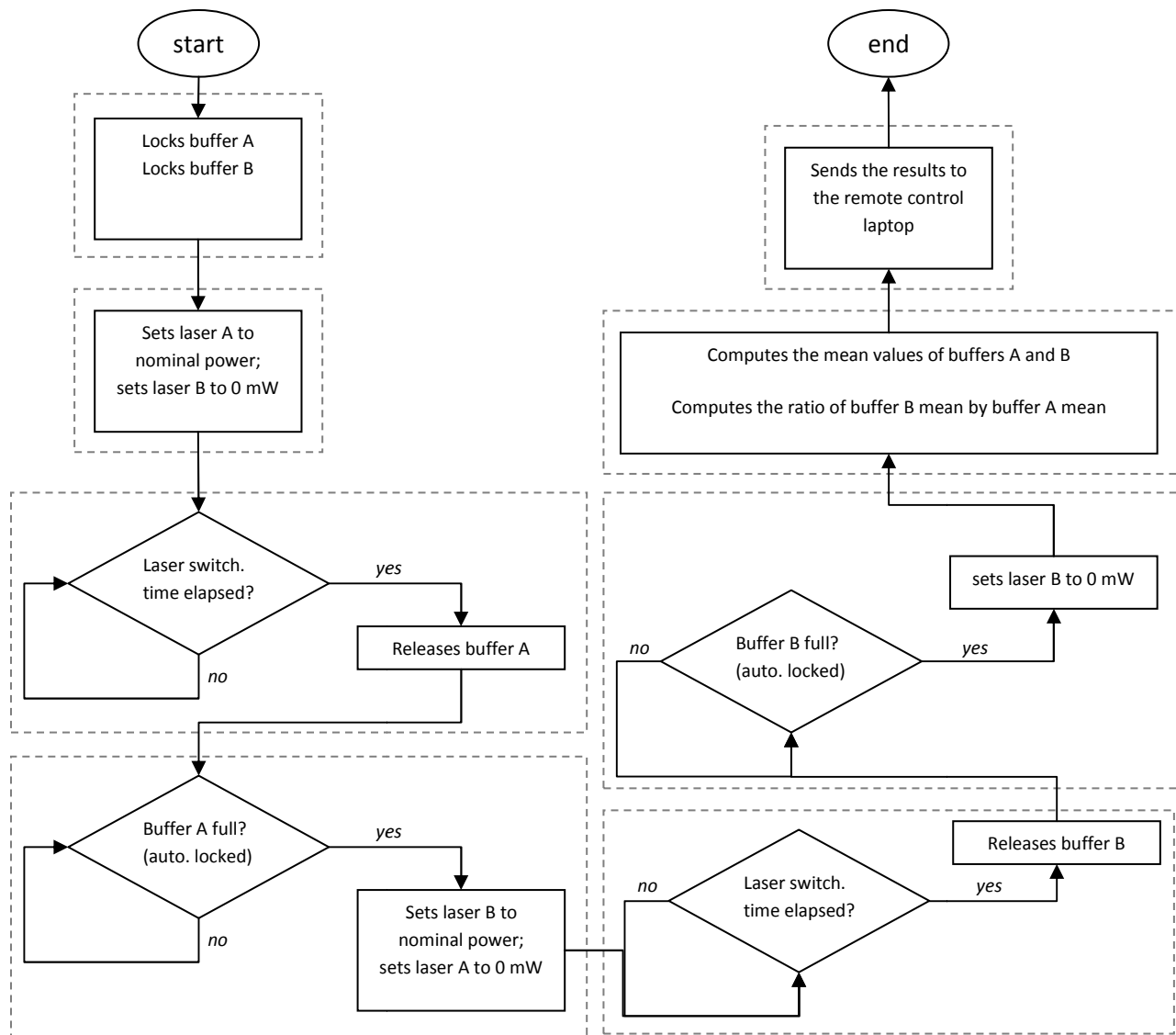


Figure 40  
 Sequential procedure executed by the pulse-oxygen algorithm

One particularity in this system is that the program can exit the sequence, execute other operations, and come back at the same point afterwards: instead of waiting for a buffer to be filled or for a temporization, the system can take care about other things such as the connection management or the execution of the received commands. The global variable *PulseOxymeterMeasurementStep* is used to store the current step of the sequence and therefore offers this possibility.

## Commands execution and status transmission

 project files: *measurements.c; wireless\_transmission.c*

At each cycle of the main loop, the methods *ExecuteCommands* and *SendStatus* are called. The first one, executed at the beginning of the main loop, checks if an order has been received from the remote control laptop; if not, it simply let the program run further. The second one is almost at the end of the main loop, and send the status of the system to the remote control application only if one of the status has changed; if not, the program can run further as well. Therefore, if the state of the system stays the same and if the user doesn't send any command, those two functions don't execute anything.

Appendix 14 shows the flow chart of those two functions. Refer to next section for further details about the content of the frame.

### 3.3.6 Wireless transmission

This section describes the protocol used in the wireless transmission. As previously mentioned, the transmission uses the *Bluetooth* technology with the SPP profile; the serial port settings correspond to the considerations of section 3.3.4 (see table 19).

#### Frame types and formats

The communication between the embedded device and the remote control laptop is executed through several types of fixed-length data packets. They all start by 4 bytes representing the *start of frame (SOF)*, and are optionally followed by some data. The SOF part differs depending on the packet type, and thus provides the information of what it is for.

Generally speaking, these packets are used to perform the following tasks:

- Initialize the connection
- Check the connection
- Send the results of the measurement from the embedded device to the laptop
- Send the status of the system from the embedded device to the laptop
- Send a command from the laptop to the embedded device

As mentioned in chapter 3.2.5, the IEEE 754 format is used to represent the numerical values such as the result of a measurement. Therefore, the SOF character is also represented in a single-precision 32 bit, and in order to avoid any misunderstanding during the frame acquisition procedure on the side of the receiver, it has to be different than the frame's content: in order to satisfy this condition, only the values representing "not a number *NaN*" are used in the SOF. The table below shows the existing frames that can be transmitted during the operation of the system.



Name	SOF	Data	Length [bytes]	Direction	
				device	laptop
Connection initialization	7F 80 00 01	-	4	⇨	
Connection acknowledge 1	7F 80 00 02	-	4		⇨
Connection acknowledge 2	7F 80 00 03	-	4	⇨	
Connection check	7F 80 00 05	-	4	⇨	⇨
Command frame	7F 80 00 08	( 6 bytes data, see details below)	10		⇨
Status frame	7F 80 00 09	( 6 bytes data, see details below)	10	⇨	
Blood flow frame	7F 80 00 10	(16 bytes data, see details below)	20	⇨	
Pulse oxymeter frame	7F 80 00 11	(12 bytes data, see details below)	16	⇨	

**Table 22**  
Frame types used in the wireless transmission

The command frame and status frame have exactly the same structure since they represent the same parameters: the only difference is that the first one is sent from the laptop to the embedded device to request something, and the second one is returned to the laptop in order to indicate what the real status are. The table below indicates which variables are concerned by such frames. Each variable can be considered as a boolean value, which state is represented by the corresponding bit.

Byte	MSB							LSB
1	Reset							CommandAccepted
2	BloodFlow.Selected	BloodFlow.Stop	BloodFlow.Play	BloodFlow.Pause	Pulseoxy.Selected	Pulseoxy.Stop	Pulseoxy.Play	Pulseoxy.Pause
3	Alternaly.Selected	Alternaly.Stop	Alternaly.Play	Alternaly.Pause	Simultaneously.Selected	Simultaneously.Stop	Simultaneously.Play	Simultaneously.Pause
4	LaserA.Main	LaserA.TempOK			LaserB.Main	LaserB.TempOK		
5	LaserA.Powser (8-bit value representing the power in milliwatts)							
6	LaserB.Powser (8-bit value representing the power in milliwatts)							

**Table 23**  
Organization of the content in the *command frame* and *status frame*

Apart from the time stamp that represents the elapsed milliseconds from the beginning of the measurement in a 32-bit integer value, the results of the measurements use the *IEEE 754* standard to represent the values. Figure 41 shows how these two frames are organized.

Blood flow frame																				
Byte-nr.	0	1	2	3	4	5	6	7	8	9	10	11	12	13	14	15	16	17	18	19
Hex. content	7F	80	00	10	xx	xx	xx	xx	xx	xx	xx	xx	xx	xx	xx	xx	xx	xx	xx	xx
Meaning	SOF				Time stamp				Signal.Mean				BloodFlow.Volume				BloodFlow.Speed			

Pulse-oxymeter frame																
Byte-nr.	0	1	2	3	4	5	6	7	8	9	10	11	12	13	14	15
Hex. content	7F	80	00	11	xx	xx	xx	xx	xx	xx	xx	xx	xx	xx	xx	xx
Meaning	SOF				Time stamp				Infra red light voltage				Red light voltage			

**Figure 41**  
Organization of the content in the *blood flow frame* and the *pulse-oxymeter frame*

### Connection initialization

After starting up, the embedded device and the laptop have first to perform a short procedure that initializes the connection and allow them to start working at the same time. This procedure is re-executed after a software reset.

It simply consists of the following frames exchange:

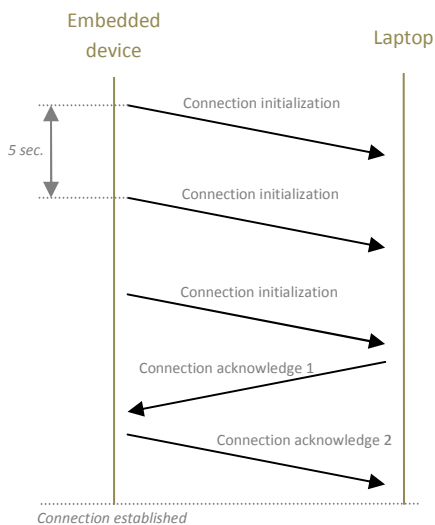


**Figure 42**  
Connection initialization procedure

The embedded device keeps sending the *Connection initialization* frame until the laptop responds by a *Connection acknowledge 1* frame. It sends it every 5 seconds (this value can be modified with the constant *CONNECTION\_INIT\_MAX\_TIME* of the DSP code).

When the embedded device receives the acknowledge, it sends the *Connection acknowledge 2* frame, and enters the main cycle of the process. By receiving this acknowledge, the laptop can also enter its main procedure.

### Connection maintenance

Once the connection is established, each device has to inform the other one that it is still running by sending a *Connection check* frame at least every 2 seconds. This interval can be modified with the constant *CONNECTION\_CHECKED\_MAX\_TIME* in the DSP code and in the control application code. If this frame is not received for more than two seconds on one side or the other, the corresponding program will perform a full software reset, i.e. return to the connection initialization procedure.

Over this frame exchange, the transmission of the results, the status, or the command, can take place.

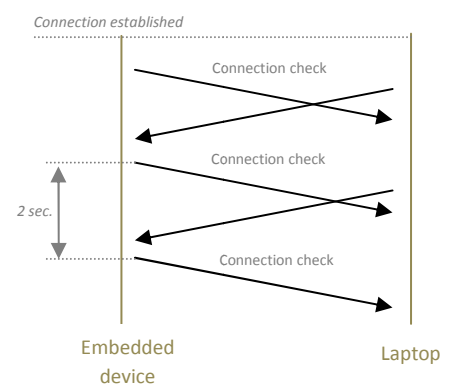


**Figure 43**  
Connection maintenance principle

### 3.3.7 Control application

The application running on the remote control laptop has been developed in *VisualBasic.NET* language, completed by an additional development tool (*Measurement Studio 8.1.2, National Instruments*) that potentiates the graphical capabilities of the application. The environment used was *Visual Studio 2005*.

In order to maintain the highest grade of readability and coherence, and to avoid any errors, all the variables and constant values that have the same name on both the DSP code and the control application represent the same thing. For example, the last byte of the SOF symbol for a blood flow frame is the hexadecimal value 10. It is declared as a constant on both sides under the name *SOF\_BYTE\_3\_BLOOD\_FLOW\_FRAME*. The constant values particularly have to be similar on both sides, otherwise some issues can occur.

The purpose of the control application is to control the embedded device, to display its status and to display the results of the measurements. As a matter of programming, it doesn't have any particular feature that requires an explanation in deep. The following part shows how it is designed and what it offers to the user.

#### Connection window

The program starts by opening a connection window, which is responsible to monitor the evolution of the connection initialization procedure. It is shown in figure 44.

The connection is composed of two different parts. The first one called *Bluetooth serial port* has to be used in order to open the COM port that allows the application to communicate with the remote device through *Bluetooth* and the SPP profile. The COM port number has to correspond with the one that the *Bluetooth* manager of the computer attributed to the connection with the *Parani-ESD200*. The second part called *Astronaut measurement system* takes place once the COM port has been successfully opened, and waits for the *connection initialization* frame to be received, before continuing the known procedure explained in the previous section.

An optional window can be opened by clicking on the button *serial port settings*, which allows changing the COM port main parameters such as baudrate, parity, etc.

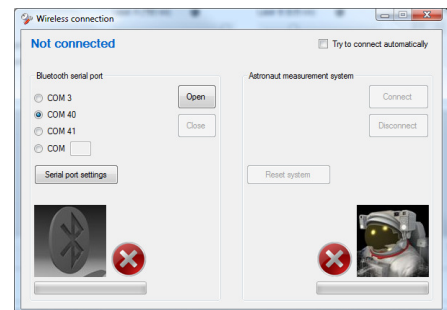


Figure 44  
Connection window of the remote control application

#### Main window

Once the connection is established, the connection window disappears and the main window is loaded. It is made of the four tabs *general*, *blood flow*, *pulse oxymeter* and *lasers control*, as shown in figure 45.

The tab *general* offers an overview of the state of the system, as well as the main results of the current measurement if one is running. The section *measurement type* permits to select the desired measurement; only the *blood flow* and *pulse-oxymeter* have been developed so far, the *alternate* and *simultaneous* measurements are basically a combination of the other two. The section *Laser's power* offers to control the output power of the lasers, and a LED lights in green when the corresponding laser is ready to operate (temperature ok). The third section *Signal* shows the voltage output of the photodiode when a measurement is running. The voltage regulation has not been developed yet.

This tab also contains the graphs of the *blood flow* and the *pulse-oxymeter*. To run, stop or pause a measurement, the user just has to click on the corresponding buttons on the right of the desired graphic. Such an operation will send a command to the remote device and, in this case, use the state machine developed in the DSP.

The bottom of the *general* tab shows, on the left, the elapsed time since the beginning of the measurement. In the middle, an optional function offers to store the measurement in a *.txt* file. In order to do so, the user just has to select a folder where to save the file, to type the desired name in the case, and to select the checkbox. The file will be created once the *play* button is clicked, and closed after the measurement is stopped. This file can afterwards easily be exported in an excel file in order to generate the graphics corresponding to the collected numerical values.

The two tabs *blood flow* and *pulse oxymeter* offer deeper views related to those measurements. For instance, the *blood flow* tab also contains the *blood volume* and *blood velocity* values.

Finally, the *lasers control* tab permits to select the main laser. This laser corresponds to the one that is used for the laser Doppler flowmetry. The pulse-oxymetry always requires the two lasers. If an external laser is used, the laser C has to be selected; in this case, the processing board will not perform a temperature test on the laser before starting the measurement, since the laser is not connected to the system.

Finally, a blue synchronization symbol on the right bottom lights in green or red everytime a command is sent. For instance, if the user clicks on the *play* button in order to start a blood flow measurement, and that the main laser is not ready (warm-up not completed for instance), the program will show that it refused the command by a red circle placed on this icon. If the measurement can start, a green circle will appear. In any case, it disappears after three seconds.

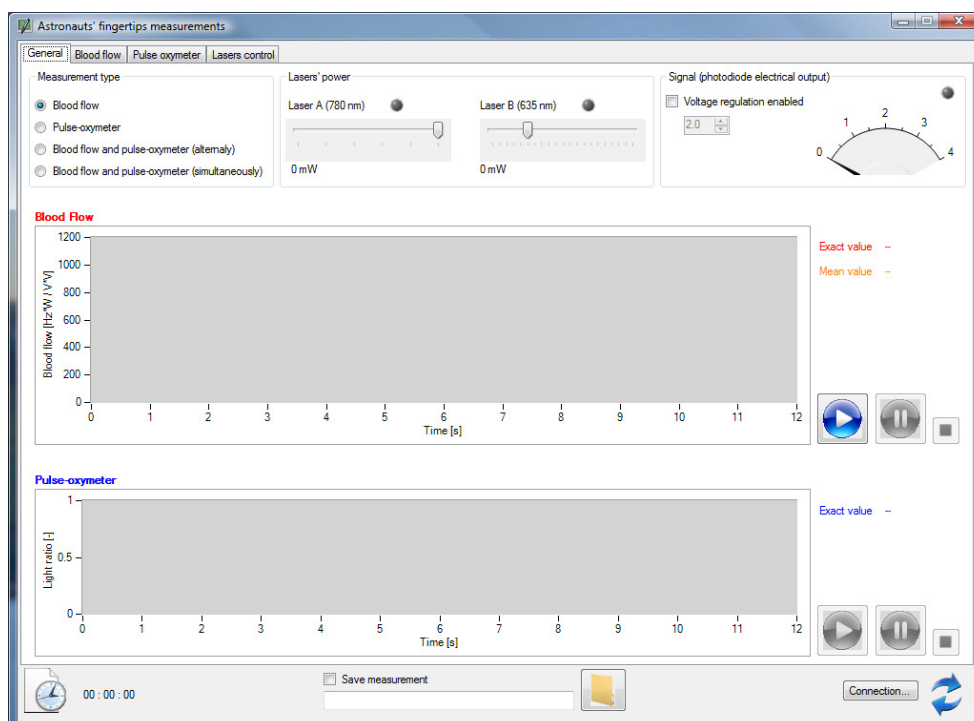


Figure 45  
Main window of the control application

## 4 CHARACTERIZATION OF THE SYSTEM

Now that the system has been developed and assembled, several tests have to be performed on it in order to guarantee that its operation will take place as expected. Most of these tests are related to the processing board.

### 4.1 CHARACTERIZATION OF THE ELECTRONIC PART

All the input signals are generated by function generator **E**.

#### 4.1.1 Voltage conversions and regulation

This section is dedicated to the tests performed on the different voltage levels of the board, in order to make sure that they are generated or regulated properly.

##### ± 15V DC/DC conversion

Instr.	Comp.	Meas. point	Expected value	Meas. value	Test passed	Comments
<b>B</b>	U2	U4 in.	+15V	+15V	✓	Figure 46 shows an oscillation of ±80mV due to the switching conversion.
<b>B</b>	U3	U5 in.	-15V	-15V	✓	

##### 3.3V, +12V, -12V regulations

Instr.	Comp.	Meas. point	Expected value	Meas. value	Test passed	Comments
<b>B</b>	U1	U1 out.	3.235..3.365	3.28 ±25mV	✓	
<b>B</b>	U4	U4 out.	11.4..12.6V	12V ±30mV	✓	Figure 12 shows the stability of this regulated voltage
<b>B</b>	U5	U5 out.	-11.4..-12.6V	-12.1V ±25mV	✓	

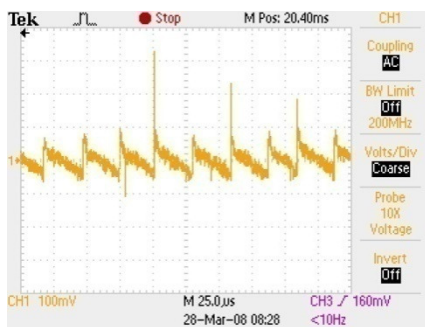


Figure 47  
Pulsed +15V voltage generated from DC/DC



Figure 46  
Stability of the regulated 12V voltage



### 4.1.2 Signal conditioning

This section shows the tests performed on the different components of the signal conditioning chain, in order to verify their correct behavior and to measure the real effect that they have on the signal (real gain of the amplifiers for instance).

#### Instrumentation amplifier (U7)

Instr.	Input	Expected value	Meas. point	Meas. value	Test passed	Comments
B	$\sin(2\pi \cdot 37\text{kHz} \cdot t) - 1.5\text{V}$ CH1, yellow	$-\sin(2\pi \cdot 37\text{kHz} \cdot t) + 1.5\text{V}$	U7 V <sub>o</sub>	$-\sin(2\pi \cdot 37\text{kHz} \cdot t) + 1.5\text{V}$ Gain = $-1.06/1.01 = -1.05$ CH2, blue	✓	Figure 48 shows result with osc. in AC-coupling

#### Voltage limitation (D6, D7)

Instr.	Input	Expected value	Meas. point	Meas. value	Test passed	Comments
B	$3 \cdot \sin(2\pi \cdot 37\text{kHz} \cdot t) + 2\text{V}$	Saturation at 3.6V and -0.25V	U7 V <sub>o</sub>	Saturation at 3V and -0.4V	✓	See Figure 49

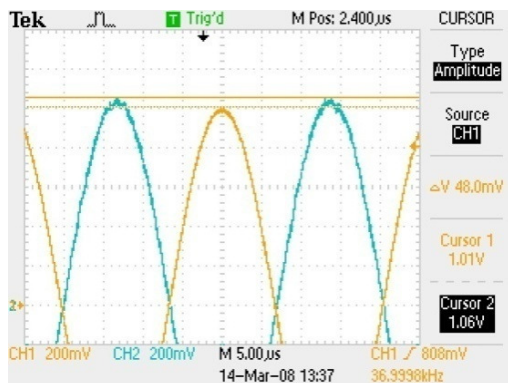


Figure 49  
Input and output of instrumentation ampl. U7

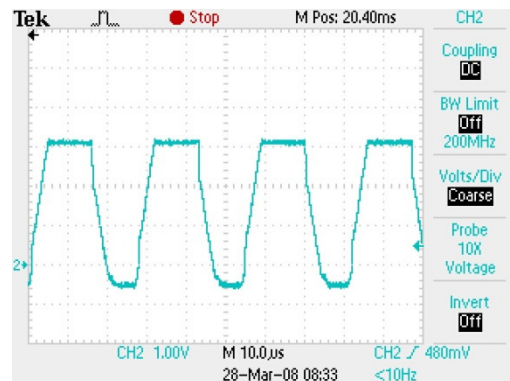


Figure 48  
Test of voltage limitation of the signal

#### Anti-aliasing filter (U8)

Instr.	Input	Expected value	Meas. point	Meas. value	Test passed	Comments
B	White noise	Cutoff freq. at ~45kHz	U8 out	Cutoff freq. at ~25 kHz	✗	See Figure 50

The cutoff frequency is not at ~45 kHz as expected, and the result obtained cannot be accepted since it will cut out a portion of the signal that is required for the processing. After several tests by changing the value of the capacitor  $C_{22}$ , a cutoff frequency of ~48 kHz has been achieved with a capacitor of 3 pF. However, according to the datasheet of the MAX295, it would mean that the internal clock of the component is

working at 11.1 MHz, but this frequency should not be higher than 2.5 MHz, which cannot be accepted. Moreover, it has been noticed afterwards that this component added so many noise in the signal that the result of the LDF measurements were clearly affected (measurement unreadable because of the noise).

The only solution at this stage is to bypass this component. For further development, it will be replaced by a passive filter.

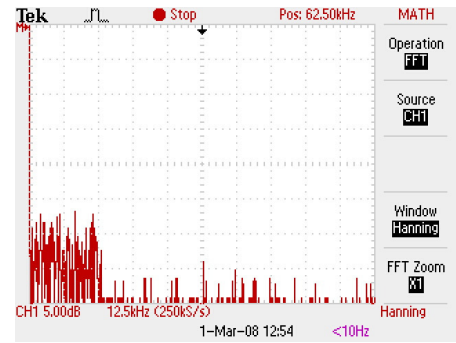


Figure 50  
Frequency analysis of the filter's output when a white noise is applied at the input

High-pass filter (U9)

This component requires a long delivery time and is not available yet, despite it has been ordered in early January 2008. Therefore, this part has to be bypassed, and the LDF algorithm will be processed after a *DC-coupled acquisition* in the mean time.

Low-noise amplifier (U10)

Since the high-pass filter is not operational yet, the values of  $R_{17}$  and  $R_{18}$  have been temporarily changed both to 5.11 k $\Omega$ , so that the theoretical gain of this amplifier is 2.

Instr.	Input	Expected value	Meas. point	Meas. value	Test passed	Comments
B	$-\sin(2\pi \cdot 37\text{kHz} \cdot t) + 1.5\text{V}$ CH2, blue	$-2 \cdot \sin(2\pi \cdot 37\text{kHz} \cdot t) + 3\text{V}$	U10 1	$-2 \cdot \sin(2\pi \cdot 37\text{kHz} \cdot t) + 3\text{V}$ Gain = $2.1/1.06 = 1.98$ CH3, purple	✓	Figure X shows result with osc. in AC-coupling

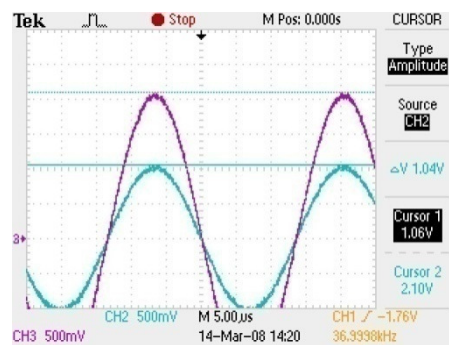


Figure 51  
Test of pre-conversion amplifier

Finally, the real gain calculated for  $U7$  and  $U10$  can be integrated in the DSP's code in order to improve the reliability of the measurement: by changing the constant values  $G_{IA}$  and  $G_A$  with the real gain, the calculation will take these values into account when it numerically reconstructs the signal during the process.

## 4.2 CHARACTERIZATION OF THE SOFTWARE PART

### 4.2.1 A/D acquisitions

This section is dedicated to verify that both internal and external A/D converters work at the desired sampling frequency of 100 kHz, and that they return the correct numerical representation of the samples in the DSP.

First, by using an auxiliary digital output that was driven by the A/D acquisition (*ADC1 interrupt*) and measuring its switching frequency with the oscilloscope, it has been verified that the signal was truly sampled at 100 kHz.

Then the conversions have been verified. The results that the DSP acquisition writes within its variables have been reported in the table below. *PORTD* is the 16-bit result of external A/D and *ADC1BUF0* is the 12-bit result of internal A/D.

Input	External A/D				Internal A/D			
	expected	measured	Measured [V]*	pass.	expected	measured	Measured [V]*	pass.
0V	0	4	$1.22 \cdot 10^{-3}$	✓	0	3	$2.42 \cdot 10^{-3}$	✓
0.5V	1'638	1'629	$497.13 \cdot 10^{-3}$	✓	621	615	$495.48 \cdot 10^{-3}$	✓
2V	6'554	6'570	2.005	✓	2'482	2'465	1.986	✓
3V	9'830	9'838	3.002	✓	3'724	3'718	2.995	✓
6V	19'661	19'665	6.001	✓	(out of range)			
-5V	49'152	49'139	-4.996	✓				

\* the transformation to this column is done by multiplying the integer value by the resolution of the converter

### 4.2.2 FFT computation

#### Frequency analysis

The first test performed in order to make sure that the FFT behaves properly has been to generate the samples of a known signal with *Matlab* and to perform an FFT on it, just like if it would have been sampled by the external A/D converter, and to watch the result. The *Matlab* program used is shown in appendix 15.

The signal that has been generated is the following:

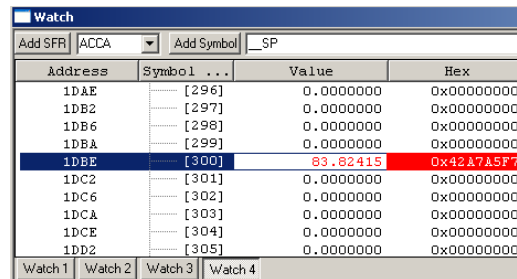
$$y = 30'000 \cdot \sin(2\pi \cdot 2'400 \cdot t)$$

at a sampling frequency of 8'192 Hz. The base-frequency of the sinusoid was 2'400 Hz and its amplitude was 30'000. Therefore,  $y$  corresponds to the integer value that is binary represented in the buffer of the converter before the program uses it.

Since the external A/D converter is used, this amplitude corresponds of  $30'000 \cdot 305.176 \mu V = 9.155 V$ . Therefore, according to the FFT theory, the expected result is a spectrum with the amplitude of 0 everywhere, excepted at the index corresponding to the base-frequency of this sinusoid, where  $Amp^2$ , that represents the power of the signal, is the amplitude of the sinusoid squared:  $Amp^2 = 83.81 V^2$ . The index corresponding of this frequency has to be calculated from the sampling frequency and the block length (which is 1'024 here):

$$\Delta f = \frac{8'192}{1'024} = 8 \text{ Hz} \quad \text{index} = \frac{2'400}{\Delta f} = 300$$

Therefore, the value 83.81 should appear at the index 300 of the resulting vector of the FFT. By stopping the DSP process right after the FFT calculation and observing this vector, the observation is the following:



Address	Symbol	Value	Hex
1DAE	[296]	0.0000000	0x00000000
1DB2	[297]	0.0000000	0x00000000
1DB6	[298]	0.0000000	0x00000000
1DBA	[299]	0.0000000	0x00000000
1DBE	[300]	83.82415	0x42.17A5F7
1DC2	[301]	0.0000000	0x00000000
1DC6	[302]	0.0000000	0x00000000
1DCA	[303]	0.0000000	0x00000000
1DCE	[304]	0.0000000	0x00000000
1DD2	[305]	0.0000000	0x00000000

Figure 52

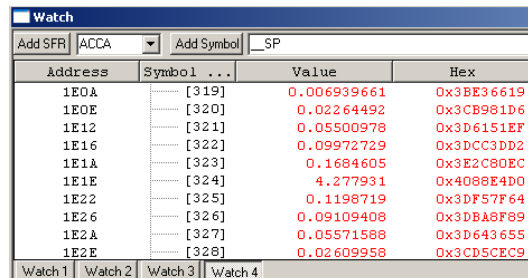
Watch window of MPLAB showing the resulting FFT vector after injecting a simulated signal

$Amp^2$  is here 83.824, which is satisfactory and proves that the result obtained is scaled.

The second test performed on the FFT process has been done with a real signal generated by the function generator  $E$ , which has been applied at the input of the external A/D converter. The signal used is:

$$y = 2V \cdot \sin(2\pi \cdot 31'641t) + 2.5V$$

The sampling frequency is now the nominal one (100 kHz) since the converter itself samples it. By repeating the same process as before, the FFT should return  $Amp^2 = 4V^2$  at the index 324. After the calculation has been performed, the resulting vector is partially:



Address	Symbol	Value	Hex
1E0A	[319]	0.006939661	0x3BE36619
1E0E	[320]	0.02264492	0x3CB981D6
1E12	[321]	0.05500978	0x3D6151EF
1E16	[322]	0.09972729	0x3DCC3DD2
1E1A	[323]	0.1684605	0x3E2C8DEC
1E1E	[324]	4.277931	0x4088E4D0
1E22	[325]	0.1198719	0x3DF57F64
1E26	[326]	0.09109408	0x3DBA8F89
1E2A	[327]	0.05571588	0x3D643655
1E2E	[328]	0.02609958	0x3CD5CEC9

Figure 53

Watch window of MPLAB showing the resulting FFT vector after injecting a known electrical signal

$Amp^2$  is here 4.278  $V^2$ . The difference of 7% compared to the theoretical value of 4  $V^2$  can be explained by the fact that the electrical signal is not as precise as the Matlab simulation, and is affected by the noise added in the system, such as the sampling noise for instance. This also explains why the values nearby the main peak are not 0 as in the ideal case described in the previous test.

### Processing time

The second feature to test is the time that the FFT requires to process the whole block of data, more particularly the time that the entire LDF processing requires. By using an auxiliary digital output and the oscilloscope, it is possible to measure how this processing is divided over the time. Table 24 shows the result of this measurement for the parts of the process that require a significant time:

<b>LDFProcessing()</b>	<b>21 ms</b>
<i>doFFT_asm</i>	<i>4 ms</i>
<i>Noise calculation</i>	<i>1 ms</i>
<i>Integrals calculation</i>	<i>16 ms</i>

**Table 24**  
Timing of the LDF processing

This measurement answers to the uncertainty that have been mentioned at the beginning, when it has been chosen to use this DSP for this application (section 3.2.4). It was not possible to know in advance if it would be able or not to compute the LDF processing in less than 10.24 ms (the required time to fill a buffer of 1'024 samples at a sampling frequency of 100 kHz).

The FFT itself (*doFFT\_asm*) is actually quite fast to be executed (4 ms). Most of the time is spent to calculate the integrals, which is a loop of 357 iterations that computes several multiplications and divisions on 32-bit float values. Since the acquisition takes 10.24 ms and the processing takes 21 ms, all the data cannot be analyzed: some of them have unavoidably to be skipped, therefore about half of the data only are processed.

This code has been carefully written so that it is the fastest achievable in C-programming language. A way to optimize it would be to develop it in assembler, but it is a long job without any guarantee of the results.

### 4.2.3 Lasers control

#### Turning on/off

The digital signals responsible to turn on/off the lasers are easy to manage, but their correct behavior has been verified since a bad functioning by interfacing the lasers could result in quite important damages.

#### Power control

The analog voltages at the outputs *Laser X power* of the board have been verified by using the function *SetLaserPower* and several power parameters. The outputs work accordingly to the table 4 and are perfectly stable when no power change is requested.

#### 4.2.4 Wireless transmission

The wireless transmission between the DSP and the laptop has been tested by generating several known trigonometric functions in the DSP, and by sending them to the laptop (*VisualBasic.NET* application) and the protocol developed for this purpose. This allows determining if the values are correct, if they are displayed in real-time, and if the system is able to work tenths of minutes without interruption. Figure 54 shows a part of the test viewed from the laptop screen. Everything has been successfully passed.

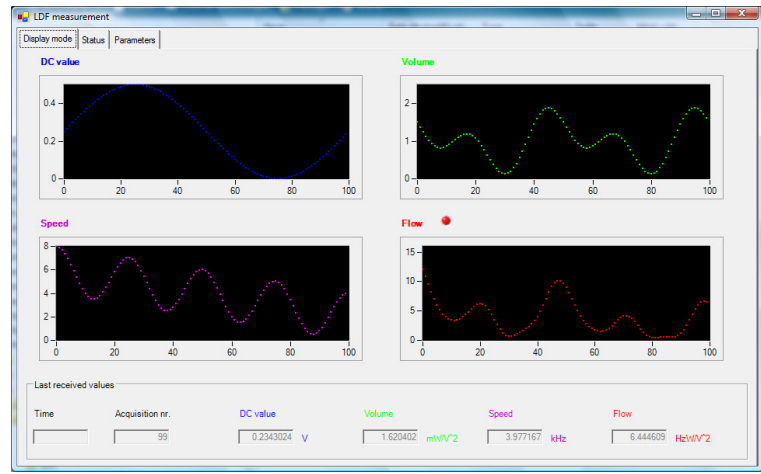


Figure 54  
Wireless transmission test with several trigonometric functions

### 4.3 CHARACTERIZATION OF THE OPTICAL SET-UP

#### 4.3.1 Photodiode

The system has been designed with the photodiode powered by the board. It requires the three voltages of -12V, 0V, and +12V. An output of the processing board is dedicated to that.

As shown in the voltage tests section (4.1.1), the  $\pm 12V$  voltages are very stable and work properly. However, by powering the photodiode this way, it has been noticed that some changes occur in the photodetected signal. During a measurement, or a test such as the one performed in section 3.1.4 and by powering the photodiode from the board, the output signal is the following:

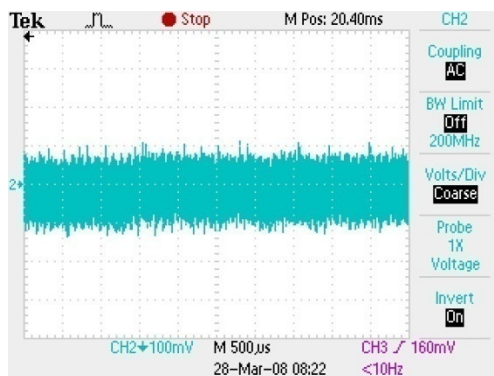


Figure 55  
Photodetected signal when photodiode is powered by the processing board

Compared to the expected signal that contains the frequencies shift, this one cannot be processed. It contains a lot of noise due to the board power supply. In fact, when the photodiode is powered by an external power supply such as the laboratory power supply, the signal is not affected by such a noise. However, the board itself can use its own  $\pm 12V$  supply without any problem, as will show the section 4.4.

### 4.3.2 Miniaturized probe

The miniaturized probe has been totally mounted, however it has not been possible to characterize it and make it operational yet: some lasers issues occurred at this time, what made this work unrealizable. However, the first observations done on the power spectrum that it returns by emitting and collecting the light to/from a finger are promising.

## 4.4 FIRST MEASUREMENTS

After the development, the mounting and the characterization of the system, it is necessary to assess if the data can be acquired by performing a real measurement. For this purpose, some alternatives have been considered since the system is not fully operational yet.

This experiment consists of the measurement of the blood circulation (*blood volume, blood speed and blood flow*) on a subject. The original set-up of the system (section 3.3.1) has been modified as follows:

- The anti-aliasing filter *U7* has been bypassed since it was not filtering at the desired cutoff frequency, and moreover it added some noise in the signal
- Since the signal conditioning cannot cut out the static component of the signal yet (component *U9* not available), this functionality is not used and the measurement is performed started from the *DC-coupled acquisition* of the signal, which obviously offers a lower resolution.
- Since it has been observed that the photodiode doesn't return a useful signal when powered by the processing board, it is supplied by the power supply *A* (see appendix 2).
- The new miniaturized probe is not operational yet, therefore the original *clip-probe* has been used with the two corresponding fiber optics. Moreover, since this experiment consists of measuring the LDF parameters only, the fiber combiner is not necessary (1 laser source is enough) and doesn't take place in the system here.

Therefore, the configuration used in this experiment can be represented by figure 56.

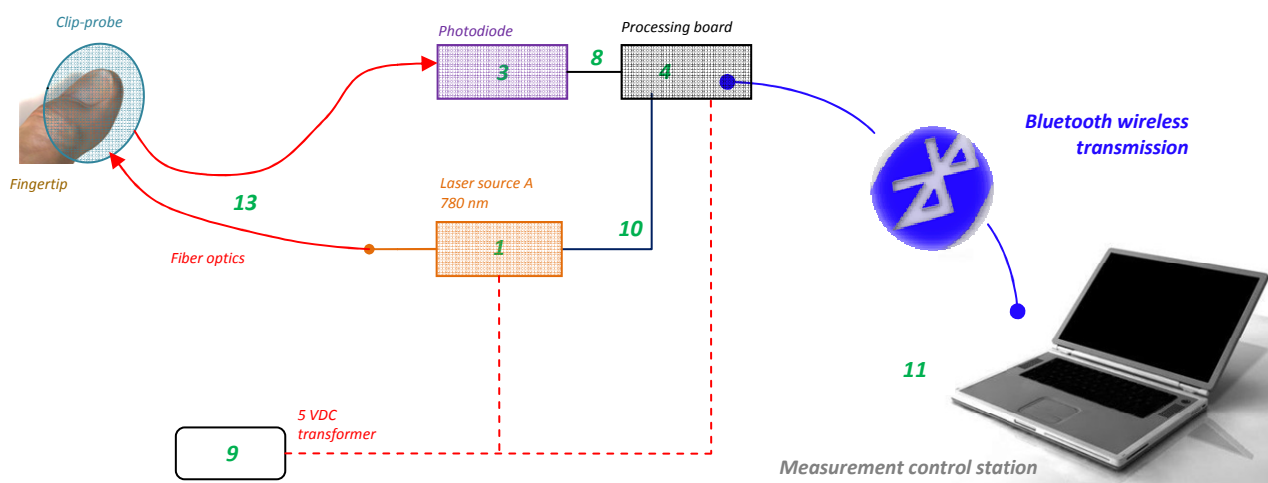


**Figure 56**  
Temporary set-up of the system for this experiment



Landmark	Device
1	Laser source A, 780 nm
3	Photodiode
4	Processing board
8	BNC cable
9	5 VDC transformer
10	Connection cable
11	Laptop
13	Fiber optics

Table 25

Caption of the figure 56. Refer to appendix 7 for detailed description of the devices

During this experiment, the subject stayed still on a chair for several minutes. The acquired data are shown in figure 57.

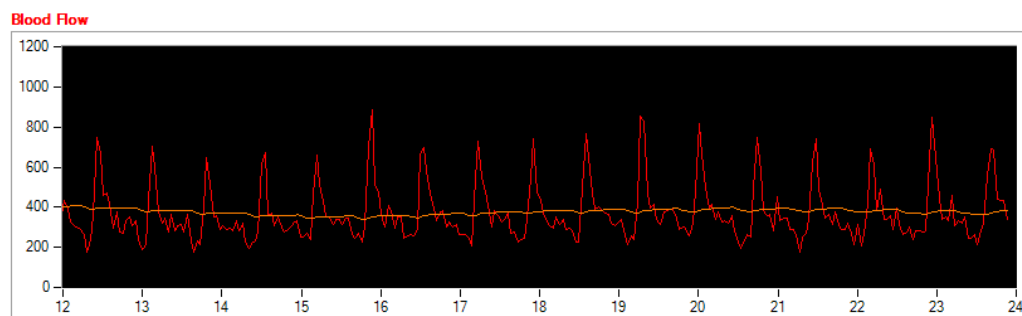


Figure 57

Measurement of the blood flow on a subject staying still. The horizontal axis represents the time in seconds, the vertical axis represents the blood flow in  $[\text{Hz}\cdot\text{W} / \text{V}^2]$ . The red points are the dynamic value of the blood flow, and the orange points are the averaged value of the blood flow.

After several minutes of experiment where the patient stayed still, it has been noticed that the mean value of the blood flow (orange line in the graphic above) kept the same level, meaning that the blood flow is constant (which makes sense in this situation). The red line clearly represents the dynamic of the blood flow and it is easy to recognize the heart beats at a regular frequency of  $\sim 1.4$  Hz (about 85 pulsations per minute), which is an acceptable value for a healthy subject.

The noise added to the dynamic of the signal is due to the resolution of the acquisition that is quite low because of the following parameters:

- The signal sampling is done on the DC-coupled signal, at 100 kHz with a low resolution of  $805.66 \mu\text{V}$  (the old system was sampling at 242 kHz with a resolution of  $30.5 \mu\text{V}$ )
- The FFT is computed on blocks of 1'024 samples, which gives a spectrum resolution of 97.65 Hz at this sampling frequency (the old system was computed blocks of 16'384 samples, thus the spectrum resolution was 14.77 Hz)

- Even though the DSP uses the maximum of its performances, it is processing about half of the data only (processing the LDF data on one block of samples requires more time than acquiring a block of data)

However, this first result is promising since it is representative of the desired parameter of the human body. The fact that the precision of this acquisition is lower than the one of the existing system [3] explains the presence of noise in the result.

Another thing that has to be mentioned is that the result is significant despite the fact that only half of the data are processed: the explanation is that the evolution of the blood flow during the time (its regular increases and decreases during a "cycle" of heart beat for instance) still occurs at a lower frequency than the natural variations of the blood flow. Actually, a group of LDF results is returned every 21 ms, which is enough to represent the blood flow behavior even in real-time.

As mentioned during the development, it was difficult to predict if the DSP used would be able to work fast enough to compute all the data, therefore it was necessary to develop a system in order to find out that. As shown here, the result is satisfactory, but it can be improved so that all the data are processed, if possible with a better resolution. This will improve the quality of the result (less noise), but the range of value will still stay the same. Refer to the last chapter for further suggestions about the possible improvements and further development.

In order to test the sensitivity of the system, two other simple tests have been done on the same subject, right after the measurement when the subject stayed still. In the second one, the measurement started when the subject was in the same position as in the first test. Then it slowly raised its arm until his hand is at the same high as the head. The result is shown in figure 58.

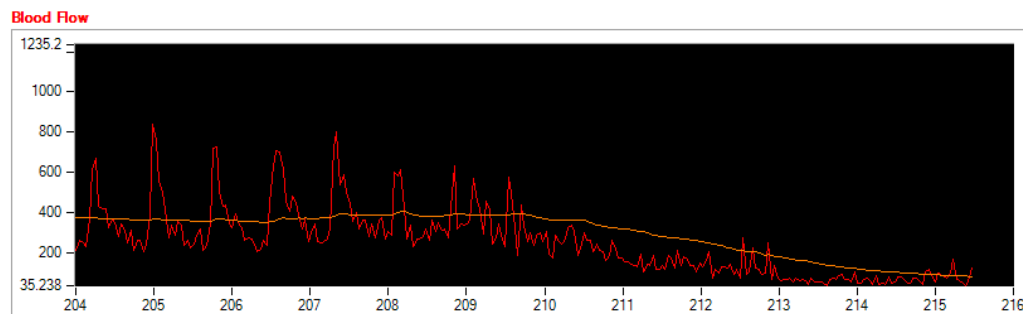
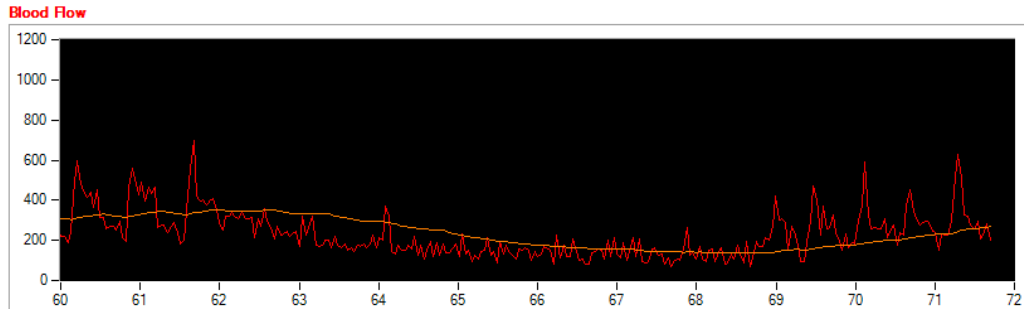


Figure 58  
Measurement of the blood flow on a subject raising his arm.

The observation is that the beginning of the measurement (from 204 sec. to 208 sec.) is comparable to the first measurement when the patient stayed still. The baseline is still the same, about  $400 \text{ Hz}\cdot\text{W}/\text{V}^2$ . Then the blood flow clearly decreases down to a mean value of about  $80 \text{ Hz}\cdot\text{W}/\text{V}^2$  when the subject raises his arm, which makes sense since it becomes more difficult for the heart to pulse the blood in such a situation for the body.

The third test was to perform an occlusion on the forearm thanks to a pressure cuff. The subject is in the same position as in the first test, and doesn't move. Then the pressure cuff is inflated so that the circulation of the blood in the arm is occluded, and released a few seconds after. The result is shown in figure 59.



**Figure 59**  
Measurement of the blood flow on a subject by occluding the blood circulation in the arm with a pressure cuff.

It is recognizable that the occlusion started at about 62 sec. and was released at about 69 sec. The blood flow decreased of more than 50% in this case.

Generally speaking for these two last measurements, it is not necessary to quantify the blood variations precisely since the influence that raising the arm or occluding the forearm cannot be quantify as well, i.e. it is not possible to establish a relationship between the cause and the effect. However it shows that the behavior of the system is promising. An important collection of data with several experiments on different subjects have now to be done in order to quantify the sensitivity of the system, and to see what are its strengths and weaknesses.

Finally, the pulse-oxymeter has not been tested yet since some issues with the lasers occurred at this time. The engineering has been totally done for this application: the board can control the two required lasers, the DSP can process the corresponding data, and the control application can display them. The optical probe has to be characterized; particularly the fibers combiner has to be tested in order to make sure that the power loss in this element is acceptable. If positive, it will be possible to run the measurement and to evaluate the results without any other modification.

## 5 CONCLUSION AND FUTURE DEVELOPMENT

### 5.1 SUMMARY

Starting from a project [3] that consisted of a computer-based system able to measure the blood flow in the fingertip using the laser Doppler flowmetry principle, a new miniaturized system was developed. The main part of the work has been focused on the development of a small electronic board, the *processing board*, that actually replaces the computer of the previous project and accurately performs the same measurement as the previous system. A new miniaturized probe has been designed and created, and the optical configuration has been partially modified.

This new system cannot be fully embedded in the astronaut's suit yet since it still requires an external power supply, and some parts of it are still too voluminous. However, its peculiar set-up makes it a very interesting model for this purpose because of the following reasons:

- The new miniaturized probe can be integrated in the astronaut's glove and connected with the rest of the system through fiber optics, which offers the possibility to place the rest of the system in another part of the suit. The fiber optics core, cladding and outer jacket provide enough flexibility to deal with small radius.
- The "brain" of the system, made of the photodiode and the processing board, is still a prototype version but takes up a volume of 120 cm<sup>3</sup> only. Further miniaturization only requires the re-design of the same electronics with smaller components, smaller connectors and multi-layers printed circuit board.
- The power consumption of the whole system is about 4.4 Watts; thus it can be powered by a battery or from the astronaut's suit power system. Moreover, this value can be further reduced by using smaller lasers.
- The wireless transmission feature using the *Bluetooth* technology provides no physical connection with the remote control laptop that controls the embedded system and displays the results. Therefore, the use of this system doesn't affect the mobility.

The electrical characteristics of the system were tested in detail, and most of the features are working accurately. The parts that require some improvement are known and discussed in the next section.

The table 25 below summarizes the technical features of the system:

<b>Optical part</b>	
Laser wavelength (LDF)	780 nm
Laser wavelength (pulse-oxymetry)	635 nm
Lasers max. power	Respectively 25 mW and 20 mW
<b>Electrical part (processing board and photodiode)</b>	
Outer dimensions	80 x 50 x 30 mm
Operating voltage	5 VDC
Power consumption	< 2 W
Wireless transmission system	<i>Bluetooth</i> with a baudrate of 57'600 bit/s
Signal processing characteristics	Computes blocks of 1'024 samples with a sampling freq. of 100 kHz

**Table 25**  
Technical features of the system

## 5.2 KNOWN WEAKNESSES AND PROBLEMS

This section summarizes the parts or features of the system that are only partially or not operational yet. The test phase has been particularly useful to detect which parts were not working as expected.

- The new miniaturized probe has been fully mounted and its characterization started. However, some laser issues occurred during this phase, which made it not usable for the time being. The first tests performed on the probe showed promising results, but it will have to be put into operation to fully test it as soon as the working lasers are available.
- The electrical part of the system can now be used for pulse-oxymetry measurements, as far as the electrical configuration (laser's control) and algorithm are concerned. Unfortunately, due to the same lasers issues, the optical part has not been characterized yet for this application. The particularity is that it requires the integration of a fibers combiner, which has to be tested before it is used for such a measurement. Once the optical part is ready for this purpose, the tests on the measurement can be performed without any other modification
- The DSP used in this application is not powerful enough to process the data at the required speed. Therefore, only half of the measured signal is analyzed during the LDF procedure. In addition to this, the resolution of the acquisition is quite low compared to the existing system (computation of blocks of 1'024 samples at 100 kHz sampling frequency instead of blocks of 16'384 samples at 242 kHz in the existing system). However, the results obtained despite this weakness are promising and encouraging to carry further development on the measurement system.
- In the signal conditioning part, the switched-capacitor anti-aliasing filter *U7* doesn't work properly, even after several tests. The real cutoff frequency value is far from the expected value that the calculation returns, and even when the good cutoff frequency is achievable, the filter adds a lot of noise to the further conditioning circuit. The use of a passive filter could solve this problem, but so far it has been bypassed.

- The developed signal conditioning (and processing) consisting of performing two different acquisitions (*DC-coupled* and *AC-coupled*) is not working because the electronic component *U9* is not available yet, despite being purchased a few months ago. It still has to be mounted and characterized.
- The photodiode, when powered by the  $\pm 12V$  of the processing board, doesn't return a useful signal: a lot of noise is added, even though the  $\pm 12V$  regulators of the circuit board work properly. As a temporary solution, a laboratory power supply has been used.

### 5.3 IDEAS AND FURTHER DEVELOPMENT

This final section contains suggestions and directions to enhance the performances of this system or to start the development of a new one based on a similar principle.

- An interesting and useful task would be to perform some relatively important measurements in order to define the sensitivity, weaknesses and performance of the system. It would be good to test both the LDF and the pulse-oxymetry measurements (once operational) first with the *clip-probe*, and then with the new miniaturized probe. In order to acquire useable values, a protocol has to be defined and repeated on several subjects. Among other things, the effect of the experiment has to be quantifiable; for instance, considering that an experiment with an occlusion on the forearm is done by means of a pressure cuff, the pressure in the cuff has to be known at any time and afterwards compared with the results of the measurements in order to establish a cause-effect relationship. Some interesting experiments could be based on temperature variations of the finger, occlusions at different pressures, repetitive movements, same tests on different fingers, etc.
- So far, the system returns LDF values with "electrical" units, such as  $\text{Hz}\cdot\text{W}/\text{V}^2$  for the blood flow. However, this parameter should scientifically be expressed in  $\text{ml}\cdot\text{g}/\text{min}$ . The transformation from the electrical unit to the real one can be done by multiplying the actual result by a calibration factor and eventually adding an offset. For this purpose, it is necessary to calibrate the system from a non-turbulent and known flow, compare the results the system returns, and establish the relationship in order to extract the corresponding calibration factor
- As mentioned in the previous section, the actual DSP is not powerful enough to process the whole data. In addition to this, the resolution of the measurement is quite low, but it already offers good enough sensitivity to prove that such a concept is realizable, according to the first results. However it will be necessary, for further development, to increase the resolution of the measurement in terms of length of blocks for the FFT processing (related to the memory that the DSP offers), sampling frequency (it could be interesting to reach a sampling frequency of 200 kHz which is close to the existing system), and to process all the data. For this purpose, the only possibility is to use another device. The *dsPIC33F* from *Microchip* that is used in this system is the most powerful DSP this manufacturer provides; therefore it is not possible to simply replace it by another one and to transfer the same code inside it. After some researches, a device able to satisfy the requirements of such a calculation has been found: it's about a floating-point digital signal processor *TMS320C6713B* from *Texas Instruments*. Of course, this is just a suggestion and it would be advisable to compare it with other similar products in order to make the best choice for this component.

- In order to achieve the miniaturization of the system, the next step would be to integrate the photodiode module and the processing board in one single circuit board, in order to save more space. Actually, the processing board already reached the same size as the photodiode module (80 x 50 mm), that's why it doesn't make any sense to reduce its size again since the photodiode module requires this space. For this reason, it is not necessary to work on the problem related to the fact that the photodiode module cannot be powered by the processing board (add of noise): the new electronic design might be different and solve this problem by itself. If not, then some considerations will be needed.
- Parallel to the further development of the electronic part of the previous point, the miniaturization of the lasers have to be considered as well. So far, it is not necessary to design customized lasers, but bearing in mind the need to do some tests with the whole system embedded in the astronaut suit in the next future, it is necessary, in order to save time and money, to think about which lasers model are available in a miniaturized version, so that the corresponding electrical interface responsible of controlling them can be developed on the board along with the future design.
- Finally, a point that has to be discussed for a future electrical design, is how the system will be powered once it is embedded. An option could be to use a battery, which has the disadvantage of increasing significantly the required space, and will limit the operating available time of the system. The second option, that seems more appropriate, is to use the already existing supply provided by the astronaut's EMU power system. If the power requirements of the system, which are quite low, can be satisfied by the EMU, the next system, even if it is not fully integrated in the suit, can already be designed with the correct operating voltages, which is a critical point according to the behavior of the photodiode when powered by the board: this kind of problems are unpredictable but can definitely affect the functioning of the system, making it useless, that's the reason why they have to be considered as early as possible.

Houston, March 31<sup>st</sup> 2008

Mikaël Rodriguez



## REFERENCES

- [1] H. Geiser, Fabrice Moret and Charles E. Riva  
**Helmet-mounted choroidal laser Doppler flowmeter**  
*Institut de recherche en ophtalmologie, Sion (Switzerland), 2001*
  
- [2] Alexander Joel D. Alon, Rafat R. Ansari, Jennifer D. Kirsop and Kwang I. Suh  
**A pilot study for using non-invasive laser Doppler flowmetry for in-vivo blood flow measurements**  
*NASA Glenn Research Center, Cleveland (Ohio), 2004*
  
- [3] Roberto Venetz  
**In-vivo blood flow measurements in distal fingertips using non-invasive laser Doppler flowmetry**  
*NASA Glenn Research Center, Cleveland (Ohio), 2006*
  
- [4] A.P. Shepherd and P.A. Oberg  
**Laser Doppler blood flowmetry**  
*Kluwer Academic Publishers, Norwell (Massachusetts), 1990*
  
- [5] Roberto Venetz  
**Manual instrument of in-vivo blood flow measurements in distal fingertips**  
*NASA Glenn Research Center, Cleveland (Ohio), 2006*
  
- [6] Robert F. Bonner and Ralph Nossal  
**Principles of laser Doppler flowmetry**  
*A.P. Shepherd and P.A. Öberg, Kluwer, Bosten, 1990*



## ADDRESSES AND CONTACT NUMBERS

**Prof. Martial Geiser**

HES-SO Wallis  
47, rte du Rawyl  
1950 Sion 2  
Switzerland

[martial.geiser@hevs.ch](mailto:martial.geiser@hevs.ch)

**Prof. Gilbert Maître**

HES-SO Wallis  
47, rte du Rawyl  
1950 Sion 2  
Switzerland

[gilbert.maitre@hevs.ch](mailto:gilbert.maitre@hevs.ch)

**Mikaël Rodriguez**

Rue St-Jean 118  
1893 Muraz  
Switzerland

[mikael.rodriguez@bluewin.ch](mailto:mikael.rodriguez@bluewin.ch)

## APPENDIX LIST

Appendix-nr.	Name	Page
1	EVA Mobility unit	79
2	Instrumentation list	81
3	Characterization of the photodetected signal	82
4	Computation of the power spectrum	84
5	LDF algorithm	85
6	IEEE 754 standard	86
7	Components list	88
8	Drawing of the probe's mechanical part	89
9	Electrical scheme of the processing board	93
10	DSP's pinout	95
11	Laser's power control flow chart	96
12	A/D conversions flow chart	97
13	Measurements state machine	98
14	Commands execution and status transmission	99
15	Matlab program for generating a sampled sinus	101

## APPENDIX 1 – EVA MOBILITY UNIT

A single EMU spacesuit is constructed from various tailor-made components produced by over 80 companies. The size of the parts varies ranging from one-eighth-inch washers to a 30 inch (76.2 cm) long water tank. The EMU consists of 18 separate items. Some of the major components are outlined below.

The primary life support system is a self-contained backpack that is fitted with an oxygen supply, carbon-dioxide removal filters, electrical power, ventilating fan and communication equipment. It provides the astronaut with most of the things needed to survive such as oxygen, air purification, temperature control and communication. As much as seven hours worth of oxygen can be stored in the suit's tank. A secondary oxygen pack is also found on the suit. This provides an additional 30 minutes of emergency oxygen.

The helmet is a large plastic, pressurized bubble that has a neck ring and a ventilation distribution pad. It also has a purge valve, which is used with a secondary oxygen pack. In the helmet, there is a straw to a drink bag in case the astronaut gets thirsty, a visor which shields rays from the bright sun, and a camera which records extra vehicular activities. The MSOR assembly attaches to the outside of the helmet. This device (also known as a "Snoopy Cap") snaps into place with a chin strap. It consists of headphones and a microphone for two way communication. It also has four small "head lamps" which shine extra light where needed. The visor is manually adjusted to shield the astronaut's eyes.

To maintain temperature, a liquid cooling and ventilation garment is worn under the outer garment. It is composed of cooling tubes, which have fluid flowing through them. The undergarment is a mesh one-piece suit composed of spandex. It has a zipper to allow for front entry. It has over 300 ft of plastic tubing intertwined within which it circulates cool water. Normally, the circulating water is maintained from 4.4-9.9°C. The temperature is controlled by a valve on the display control panel. The lower garment weighs 3.8 kg when loaded with water.

The lower torso assembly is made up of the pants, boots, brief unit, knee and ankle joints and the waist connection. It is composed of a pressure bladder of urethane-coated nylon. A restraining layer of Dacron and an outer thermal garment composed of Neoprene-coated nylon. It also has five layers of aluminized Mylar and a fabric surface layer composed of Teflon, Kevlar, and Nomex. This part of the suit can be made shorter or longer by adjusting the sizing rings in the thigh and leg section. The boots have an insulated toe cap to improve heat retention. Thermal socks are also worn.

The arm assembly is adjustable just like the lower torso assembly. The gloves contain miniature battery-powered heaters in each finger. The rest of the unit is covered by padding and an additional protective outer layer.

The hard upper torso is constructed with fiberglass and metal. It is where most of the suit pieces attach including the helmet, arms, life support system display, control module and lower torso. It includes oxygen bottles, water storage tanks, a sublimator, a contaminant control cartridge, regulators, sensors, valves, and a communications system. Oxygen, carbon dioxide and water vapor leave the suit through the ventilation



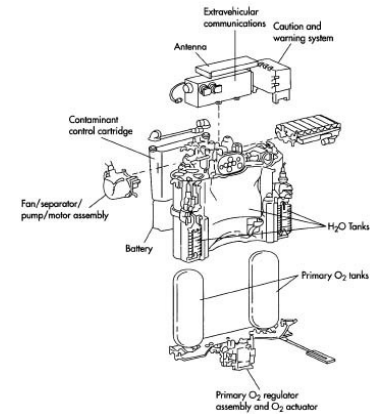
An extravehicular mobility unit (EMU)

garment near the astronaut's feet and elbows. A drinkbag in the upper torso can hold as much as 907.2 g of water. The astronaut can take a drink through the mouthpiece that extends into the helmet.

Chest mounted control module lets the astronaut monitor the suit's status and connect to external sources of fluids and electricity. It contains all the mechanical and electrical operating controls and also a visual display panel. A silver zinc, rechargeable battery which operates at 17 volts is used to power the suit. This control module is integrated with the warning system found in the hard upper torso to ensure that the astronaut knows the status of the suit's environment. The suit connects to the orbiter through an umbilical line. It is disconnected prior to leaving the airlock.

The white suit weighs about 124.8 kg on Earth and has a product life expectancy of about 15 years. It is pressurized to 1.95 kg per square inch and can be recharged by hooking up directly to the orbiter. The existing spacesuits are modular so they can be shared by multiple astronauts. The four basic interchangeable sections include the helmet, the hard upper torso, the arms and the lower torso assembly. These parts are adjustable and can be resized to fit over 95% of all astronauts. Each set of arms and legs comes in different sizes which can be fine-tuned to fit the specific astronaut. The arms allow for as much as a one inch adjustment. The legs allow for up to a three inch adjustment.

It takes about 15 minutes to put on the spacesuit. To put the spacesuit on the astronaut first puts on the lower garment that contains the liquid cooling and ventilation system. The lower torso assembly is put on next with the boots being attached. Next, the astronaut slides into the upper torso unit which is mounted with the life-support backpack on a special connector in the airlock chamber. The waste rings are connected and then the gloves and helmet are put on.



The primary life support system is a self-contained backpack that is fitted with an oxygen supply, carbon-dioxide removal filters, electrical power, ventilating fan, and communication equipment



A partially-unmounted EMU

## APPENDIX 2 – INSTRUMENTATION LIST

Landmark	Instrument	Brand	Model	Description, main features	Serial number
<i>A</i>	Laboratory power supply	Tenma	72-6905	4 channels DC power supply; outputs up to 30V, 3A	0700045
<i>B</i>	Oscilloscope	Tektronix	TDS 2024B	4 channels digital storage oscilloscope	C037453
<i>C</i>	Multimeter	Fluke	179	True RMS multimeter	3529602
<i>D</i>	Laser power meter	Ophir	Nova	High range laser power meter	112222
<i>E</i>	Functions generator	SRS	DS360	Ultra low distorsion function generator	61622

## APPENDIX 3 – CHARACTERIZATION OF THE PHOTODETECTED SIGNAL

### Explanation of the setup shown in figure 14

The *5VDC transformer* and the *laboratory power supply* are powered by the industrial network (110V, 60Hz). They respectively provide a single voltage of 5V to the *control box* and a bipolar voltage of  $\pm 12V$ , 0V to the *photodiode*.

The *control box* is connected to the *laser source* by a DB9 connector and it has to aim to turn on the laser, as well as controlling its power thanks to a potentiometer (controlled by the user).

Two identical *fiber optics* connect the *laser source* to the *clip-probe*, and the *clip-probe* to the *photodiode*. The *photodiode* is finally connected with the *oscilloscope* and the *multimeter* by standard BNC cables and T-connector.

### Technical features of instruments and devices

The *laboratory power supply*, *oscilloscope* and *multimeter* correspond respectively to instruments *A*, *B* and *C* (see appendix 2). The other devices are described below:

Device	Brand	Model	Description, main features	Serial number
<i>5VDC transformer</i>	Phihong	PSA31U-050	Switching AC adaptor; DC output 5V, 4A	P60900339A3
<i>Control box</i>	OZ Optics	OZ-X000-CTRL-BOX	Station for monitoring the temperature of the laser and controlling its power	101070-01
<i>Laser source</i>	OZ Optics	OZ-2000-780-5/ 125-S-40-3S-3A-1-25	Stable laser source, wavelength 780 nm, output power variable up to 25 mW	101068-02
<i>Fiber optics (2x)</i>	OZ Optics	MMJ-31-IRVIS-50/ 125-3-2	2 meters long, 3 mm OD cabled 50/125 IRVIS MM patchcord terminated with a FC/PC connector on one end, 1.8 mm ferrule on the other	a) T895801-01 b) T895801-02
<i>Clip-probe</i>	-	-	Home-made clip-probe from system developed at NASA GRC (see ch. 3.1.1)	-
<i>Photodiode</i>	Hamamatsu	C5460-01	Avalanche photodiode module integrated with peripheral circuits	01724

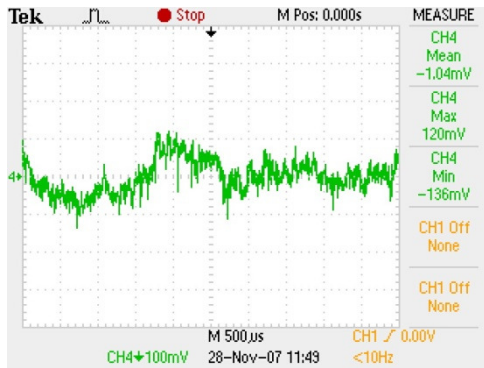
### Protocol and results

Sample	Subject	Laser power	Static component [V]	Dynamic component [mV]
1	Rafat R. Ansari	~18mW	-1.8	-120..+136
2	Rafat R. Ansari	25 mW	-2.3	-224..+272
3	Mikaël Rodriguez	~18mW	-1.5	-132..+96
4	Mikaël Rodriguez	25 mW	-2.0	-256..+196
5	Mikaël Rodriguez	~10mW	-0.9	-72..+96

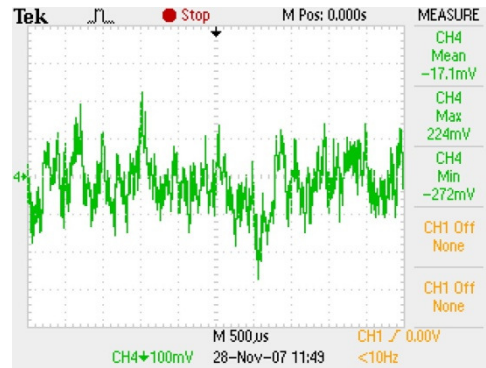


Oscilloscope views

The oscilloscope was configured with an AC coupling, the input inverted, and a voltage resolution of 100 mV per division versus a time resolution of 500  $\mu$ s per division.



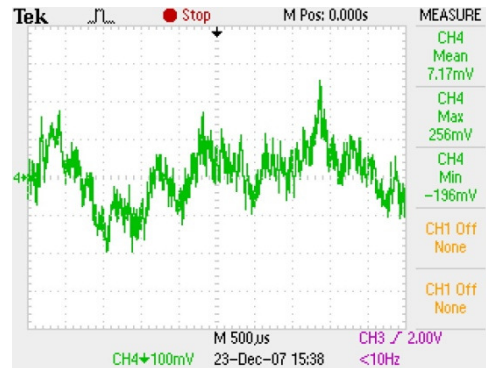
Sample 1



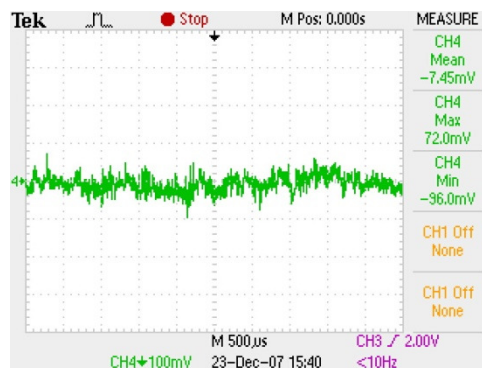
Sample 2



Sample 3



Sample 4



Sample 5





## APPENDIX 4 – COMPUTATION OF THE POWER SPECTRUM

After signal conditioning (inversion among other things) and analog-to-digital conversion (AD), a fixed quantity of samples (block) is used to compute the power spectrum of the signal. This procedure is repeated as soon as a full block has been filled, and then the LDF parameters are calculated from the power spectrum.

In order to extract the power spectrum of the acquired signal, it is first necessary to compute a *Fast Fourier Transform (FFT)* on it; this calculation returns an array of values which dimension is the same as the input block, and each is composed of a *real part (Re)* and an *imaginary part (Im)*. Depending on how they are used in further calculation, they can be representative of either the *amplitude (Amp)* or the *phase* of the signal. In the case of the LDF measurement, the interest is in the power of the signal, which can be calculated from the *amplitude* of the signal; therefore, the *phase* calculation is not required in this application. The following calculation shows the principle to obtain such values:

$$Amp = \sqrt{Re^2 + Im^2}$$

$$Mag = 20 \cdot \log(Amp) = 10 \cdot \log(Amp^2)$$

where *Mag* is the magnitude of the power spectrum. The *amplitude* has the units of *V* (Volts), and the magnitude *dBV*. The calculation above has to be applied on each single element of the array in order to reproduce the correct spectrum. However, the calculation based on the LDF theory (see 2.1.3) refers to *P(f)*, which is actually the power spectrum, but in "true" values: such a calculation cannot be applied on values expressed in *dBV*, but they have to be in *V<sup>2</sup>*. Therefore, the values of *P(f)* have to be calculated as follows:

$$Amp^2 = Re^2 + Im^2$$

Where *Amp<sup>2</sup>* effectively represents the power of the signal in *V<sup>2</sup>*; the latter value is just different from the *magnitude* by its unit, but still represent the same parameter.

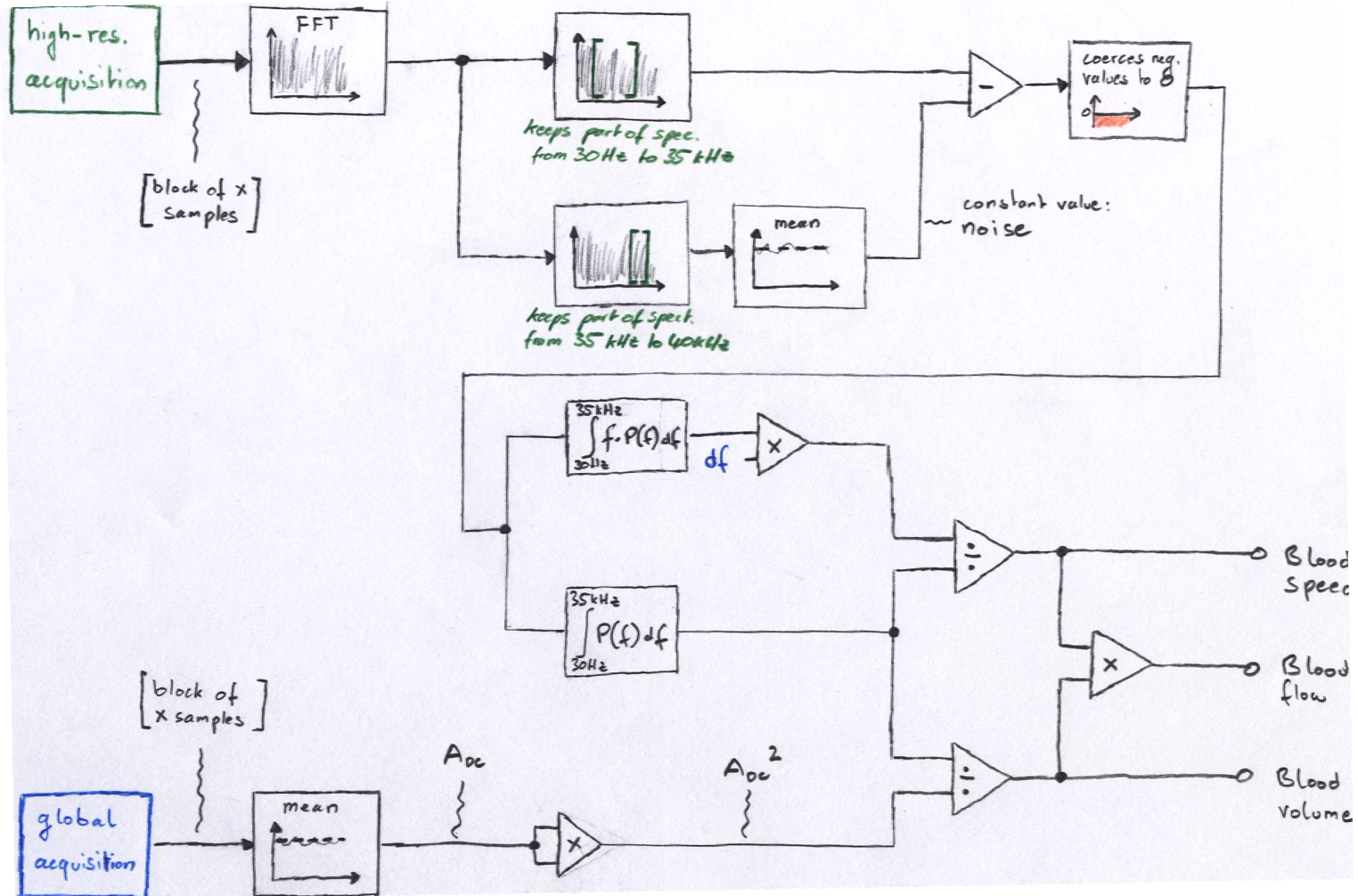
Whatever is the interest (*Amp*, *Amp<sup>2</sup>* or *Mag*), each of these parameters has to be calculated for each single result of the FFT, meaning that they can be arranged within a vector, and displayed in a graph. The scale and units of the y-axis depend on which of the three parameters above is chosen.

The x-axis is composed of a number of values equals to half of the number of samples used in the analyzed block, and represents the corresponding frequency to which *Amp*, *Amp<sup>2</sup>* or *Mag* refers. The axis range is from 0 Hz to  $f_s/2$  with a discrete increment of  $\Delta f$  equal to:

$$\Delta f = \frac{f_s}{\text{num. of samples}} = df$$

The existing system [3] samples blocks of 16'384 samples ( $2^{14}$ ) at a frequency  $f_s$  of 242 kHz. Therefore,  $\Delta f \approx 14.77$  Hz. *Amp<sup>2</sup>* is calculated for each result of the FFT according to the formula mentioned above and the resulting vector can be displayed in a graph called power spectrum.

### APPENDIX 5 – LDF ALGORITHM



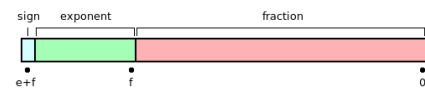
## APPENDIX 6 – IEEE 754 STANDARD

The *IEEE 754* standard defines formats for representing floating-point numbers and special values (infinity and *NaN* (Not a Number)) together with a set of floating-point operations that operate on these values.

*IEEE 754* specifies four formats for representing floating-point values: single-precision (32 bit), double precision (64 bit), single-extended precision ( $\geq 43$  bit, not commonly used) and double-extended precision ( $\geq 79$  bit, usually implemented with 80 bits). Only 32-bit values are required by the standard; the others are optional. Many languages specify that *IEEE* formats and arithmetic be implemented, although sometimes it is optional. For example, the C programming language, which pre-dated *IEEE 754*, now allows but does not require *IEEE* arithmetic (the C float typically is used for *IEEE* single-precision).

### General layout for a floating-point number

Binary floating-point numbers are stored in a sign-magnitude form where the most significant bit is the sign bit, *exponent* is the biased exponent, and *fraction* is the significand (or mantissa) minus the *most significant bit*.



The exponent is biased by  $2^{e-1}-1$ , where  $e$  is the number of bits used for the exponent field. Biasing is done because exponents have to be signed values in order to be able to represent both tiny and huge values, but two's complement, the usual representation for signed values, would make comparison harder. To solve this, the exponent is biased before being stored by adjusting its value to put it within an unsigned range suitable for comparison.

For example, to represent a number which has exponent of 17, *exponent* is  $17 + 2^{e-1}-1$ . Assuming  $e = 8$ , the exponent is equal to  $17 + 128 - 1 = 144$

The most significant bit of the significand (not stored) is determined by the value of *exponent*. If  $0 < \textit{exponent} < 2^{e-1}-1$ , the most significant bit of the *significand* is 1, and the number is said to be *normalized*. If *exponent* is 0, the most significant bit of the *significand* is 0 and the number is said to be *de-normalized*. Three special cases arise:

1. If *exponent* is 0 and *fraction* is 0, the number is  $\pm 0$  (depending on the sign bit)
2. If *exponent* =  $2^e-1$  and *fraction* is 0, the number is  $\pm$  infinity (again depending on the sign bit)
3. If *exponent* =  $2^e-1$  and *fraction* is not 0, the number being represented is not a number (NaN)

This can be summarized as:

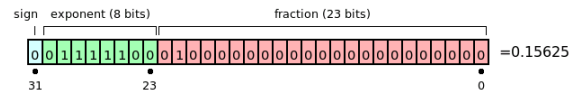
Type	Exponent	Fraction
Zeros	0	0
Denormalized numbers	0	Non zero
Normalized numbers	1 to $2^e-2$	Any
Infinities	$2^e-1$	0
NaNs	$2^e-1$	non zero



Single-precision 32 bit

A single-precision binary floating-point number is stored in 32 bits.

The exponent is biased by  $2^{8-1}-1 = 127$  in this case (exponents in the range -126 to +127 are representable). An exponent of -127 would be biased to the value 0 but this is reserved to encode that the value is a denormalized number or zero. An exponent of 128 would be biased to the value 255 but this is reserved to encode an *infinity* or *not a number (NaN)*.



For normalized numbers, which are the most common, the *exponent* is the biased exponent and *fraction* is the significand without the most significant bit.

The number has value  $v$ :

$$v = s \cdot 2^e \cdot m$$

Where

- $s = +1$  (positive numbers and +0) when the sign bit is 0
- $s = -1$  (negative numbers and -0) when the sign bit is 1
- $e = \text{exponent} - 127$  (in other words, the exponent is stored with 127 added to it, also called "biased with 127")
- $m = 1.\text{fraction}$  in binary (that is, the significand is the binary number 1 followed by the radix point followed by the binary bits of the *fraction*). Therefore,  $1 \leq m < 2$

In the example shown above, the *sign* is zero so  $s$  is +1, the *exponent* is 124 so  $e$  is -3, and the significand  $m$  is 1.01 (in binary, which is 1.25 in decimal). The represented number is therefore  $+1.25 \cdot 2^{-3}$ , which is +0.15625.

Here is the summary table from the previous section with some 32-bit single-precision examples:

Type	Sign	Exponent	Significand	Value
Zero	0	0000 0000	000 0000 0000 0000 0000 0000	0.0
One	0	0111 1111	000 0000 0000 0000 0000 0000	1.0
Minus one	1	0111 1111	000 0000 0000 0000 0000 0000	-1.0
Smallest denorm. number	*	0000 0000	000 0000 0000 0000 0000 0001	$\pm 2^{-23} \cdot 2^{-126} = \pm 2^{-149} \approx \pm 1.4 \cdot 10^{-45}$
"Middle" denorm. number	*	0000 0000	100 0000 0000 0000 0000 0000	$\pm 2^{-1} \cdot 2^{-126} = \pm 2^{-127} \approx \pm 5.88 \cdot 10^{-39}$
Largest denorm. number	*	0000 0000	111 1111 1111 1111 1111 1111	$\pm (1-2^{-23}) \cdot 2^{-126} \approx \pm 1.18 \cdot 10^{-38}$
Smallest normal. number	*	0000 0001	000 0000 0000 0000 0000 0000	$\pm 2^{-126} \approx \pm 1.18 \cdot 10^{-38}$
Largest normal. number	*	1111 1110	111 1111 1111 1111 1111 1111	$\pm (2-2^{-23}) \cdot 2^{-127} \approx \pm 3.4 \cdot 10^{38}$
Positive infinity	0	1111 1111	000 0000 0000 0000 0000 0000	$+\infty$
Negative infinity	1	1111 1111	000 0000 0000 0000 0000 0000	$-\infty$
Not a number	*	1111 1111	non zero	NaN

\* sign bit can be either 0 or 1

## APPENDIX 7 – COMPONENTS LIST

### Miniaturized probe

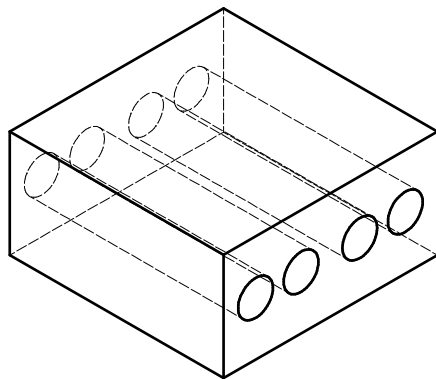
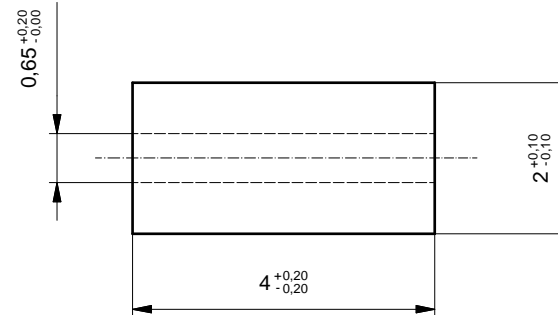
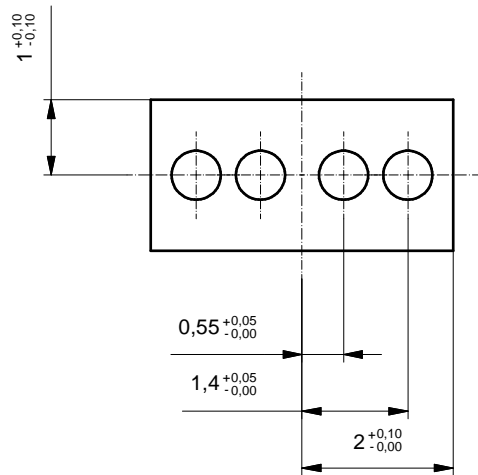
Landmark	Req. quantity	Component	Brand	Model	Description, main features	Serial number
5a	1	Mechanical holder for fiber optics	-	-	Aluminium, 4 holes $\varnothing$ 650 $\mu$ m fiber optics holder	-
5b	2	Mirror	Edmund Optics	NT45-385	Techspec right angle prism	-
7a	2	600 $\mu$ m core fiber optics	Thor Labs	BFL37-600	Standard hard cladding multimode fiber, low OH, 600 $\mu$ m core, 0.37 NA	-
7b	2	SMA connector	Thor Labs	10640A	SMA 905 fiber connector: multi-mode, fiber size 630 $\mu$ m	-

### Optical set-up

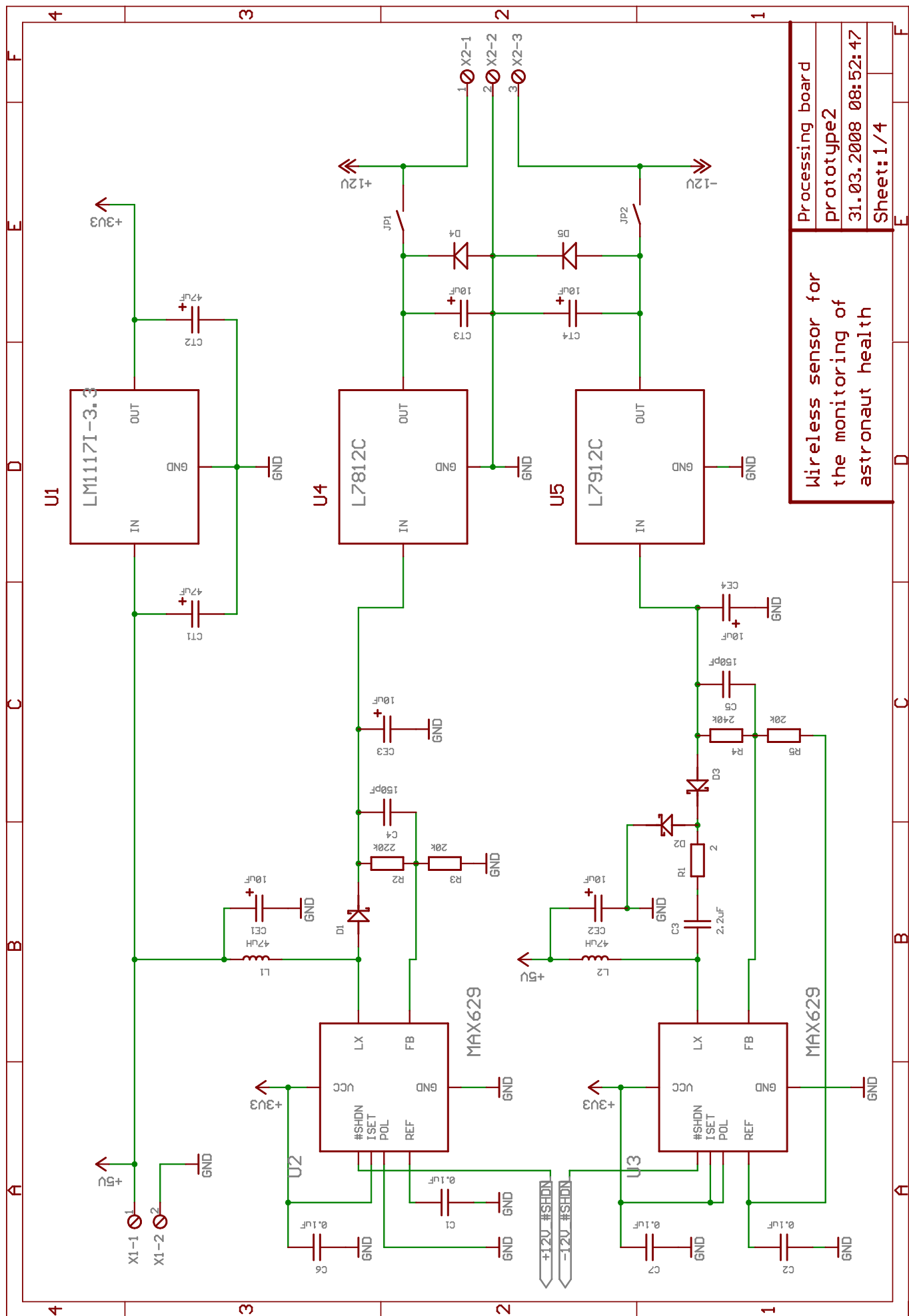
Landmark	Req. quantity	Component	Brand	Model	Description, main features	Serial number
1	1	Laser A	OZ Optics	OZ-2000-780-5/ 125-S-40-3S-3A-1-25	Stable laser source, wavelength 780 nm, output power variable up to 25 mW	101068-02
2	1	Laser B	OZ Optics	OZ-2000-635-4/ 125-S-40-3S-3A-1-20	Stable laser source, wavelength 635 nm, output power variable up to 20 mW	101067-1
3	1	Photodiode	Hamamatsu	C5460-01	Avalanche photodiode module integrated with peripheral circuits	01724
6	1	Fibers combiner	Font Canada	SLC128	400 $\mu$ m core "2 to 1" multimode fibers combiner	-
10	2	Connection cable	OZ Optics	OZ-X000-CABLE-SA	Cable fitted with DB9-connector on one side, and laser signals wires on the other (for interfacing OZ-2000 lasers series)	a) 100022-5 b) 100022-6
12	2	FC/PC to SMA connector	-	-	Metallic adapter from FC/PC to SMA	-
13	2	Fiber optics	OZ Optics	MMJ-31-IRVIS-50/ 125-3-2	2 meters long, 3 mm OD cabled 50/125 IRVIS MM patchcord terminated with a FC/PC connector on one end, 1.8 mm ferrule on the other	a) T895801-01 b) T895801-02

Electrical set-up

Landmark	Req. quantity	Component	Brand	Model	Description, main features	Serial number
4	1	Processing board	-	-	Prototype 2 of the developed processing board	-
8	1	BNC cable	-	-	Standard BNC cable	-
9	1	5VDC transformer	Phihong	PSA31U-050	Switching AC adaptor; DC output 5V, 4A	P60900339A3

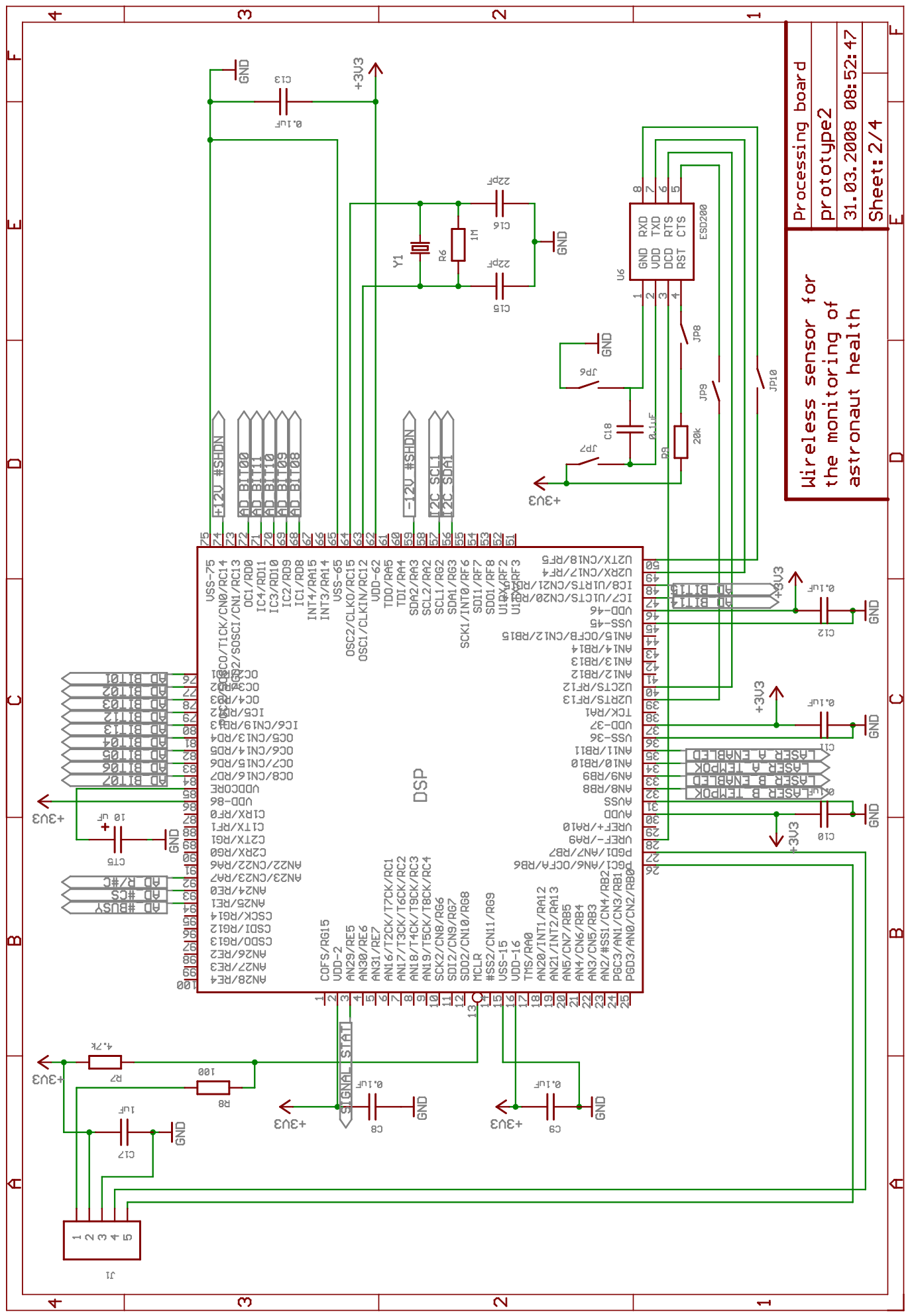


1	1	Aluminium	Canal, dia 650, 4 holes				
Pos.	Quantité	Matière	Dénomination / caractéristiques				
Pos.	Menge	Werkstoff	Benennung / Merkmale				
Astronaut fingertip measurement Fiber optic canal, diameter 650				Dessiné Gezeichnet	Mikaël Rodriguez	08.02.2008	Echelle Massstab
				Contrôlé Geprüft			10:1
Fichier Datei	C:\Documents and Settings\Mikaël\Inventor\LDF\canal_dia650_4holes.idw						
Haute école valaisanne Hochschule Wallis				All the dimensions are in millimeters			



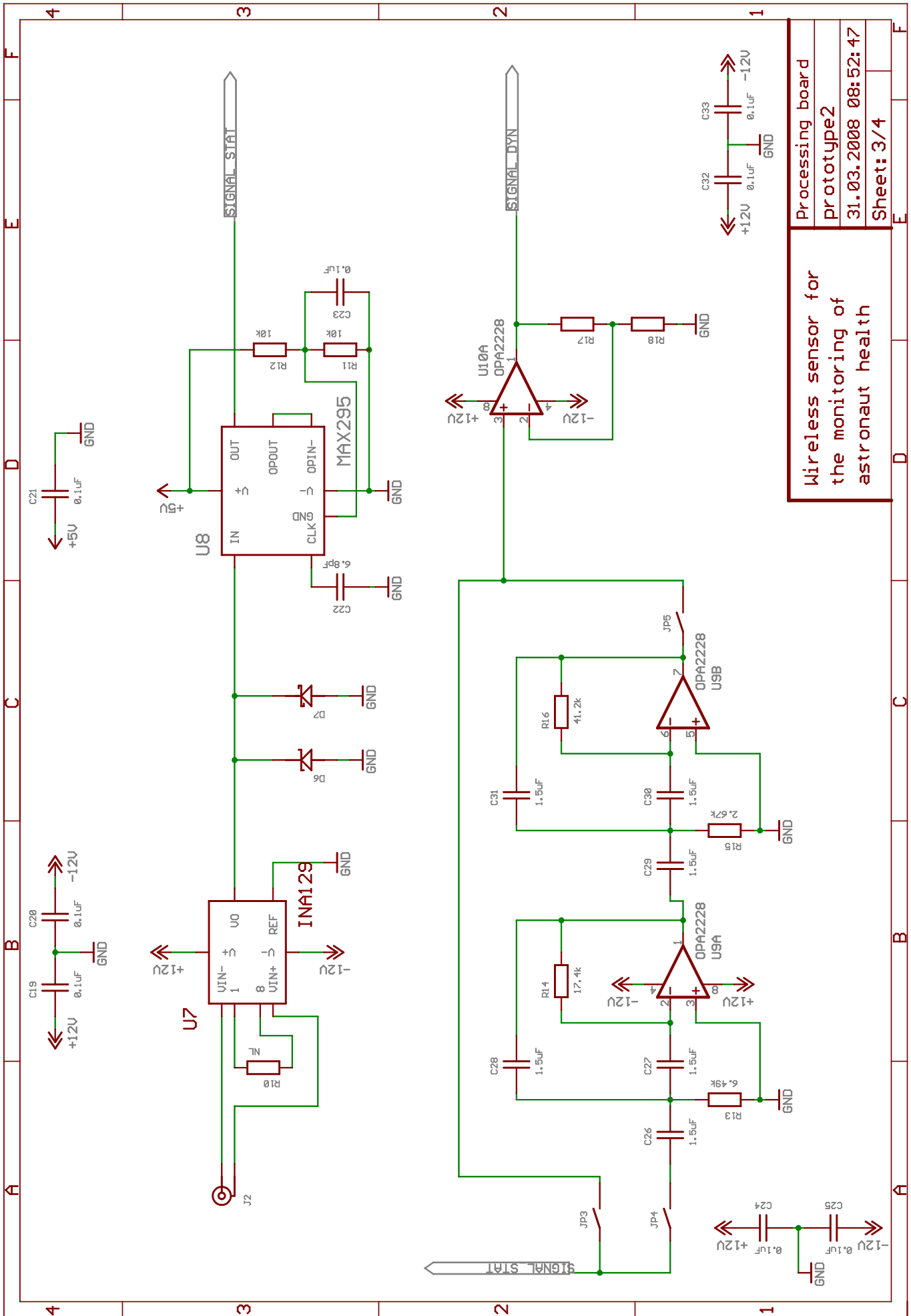
Processing board  
 prototype2  
 31.03.2008 08:52:47  
 Sheet: 1/4

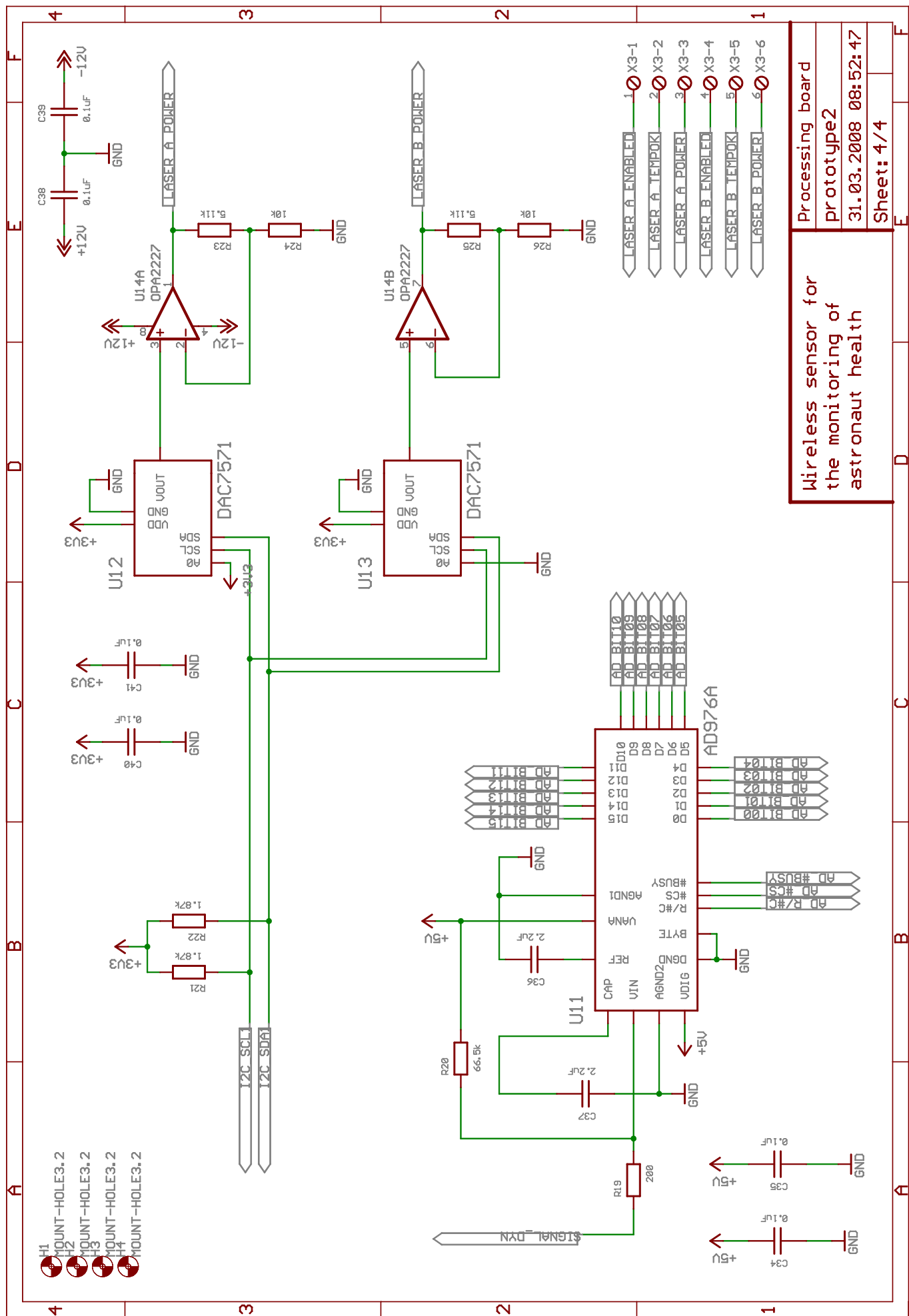




Processing board  
 prototype2  
 31.03.2008 08:52:47  
 Sheet: 2/4

Wireless sensor for  
 the monitoring of  
 astronaut health





Processing board  
 prototype2  
 31.03.2008 08:52:47  
 Sheet: 4/4

Wireless sensor for  
 the monitoring of  
 astronaut health

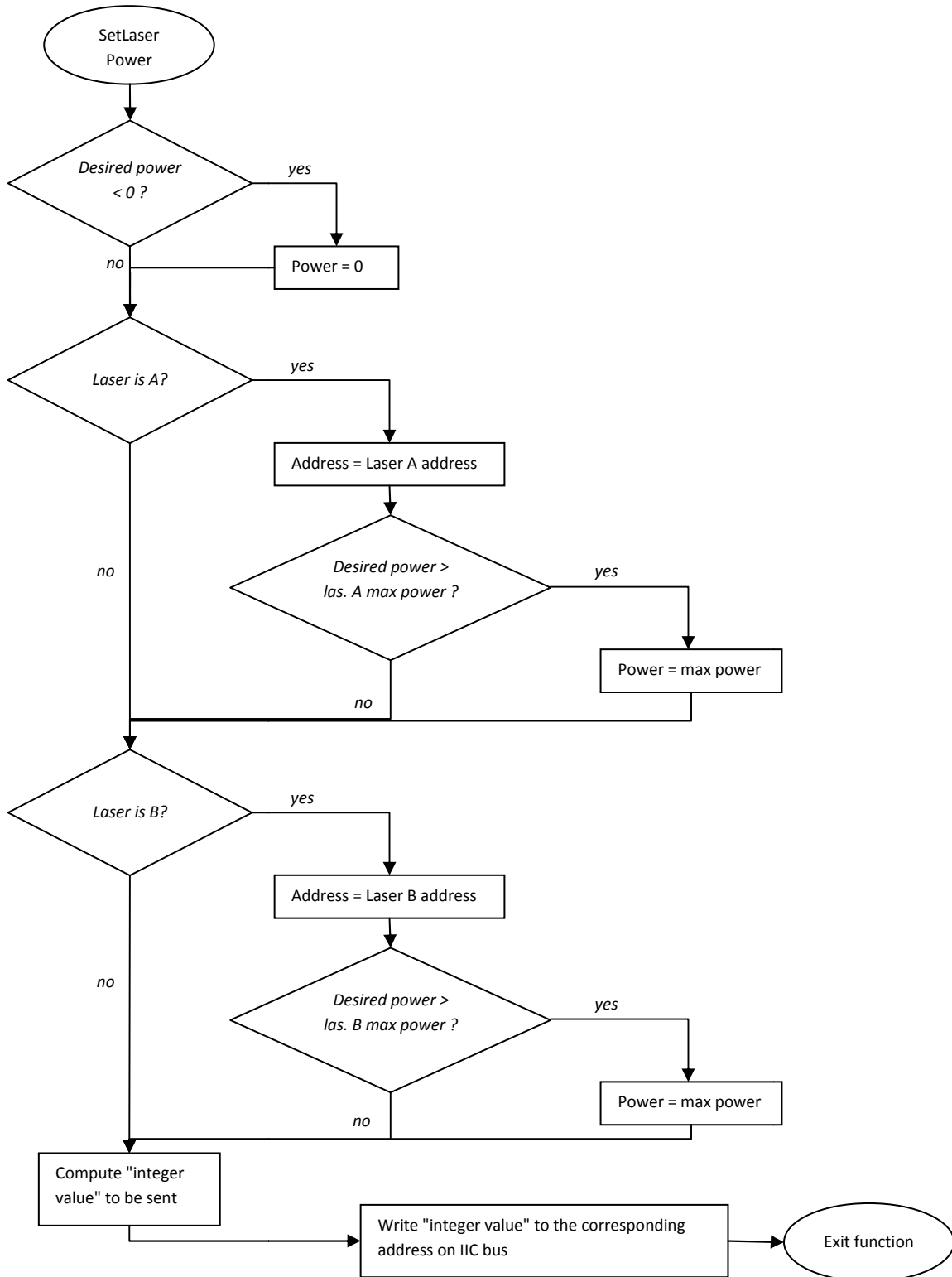


## APPENDIX 10 – DSP'S PINOUT

Pin-nr	Pin name	Type	Connection
2	V <sub>dd</sub>	Power input	To 3.3V
3	AN29	Analog input	(operates the DC-coupled acquisition)
13	MCLR (ac. low)	(master clear)	Used when programming occurs
15	V <sub>ss</sub>	Power input	To ground
16	V <sub>dd</sub>	Power input	To 3.3V
26	PGC1	Programming clock	To programming connector
27	PGD1	Programming data	To programming connector
28	RA9	Digital input	Bluetooth module U6, pin <i>DCD</i>
30	V <sub>dd</sub>	Power input	To 3.3V
31	V <sub>ss</sub>	Power input	To ground
32	RB8	Digital input	To <i>Laser B temperature OK</i>
33	RB9	Digital output	To <i>Laser B enable</i>
34	RB10	Digital input	To <i>Laser A temperature OK</i>
35	RB11	Digital output	To <i>Laser A enable</i>
36	V <sub>ss</sub>	Power input	To ground
37	V <sub>dd</sub>	Power input	To 3.3V
39	U2RTS	UART module, RTS signal	Bluetooth module U6, pin <i>CTS</i>
40	U2CTS	UART module, CTS signal	Bluetooth module U6, pin <i>RTS</i>
45	V <sub>ss</sub>	Power input	To ground
46	V <sub>dd</sub>	Power input	To 3.3V
47	RD14	Digital input	External AD converter U11, pin <i>D14</i>
48	RD15	Digital input	External AD converter U11, pin <i>D15</i>
49	U2RX	UART module, RX signal	Bluetooth module U6, pin <i>TXD</i>
50	U2TX	UART module, TX signal	Bluetooth module U6, pin <i>RXD</i>
56	I <sup>2</sup> C SDA1	I <sup>2</sup> C module, data	D/A converters U12 and U13, pin <i>SDA</i>
57	I <sup>2</sup> C SCL1	I <sup>2</sup> C module, clock	D/A converters U12 and U13, pin <i>SCL</i>
59	RA3	Digital output	Negative-voltage DC/DC converter U3, pin <i>SHDN</i>
62	V <sub>dd</sub>	Power input	To 3.3V
63	OSC1	Clock input	External crystal Y1
64	OSC2	Clock input	External crystal Y1
65	V <sub>ss</sub>	Power input	To ground
68	RD8	Digital input	External AD converter U11, pin <i>D8</i>
69	RD9	Digital input	External AD converter U11, pin <i>D9</i>
70	RD10	Digital input	External AD converter U11, pin <i>D10</i>
71	RD11	Digital input	External AD converter U11, pin <i>D11</i>
72	RD0	Digital input	External AD converter U11, pin <i>D0</i>
74	RC14	Digital output	Positive-voltage DC/DC converter U2, pin <i>SHDN</i>
75	V <sub>ss</sub>	Power input	To ground
76	RD1	Digital input	External AD converter U11, pin <i>D1</i>
77	RD2	Digital input	External AD converter U11, pin <i>D2</i>
78	RD3	Digital input	External AD converter U11, pin <i>D3</i>
79	RD12	Digital input	External AD converter U11, pin <i>D12</i>
80	RD13	Digital input	External AD converter U11, pin <i>D13</i>
81	RD4	Digital input	External AD converter U11, pin <i>D4</i>
82	RD5	Digital input	External AD converter U11, pin <i>D5</i>
83	RD6	Digital input	External AD converter U11, pin <i>D6</i>
84	RD7	Digital input	External AD converter U11, pin <i>D7</i>
85	VDD core	-	Tantalum capacitor CT5
86	V <sub>dd</sub>	Power input	To 3.3V
92	RA7	Digital output	External AD converter U11, pin <i>R/C</i>
93	RE0	Digital output	External AD converter U11, pin <i>CS</i>
94	RE1	Digital input	External AD converter U11, pin <i>BUSY</i>

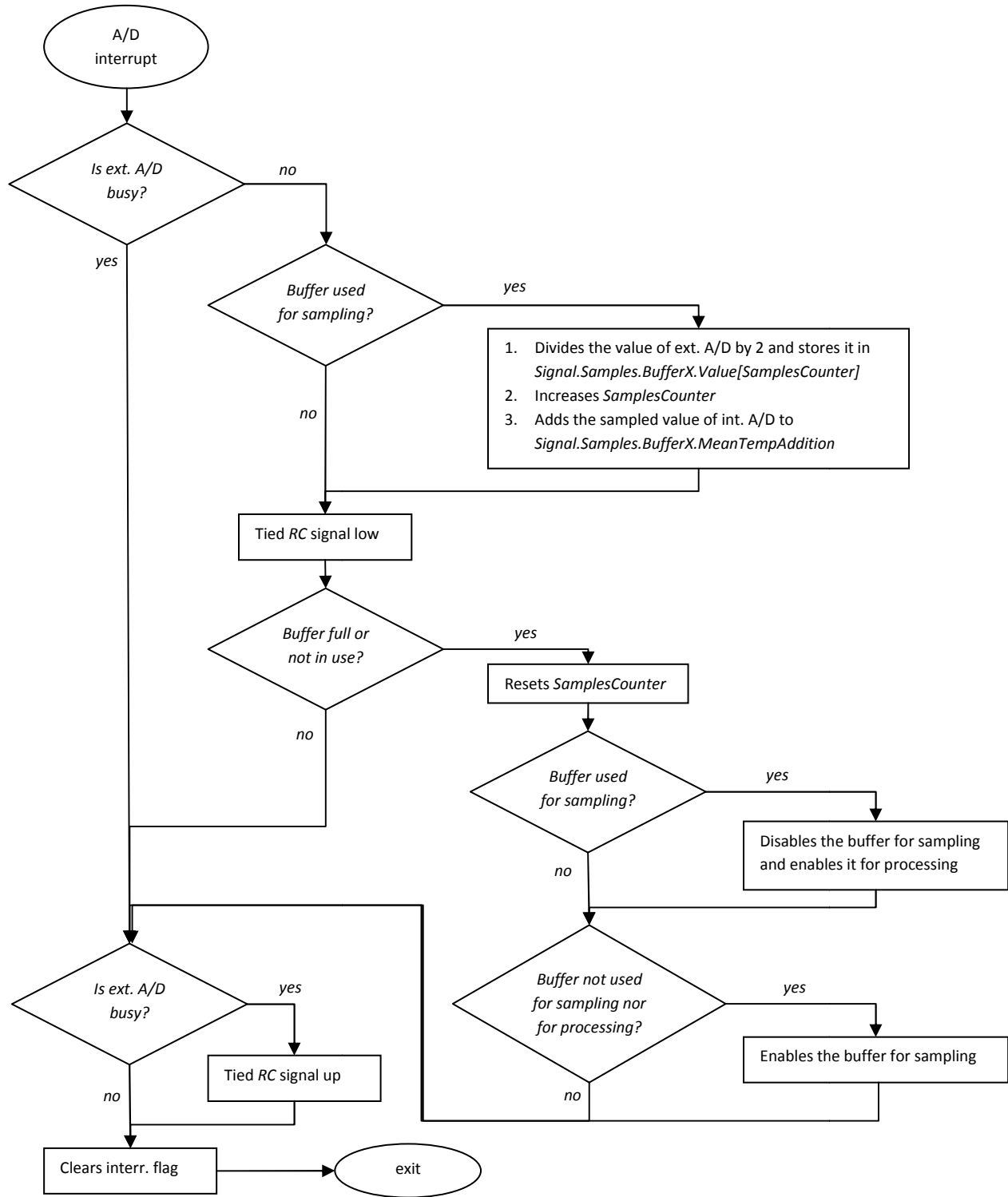


## APPENDIX 11 – LASER'S POWER CONTROL FLOW CHART

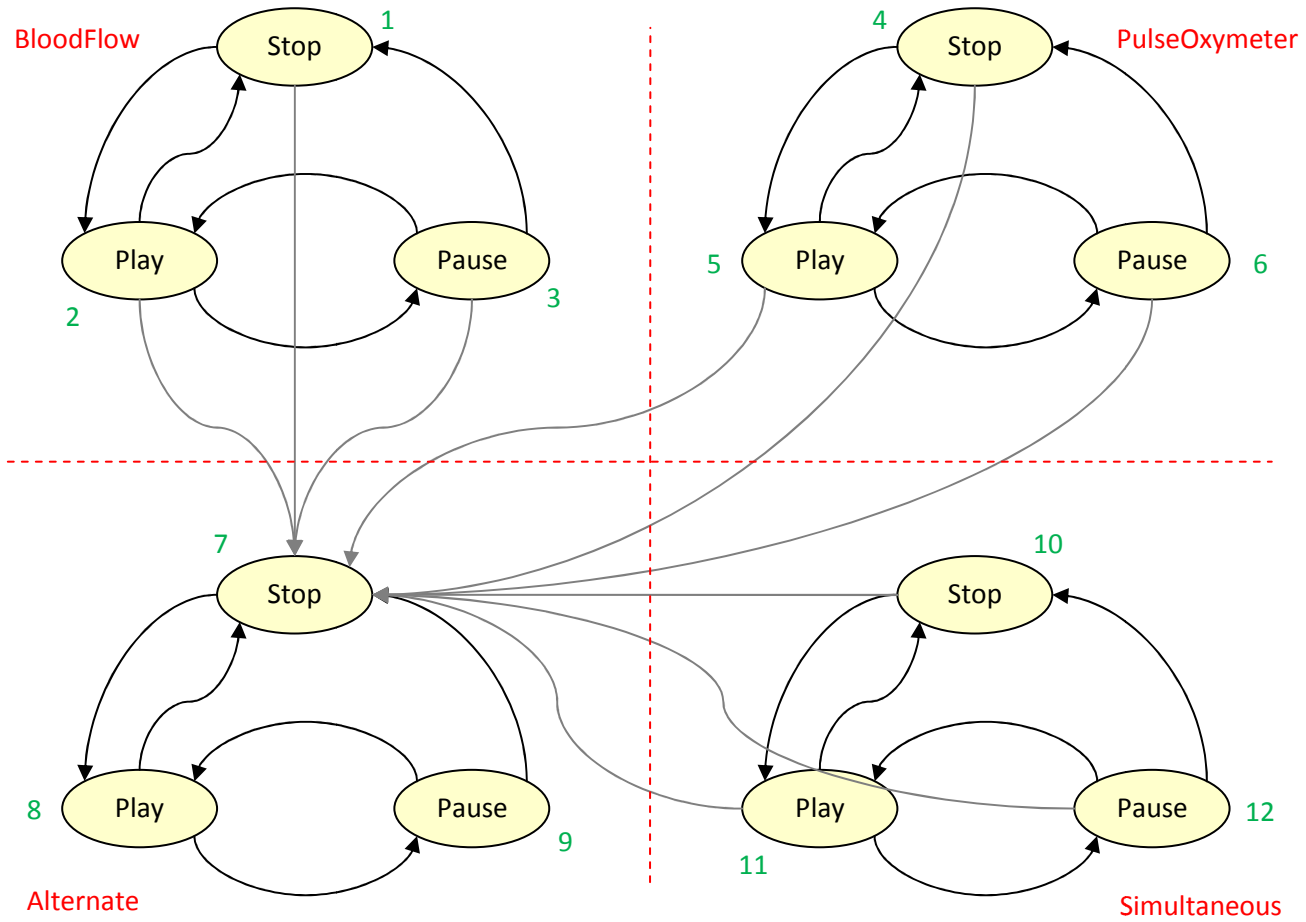




## APPENDIX 12 – A/D CONVERSIONS FLOW CHART

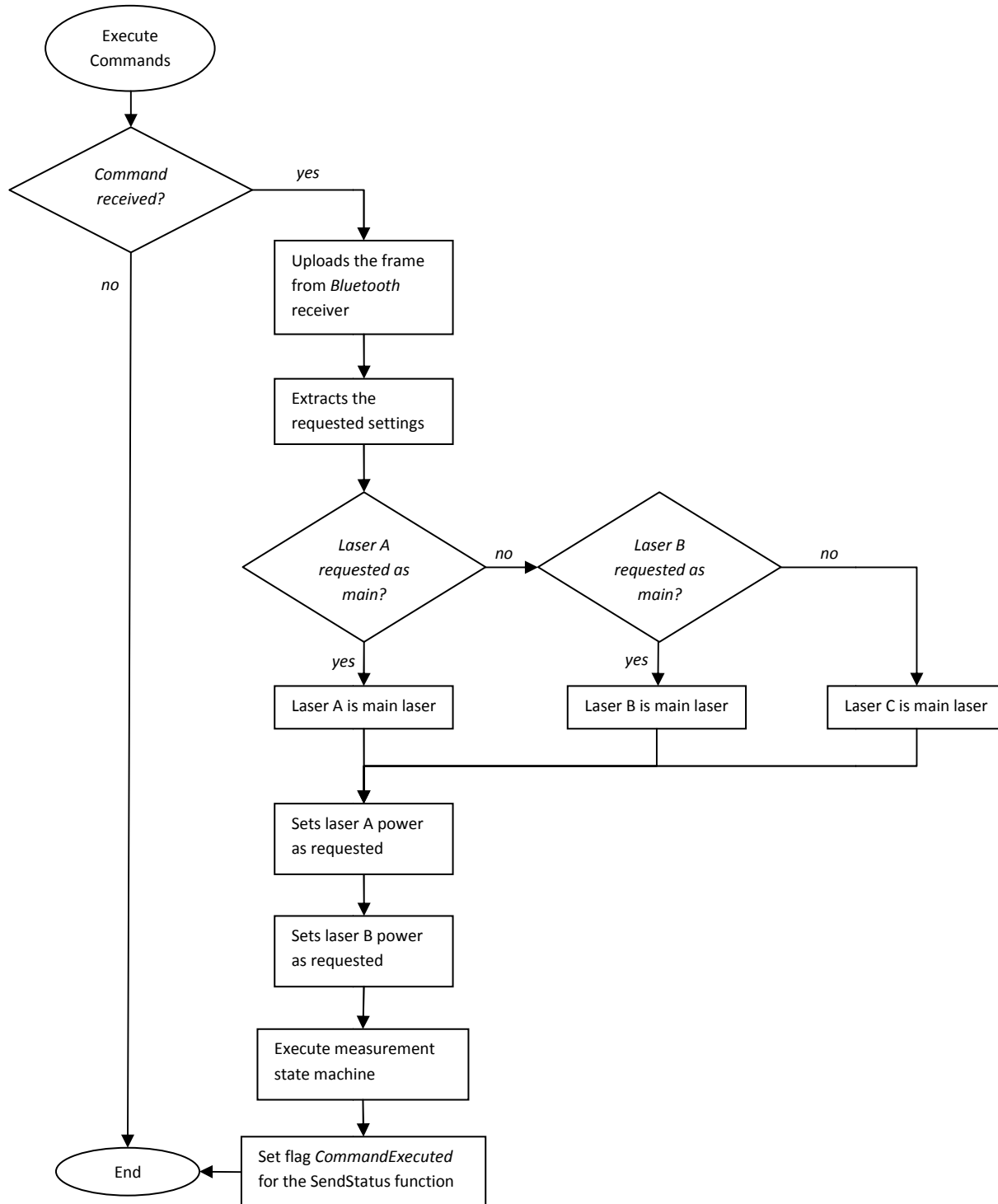


### APPENDIX 13 – MEASUREMENTS STATE MACHINE

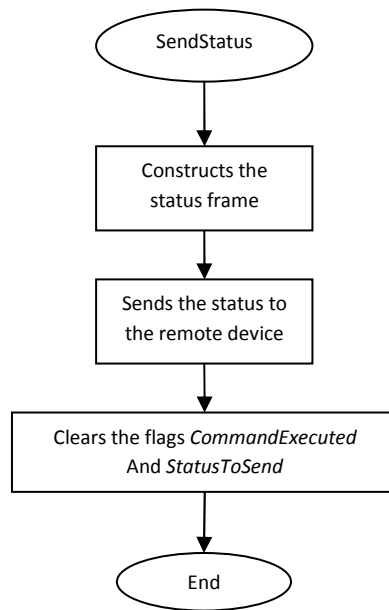




## APPENDIX 14 – COMMANDS EXECUTION AND STATUS TRANSMISSION









## APPENDIX 15 – MATLAB PROGRAM FOR GENERATING A SAMPLED SINUS

```
clear all
close all
format short g

frequency=2400;
sampling_frequency=8192;
N=1024;

t = linspace(0,N,N*sampling_frequency);
y = 15000*sin(2*pi*frequency*t);
y = y(1:N);
t=t(1:N);
binary=(round(y));
plot(t,binary)

fid = fopen('c:\sine.txt','w');
fprintf(fid,'%d,\t\n ',binary);
fclose(fid);
```